DISSERTATION

Submitted to

the combined faculties for Natural Sciences and Mathematics

of the Ruperto-Carola University of Heidelberg, Germany

for the degree of

Doctor of Natural Sciences

presented by

Sirikamol Srismith (M. Sc.)

born in Chiang Mai, Thailand

Date of oral examination: 10. 09. 2018

Protection against severe malaria by haemoglobinopathic erythrocytes

Referees: Prof. Dr. Michael Lanzer

Prof. Dr. Fredrich Frischknecht

Ich erkläre hiermit, dass ich die vorliegende Doktorarbeit selbstständig unter Anleitung verfasst und keine anderen als die angegebenen Quellen und Hilfsmittel benutzt habe.

Ich erkläre hiermit, dass ich an keiner anderen Stelle ein Prüfungsverfahren beantragt bzw. die Dissertation in dieser oder anderer Form bereits anderweitig als Prüfungsarbeit verwendet oder einer anderen Fakultät als Dissertation vorgelegt habe.

Die vorliegende Arbeit wurde am Department für Infektologie, Abteilung Parasitologie des Universitätsklinikum Heidelberg in der Zeit von März 2014 bis September 2017 unter der Leitung von Prof. Dr. Michael Lanzer ausgeführt.

…… ……

Datum Sirikamol Srismith

Acknowledgements

"*No man is an island, entire of itself;*" (Donne, 1624)

My PhD and this thesis would have never been possible without the help and support of the following people:

First and foremost, I would like to thank Prof. Dr. Michael Lanzer, both for the opportunity to work on this vastly interesting topic and his understanding, help and guidance along the way.

Thank you to Prof. Dr. Friedrich Frischknecht, Prof. Dr. Ulrich Schwarz and Prof. Dr. Mike Heilemann for their suggestions, guidance and participation in my TAC meetings. Further thanks to Prof. Dr. Frauke Melchior and Dr. Faith Osier for agreeing to be a part of my thesis defence committee.

Thank you to Dr. Marek Cyrklaff for his invaluable support, encouragement and guidance, the last-minute consultations and the scientific as well as general discussions we have had throughout my time here.

Thank you to my collaborators for helping me with various parts of my projects: Dr. Benjamin Flottmann for introducing me to *d*STORM imaging; Dr. Varun Venkataramani and Dr. Frank Herrmannsdörfer for the discussion on the *d*STORM reconstructions and the SuReSim software; Dr. Janina Hahn for her help with STED imaging and Dr. Sophie Adjelley for her assistance with qRT-PCR. Thank you also to Dr. Cecilia Sanchez for her help with the confocal microscope and other molecular biological techniques in the lab.

Thank you to my lovely, lovely lab mates, past and present – in no particular order (you know I love you all!): Dr. Christine Lansche, Dr. Maelle Duffey, Monika Jankowska, Dr. Sonia Molliner, Dr. Sebastiano Bellanca, Dr. Britta Nyboer, Stephan Prior, Marina Müller, Dr. Hani Kartini, Dr. Nicole Killan, Dr. Martin Dittmer, Dr. Harden Rieger, Maillin Waldecker, Costanza Tacolli, Marvin Haag. Thank you for all of your help and support, both academically and personally, and thank you for making the lab more like a family than a workplace! You guys are the best, seriously!!! HUGSSSS!!

Thanks to Miriam Griesheimer and Sandra Niebel for their tremendous help with various paperwork and administrative issues as well as their support during the last stages of this thesis!

Another big hug and thank you goes to my friends, both here in Heidelberg and abroad. I've learnt so much and experienced so much over the past six years in Germany – and a lot of things wouldn't have been possible without you guys :) A special shout-out to Priyata for finally

dragging me to the pool to learn how to swim(-ish)! And another huge thank you to Noom and Punch for all of those cooking evenings and associated gossip sessions! Thanks also to those friends who aren't physically within reach – with the amount of time I generally spend on my phone/laptop, I don't think distance was much of an issue, was it? :p

Last but not least, my family. My mother, Butsaba Srismith, my late-father, Chartchai Srismith, and my little sister, Duangkamol (Nack) Srismith. Words cannot express how grateful I am to have you guys in my life. Mama and Papa, thank you for your love, support and guidance. Thank you for your vision and sacrifice - I literally would not be here today if not for you. Thank you for a great childhood, full of laughter and love. Nack, thank you for being the best little sister I could hope for. I hope you know how much I value our discussions and your thoughts and input. I love how we can just talk about anything and everything! I don't think my 3-year old self would believe that the little (possibly screaming) bundle I attempted to drag around the house in a laundry basket would one day become one of my best friends!! They say you can't choose your family – well, it seems I'm pretty lucky with this one :)

Summary

Although the molecular mechanisms by which haemoglobinopathic erythrocytes protect their carriers against life-threatening complications of severe malaria have yet to be elucidated, one of the contributing factors is believed to be reduced cytoadhesion in the microvasculatures of vital organs. Previous studies have described perturbations in host actin remodelling, reduced surface levels of PfEMP1 adhesin, abnormal knob sizes and distributions as well as malformed Maurer's clefts in infected haemoglobinopathic erythrocytes, relative to those seen in infected HbAA erythrocytes.

We attempted to establish super-resolution imaging with direct stochastic optical reconstruction microscopy (*d*STORM) as an intermediate throughput method of visualising host actin remodelling in infected erythrocytes. Unfortunately, individual F-actin and spectrin filaments could not be resolved and no significant differences in the actin and spectrin labelling of uninfected versus infected erythrocytes were distinguishable.

We also further explored the kinetics of adhesion phenotype and protein transport in haemaglobinopathic erythrocytes. We found that infected HbAS erythrocytes exhibited slower temporal increase in number of adherent cells as well as a lower total number of adherent cell relative to infected HbAA erythrocytes. A delay in the establishment of new permeability pathway (NPP) was also observed in infected haemoglobinopathic erythrocytes.

We tested the hypothesis that the inherent redox imbalance found in uninfected haemoglobinopathic erythrocytes is the beginning of a cascade of events which precipitates in the reduced cytoadhesive phonotype associated with protection against severe malaria. By exposing uninfected HbAA erythrocytes to transient oxidative stress, we were able to mimic various phenotypes associated with the protective traits, including reduced cytoadhesion and surface PfEMP1 levels, malformed and dispersed knobs, aberrant Maurer's cleft morphologies and inability to remodel host actin cytoskeleton.

Taken together, our findings describe a cascade of events which begins with the redox imbalance inherent to uninfected haemoglobinopathic erythrocytes. This oxidative milieu interferes with parasitic protein export, host actin remodelling and knobs and Maurer's cleft formation, which leads to aberrant display of PfEMP1 on the cell surface and a reduced level of cytoadhesion. This helps to alleviate the life-threatening consequences of severe malaria.

Zusammenfassung

Obwohl die molekularen Mechanismen durch die hämoglobinopathische Erythrozyten ihre Träger gegen lebensbedrohliche Komplikationen schwerer Malaria schützen noch nicht geklärt sind, wird als einer der beitragenden Faktoren eine verminderte Zytoadhäsion in der Mikrovaskulatur lebenswichtiger Organe vermutet. Frühere Studien haben Störungen der Wirts-Aktin Remodellierung, eine reduzierte Expression des Adhäsins PfEMP1 an der Oberfläche von Erythrozyten, eine abnormale Größe und Verteilung von Knobs sowie fehlgeformte Maurer-Spalten in infizierten hämoglobinopathischen Erythrozyten im Vergleich zu infizierten HbAA-Erythrozyten beschrieben.

Wir haben versucht, eine hochauflösende Bildgebung mittels direkter stochastischer optischer Rekonstruktionsmikroskopie (dSTORM) als intermediärer Durchsatzmethode zur Visualisierung der Wirts-Aktin Remodellierung in infizierten Erythrozyten zu etablieren. Unglücklicherweise konnten einzelne F-Aktin- und Spektrinfilamente nicht aufgelöst werden, zudem wurden keine signifikanten Unterschiede in der Aktin- und Spektrinmarkierung von nicht-infizierten gegenüber infizierten Erythrozyten gefunden.

Wir untersuchten auch die Kinetiken des Adhäsionsphänotyps und des Proteintransports in hämoglobinopathischen Erythrozyten. Wir konnten zeigen, dass infizierte HbAS-Erythrozyten einen langsameren zeitlichen Anstieg der Anzahl adhärenter Zellen sowie eine geringere Gesamtanzahl adhärenter Zellen im Vergleich zu infizierten HbAA-Erythrozyten aufwiesen. Des Weiteren konnte auch eine Verzögerung bei der Etablierung des neuen Permeabilitätsweges (NPP) in infizierten hämoglobinopathischen Erythrozyten beobachtet werden.

Wir testeten die Hypothese, dass das in nicht infizierten hämoglobinopathischen Erythrozyten vorhandene inhärente Redox-Ungleichgewicht der Beginn einer Kaskade von Ereignissen ist, die schlußendlich zu dem reduzierten zytoadhäsiven Phänotyp führen, der mit dem Schutz vor schwerer Malaria assoziiert ist. Indem wir nicht infizierte HbAA-Erythrozyten transientem oxidativen Stress aussetzten, konnten wir verschiedene, mit den schützenden Eigenschaften assoziierte Phänotypen nachahmen, einschließlich verringerter Zytoadhäsion und Oberflächenexpression von PfEMP1, fehlgebildeter und weit verteilter Knobs, abweichender Maurer-Spalten Morphologie und der Unfähigkeit, das Wirts-Aktinzytoskelett umzuformen.

Zusammengefasst beschreiben unsere Ergebnisse eine Kaskade von Ereignissen, die mit dem Redox-Ungleichgewicht beginnt, das nicht infizierte hämoglobinopathische Erythrozyten aufweisen. Dieses oxidative Milieu stört den parasitären Proteinexport, die Remodellierung des Wirts-Aktins, die Ausbildung von Knobs und Maurer-Spalten, was ultimativ zu einer anomalen Präsentation von PfEMP1 auf der Zelloberfläche und einem verringerten Grad an Zytoadhäsion führt. Dies trägt dazu bei, die lebensbedrohlichen Folgen einer schweren Malaria zu verringern.

Table of Contents

List of Abbreviations

°	degrees
*	times/multiply
·	free radical
α	alpha
β	beta
±	plus or minus
&	and
Ab	antibody
AFM	atomic force microscopy
BSA	bovine serum albumin
C	celcius
C4S	chondroitin-4-sulfate
CD	cluster of differentiation
CDC	Centers for Disease Control and Prevention
cDNA	complementary DNA
CSA	chondroitin sulfate A
CSPG	chondroitin sulfate proteoglycan
Da	Dalton
DAB	diaminobenzidine
DCF	2',7'-dichlorofluorescein
DCF-DA	dichlorofluorescein diacetate
DNA	deoxyribonucleic acid
DTT	dithiothreitol

ECM	experimental cerebral malaria
EM	electron microscopy
et al.	et alii
FOV	field of view
Fwd	forward
FS	freeze substitution
GA	glutaraldehyde
GSH	gluthathione
GSSG	gluthathione disulfide
MEA	cysteamine hydrochloride
P.	*Plasmodium*
PAM	pregnancy-associated malaria
PFA	paraformaldehyde
PfEMP	Plasmodium falciparum Erythrocyte membrane protein
H_2O_2	hydrogen peroxide
Hb	haemoglobin
HCM	human cerebral malaria
HDMEC	human dermal microvascular endothelial cells
HDMS	1,1,1,3,3,3-Hexamethyldisilazane
HPF	high pressure freezing
h	hour
ICAM	intercellular adhesion molecule
Ig	Immunoglobulin
iRBC	infected red blood cell
k	kilo
KAHRP	knob-associated Histidine-rich protein

kDa	kilo Dalton
KOH	potassium chloride
kV	kilo volts
m	mili
M	molar
MACS	Magnetic Activated Cell Sorter
MC	Maurer's cleft
mg	milligram
µg	microgramm
min	minutes
ml	millilitre
µl	microliter
mM	millimolar
mRNA	messenger ribonucleic acid
MW	molecular weight
NADP	nicotinamide adenine dinucleotide phosphate
NADPH	reduced nicotinamide adenine dinucleotide phosphate
NaOH	sodium hydroxide
PBS	phosphate-buffered saline
PCR	polymerase chain reaction
pH	potential hydrogenii
PM	plasma membrane
PV	parasitophorous vacuole
PVP	polyvinyl pyrrolidone
qPCR	quantitative/real-time polymerase chain reaction
qRT-PCR	quantitative reverse transcription polymerase chain reaction

RBC	red blood cell
Rev	reverse
RNA	ribonucleic acid
ROS	reactive oxygen species
rpm	revolutions per minute
RT	room temperature
sec	seconds
SEM	scanning electron microscopy/standard error of mean
tBOOH	tert-butyl hydroperoxide
TEM	transmission electron microscopy
UV	ultra violet
vs	versus
WHO	world health organisation

1 Introduction

1.1 Malaria Disease Burden

Malaria is amongst the oldest and most influential of diseases, with written records of its characteristic cyclic fever stretching back to ancient civilisations in China (2700 BC), India and Egypt (1500 – 1600 BC) (Carter and Mendis, 2002; Cox, 2010). Many attempts at malaria control and eradication have been made over the years, both at the local and global levels, to varying degrees of success (Carter and Mendis, 2002; Nájera *et al.*, 2011). In the year 2000, all members of the United Nations (UN) agreed to strive towards a set of eight goals, referred to as the Millennium Development Goals (MDGs), and achieve certain milestones by the year 2015. One of this was Goal 6C: "Have halted by 2015 and begun to reverse the incidence of malaria and other major diseases." (MDG-Monitor, 2016).

Malaria exerts a great toll on the human population – not only in terms of morbidity and mortality, but also in terms of economic and social burden. Beyond the direct economic costs of medical treatments and income loss due to disease episodes, indirect costs such as changes in household behaviours, including schooling and migration, as well as macroeconomic effects, such as tourism and foreign investments, should also be taken into account when considering the impact of malaria as a disease (Sachs and Malaney, 2002). The influence of malaria on economic development is such that a comparison of average gross domestic product (GDP) between endemic and non-endemic countries shows more than a five-fold difference (US$1,526 and US$8,268 respectively) (Gallup and Sachs, 2001). More importantly, this trend also applies to the rate of economic growth, where malaria endemic countries showing, on average, 0.4% economic growth rate per capita per year between 1965 – 1990, compared to 2.3% for their non-endemic counterparts. A 10% reduction in malaria index was also associated with a 0.3% rise in annual economic growth (Gallup and Sachs, 2001).

With the UN declaring 17 "sustainable development goals" (SDGs) to succeed the MDGs which ended in 2015, global efforts to control and eradicate malaria will play a major role in how far we are able to achieve the SDGs by the target year of 2030, including the goal to end poverty, ensure healthy lives and well-being for all and promote sustainable economic growth (United Nations, 2017).

The world health organisation (WHO) estimated the number of malaria cases in 2016 to be 216 million. Of the resulting 445,000 deaths, 70% are children under the age of 5 (WHO, 2017b). Moreover, previously published reports suggest that malaria may indirectly contribute to an increasing number of deaths through its interaction with other diseases such as HIV and invasive bacterial diseases (van Eijk *et al.*, 2007; Scott *et al.*, 2011; Church and Maitland, 2014; Cowman *et al.*, 2016).

There is a marked decrease in the number of malaria cases and mortality in 2016 compared to 2010, where 237 million cases and 591,000 deaths were reported. This is reflected in the 18% reduction in incidence rate (the number of cases per 1000 population at risk) between 2010 – 2016 (WHO, 2017b). The number of malaria endemic countries have also decreased from 106 countries in 2000 to 95 countries in 2015 (Fig 1-1) (Phillips *et al.*, 2017). Despite these encouraging news, the road to malaria eradication is still a long one, further complicated by emergence of insecticide and antimalarial drug resistance as well as climate change (Klein, 2013; WHO, 2017b, a)

Malaria is a disease centred in the tropical and subtropical zone, with 90% of cases and 91% of deaths reported in 2016 occurring in Africa (WHO, 2017b). This geographical distribution is partially governed by the effect of temperature on the development of *Plasmodium* parasites themselves as well as the availably of the female *Anopheles* vector (Gething *et al.*, 2011; Phillips *et al.*, 2017; Shapiro *et al.*, 2017). Of the many members in the *Plasmodium* species, five causes malaria in human: *Plasmodium falciparum, Plasmodium vivax, Plasmodium ovale* and *Plasmodium malariae* can also be transmitted by human while *Plasmodium knowlesi* is a zoonotic disease from long-tailed macaques (*Macaca fascicularis*) (Singh and Daneshvar, 2013).

Plasmodium falciparum, the deadliest of the five species, is most prevalent in Africa and South East Asia, whereas *Plasmodium vivax* has a wider geographical reach, including the colder temperate regions such as China and Korea (Fig 1-1) (Martens *et al.*, 1999; Howes *et al.*, 2016; Phillips *et al.*, 2017; WHO, 2017b). The ability of *Plasmodium vivax* to survive in colder climates has been partially attributed to the presence of hypnozoites, a dormant hepatic stage which could escape treatment with standard antimalarial drugs and causes a relapse months or years after the initial infection (Campo *et al.*, 2015). *Plasmodium falciparum* seems to be more sensitive to changes in temperature - a predicted rise of 2-3°C in global temperature could result in an additional 5% of the global population being at risk of malarial infection (Phillips *et al.*,

2017; WHO, 2017a). Not only that, the effects of climate change on other factors including length of seasons, amount of rainfall, vector availability, urbanisation, migration and increase in infrastructures such as dams and reservoirs would all contribute to changes in transmission intensities and the success of global malaria control strategies (Gething *et al.*, 2011; Caminade *et al.*, 2014).

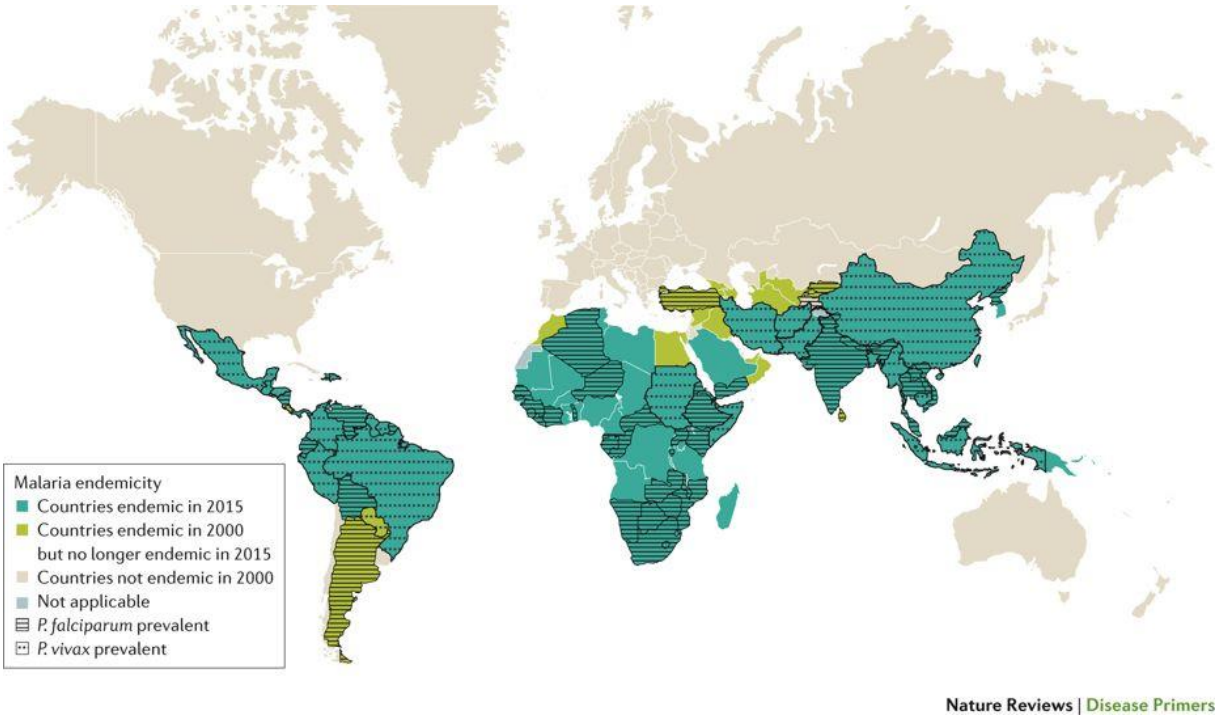

Figure 1-1 Global distribution of malaria in the year 2000 and 2015.

The number of malaria endemic countries decreased from 106 in 2000 to 95 in 2015. *Plasmodium falciparum* cases are predominantly found in tropical areas such as Africa and South East Asia, whereas *Plasmodium vivax* has a slightly larger geological distribution, including countries with colder temperate climate such as china and korea. 'Not applicable' denotes countries which had not been separately surveyed. Figure reproduced from Phillips *et al.*, (2017), with data from WHO, (2015b).

1.2 Life cycle of *Plasmodium falciparum*

Plasmodium falciparum goes through a complex series of sexual and asexual developmental stages in both the human host and the female *Anopheles* mosquito vector (Fig 1-2). The transmission begins with the bite of an infected mosquito, when approximately 100 sporozoites are deposited in the dermis of the human host. The sporozoites exhibit random gliding motility

until they encounter a blood vessel or a lymph node, while others remain in the skin (Amino *et al.*, 2006; Jin *et al.*, 2007; Ejigiri and Sinnis, 2009). Exiting the dermis through a process termed "cell traversal", the sporozoites actively trespass through the endothelium of the blood vessel to be taken by the blood circulation, sweeping towards their next destination – the liver (Mota and Rodriguez, 2004; Amino *et al.*, 2008).

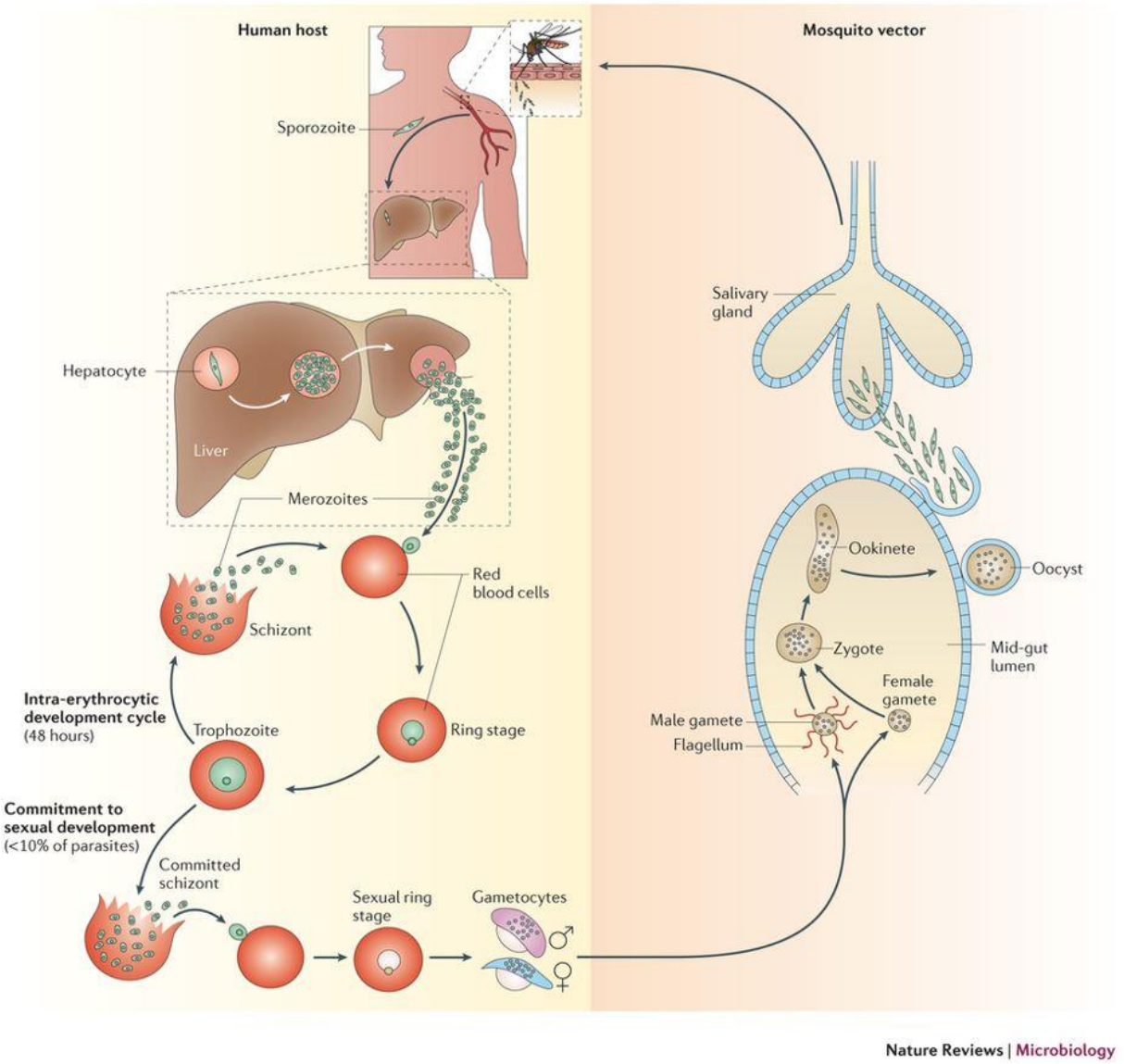

Figure 1-2 Life cycle of *Plasmodium falciparum*.

Reproduced from Josling and Llinás, (2015).

The slow rate of blood flow in the liver sinusoid allows the sporozoites to bind to the endothelium and interact with liver-specific, highly sulfated heparan sulfate proteoglycans

(HPSGs) found protruding through the fenestration into the sinusoid (Vaughan *et al.*, 2008; Graewe *et al.*, 2012). These interactions also trigger calcium signaling pathways, one of the factors believed to be involved in switching the sporozoites from "migratory" to "invasive" mode (Coppi *et al.*, 2007) (Cowman *et al.*, 2016). Individual sporozoites gain access to the liver parenchyma by transmigrating through Kupffer cells, resident hepatic macrophages, then continue to traverse through several hepatocytes before finally establishing a parasitophorous vacuole (PV) upon invasion of the final cell (Vaughan *et al.*, 2008). The reason why the sporozoite traverses through several hepatocytes before finally infecting one remains under investigation, but it has been suggested that the traversal could both prime the sporozoite for invasion as well as render the hepatocytes more susceptible (Carrolo *et al.*, 2003; Mota and Rodriguez, 2004). Another hypothesis is that it simply takes time to fully switched from migratory to invasive mode, and the cell traversal would continue to take place until the switching is complete (Graewe *et al.*, 2012).

After the sporozoite establishes itself inside a parasitophorous vacuole membrane (PVM), it undergoes changes from the elongated, motile sporozoite to a small, rounded trophozoite, called liver-stage (LS) or exo-erythrocytic form (EEF), before going through rounds of intense schizogony, producing up to 30,000 merozoites (Graewe *et al.*, 2012). Membrane-bound vesicles termed merosomes containing these merozoites are found to bud from the hepatocytes into the sinusoid and directly release the merozoites into the circulation in order to avoid detection by Kupffer cells and other phagocytes (Sturm *et al.*, 2006).

Once a merozoite encounters an uninfected red blood cell, invasion is completed within 2 minutes (Cowman *et al.*, 2016). The steps include pre-invasion, active invasion and echinocytosis. Pre-invasion refers to the initial interaction of the merozoite with the erythrocyte which results in the deformation of the erythrocyte surface (Cowman *et al.*, 2016). Active invasion then begins with the reorientation of the merozoite so that its apex faces the erythrocyte membrane. The binding of *Plasmodium falciparum* reticulocyte-binding protein homolog 5 (PfRh5) to host receptor basignin initiates a series of downstream events, including the influx of calcium into the erythrocytes as well as the release of the microneme proteins such as the Rhoptry Neck Protein (RON) complex into the erythrocyte membrane (Weiss *et al.*, 2015). The merozoite then invades the erythrocyte by establishing a Moving Junction through the binding of the surface protein Apical Membrane Antigen 1 (AMA1) to the RON complex (Delgadillo *et al.*, 2016) and using the forces generated by the parasite actin-myosin motor to propel itself forward (Riglar *et al.*, 2011). The parasitophorous vacuole membrane is believed to be formed

from the rhoptries content and membrane fusion at the posterior of the merozoite as it completes the active invasion seals the parasite inside the parasitophorous vacuole (Cowman *et al.*, 2016). The brief formation of echinocytes after the active invasion phrase is believed to be due to the calcium influx instigated when PhRh5 binds to basignin at the beginning of the invasion process (Weiss *et al.*, 2015).

Once inside the host erythrocyte, the parasite undergoes an asexual replication cycle lasting approximately 48 h. This is the stage associated with most of the malaria pathophysiology such as fever, anaemia and further complications (Miller *et al.*, 2002). During the intra-erythrocytic cycle, the parasite goes through three distinct stages: rings, trophozoite and schizont (Fig 1-2). The extensive remodelling of the host erythrocyte carried out by the parasite during this developmental stage will be covered in a later section of this thesis. At the end of the cycle, approximately 16 – 32 daughter merozoites are released – the parasite egress causing the destruction of the infected erythrocyte (Cowman *et al.*, 2016). These daughter merozoites then continue the asexual replication cycle by infecting new red blood cells.

During the intra-erythrocytic cycle, some parasites become committed to sexual development (Fig 1-2). Although the molecular mechanisms and factors behind this 'switching' remain unclear, increase in drug pressure as well as high parasitemia have been observed to increase gametocyte production (Price *et al.*, 1996; Talman *et al.*, 2004; Pietro, 2007). Five different stages of gametocyte maturation have been described for *P. falciparum* (Talman *et al.*, 2004) and the immature gametocytes are found to sequester in the bone marrow during their development (Joice *et al.*, 2014). Once the mature male and female gametocytes, termed micro- and macrogametocytes respectively, emerge into the blood stream, they are picked up by the *Anopheles* mosquito vector during a blood meal.

The sexual development continues after the micro- and macrogametocytes are ingested by the mosquito. The abrupt decrease in temperature of approximately 5° C, the presence of xanthurenic acid (XA), a mosquito- derived molecule, as well as the increase in extracellular pH from 7.2 to about 8 are all reported triggers for the initiation of gametogenesis, which is when the microgametocytes exflagellate to produce motile microgametes and the macrogametocytes emerge from the erythrocytes and mature into rounded macrogametes (Billker *et al.*, 1997; Billker *et al.*, 1998; Pietro, 2007; Bennink *et al.*, 2016). The fertilisation of micro- and macrogametes is followed by nuclear fusion and meiosis, resulting in a tetraploid zygote (Janse *et al.*, 1986; Bennink *et al.*, 2016).

The zygote matures into an elongated, motile ookinete containing micronemes, secretory organelles containing proteins involved in invasion, motility and tissue traversal. The ookinete exits the midgut lumen and traverses through several epithelial cells before exiting the epithelium through the basal side and transforms into an oocyst. The traversal of epithelial cells is believed to switch the ookinete from "traversal" to "sessile" mode (Aly *et al.*, 2009). Laminin and other components of the mosquito's basal lamina are also believed to be involved in the induction of the ookinete's "sessile" mode and its development into an oocyst (Adini and Warburg, 1999).

After several rounds of mitotic divisions, the oocyst grows to 50–60 μm in diameter and contains thousands of sporozoites, waiting to be released. The precise sequences and molecular mechanisms of sporozoite egress from the oocyst is still under investigation but a putative cystein protease named ECP1 (egress cysteine protease 1) is believed to be involved (Aly and Matuschewski, 2005; Aly *et al.*, 2009).

Once released into the hemocoel, the sporozoites are carried around the mosquito by the circulation (Rodriguez and Hernández-Hernández, 2004; Vlachou *et al.*, 2006). Specific host receptors allow recognition and attachment to the basal lamina of the salivary glands, followed by transmigration through the acinar cells and exit into the salivary gland cavity (Pimenta *et al.*, 1994; Aly *et al.*, 2009). Gliding motility is reported to be involved in the migration of the sporozoite from the cavity into the salivary ducts, which allows transmission of the sporozoite to the human host upon injection of mosquito saliva while those remaining in the gland cavity are either lost or would have to be transmitted during future bites (Frischknecht *et al.*, 2004; Rodriguez and Hernández-Hernández, 2004; Vlachou *et al.*, 2006). The inoculated sporozoites then glide around the dermis until they encounter a blood vessel and thus the cycle begins again.

1.3 Malaria Pathogenesis

1.3.1 Clinical manifestations and pathogenesis

Clinical manifestations and the outcome of malaria infection can vary depending on a combination of parasite and host factors, including parasite species, age, immune status and

genetics of the host, as well as interaction with other infections and access to care (Miller *et al.*, 2002; Bartoloni and Zammarchi, 2012a; Acharya *et al.*, 2017).

The initial presentation of malaria is rather unspecific, including flu-like symptoms such as fever, headaches, nausea, vomiting and diarrhoea (Bartoloni and Zammarchi, 2012a). The incubation period, the time between the infection and the onset of symptoms, can vary from approximately 9 – 30 days, depending on the *Plasmodium* species as well as host immune status and use of prophylactic anti-malarial drugs (Miller *et al.*, 2002; Bartoloni and Zammarchi, 2012a).

Although fever is generally present since the initial onset of symptoms, they do not exhibit the trademark periodicity until approximately 5-7 days after infection, when the asexual replication cycle becomes synchronous. The cyclic nature of these febrile paroxysms also gave rise to the name "benign tertian", "quartian" and "malignant subtertian" fevers for *P.vivax, P.malariae* and *P. falciparum* malaria, respectively (Carter and Mendis, 2002).

There are three stages to the classical malaria paroxysm: a cold stage, a hot stage and a sweating stage (Bartoloni and Zammarchi, 2012b). As the name implies, the cold stage is when the patient feels extremely cold, starts shivering and their skin feels cold and dry. During these 10-30 minutes, their body temperature gradually rises, reaching a peak of 39 – 41°C and the shivering stops as they enter the hot stage of the attack. Their skin now feels hot and dry, their face is flushed, and vomiting is common at this stage. Other symptoms including diarrhoea, severe headache and dizziness are also possible, including convulsions in younger patients. Within 2-6 hours after the onset, the patient enters the last stage of the attack, the sweating stage. After sudden and profuse sweating, lasting between 2-3 hours, the temperature falls and the patient feels well again, although sleepy and tired. The entire cycle lasts between 6 – 10 h and most often manifests in the late afternoon to evening (Bartoloni and Zammarchi, 2012b).

These "mild" or "uncomplicated" malaria constitutes the majority of cases, with pathogenesis attributed to the release of parasitic factors and erythrocyte materials upon schizont rupture, triggering cytokine cascades responsible for many of the symptoms (Trampuz *et al.*, 2003a; Fairhurst *et al.*, 2012). However, sudden development of severe and life-threatening complications can occur in 1-3% of the cases. Despite timely treatment, the mortality rate for severe malaria is still very high: 20% in adult and 15% in children (Mackintosh *et al.*, 2004; Bartoloni and Zammarchi, 2012b; WHO, 2017b). Without treatment, it is nearly always fatal.

"Severe malaria" is a complex mixture of overlapping syndromes involving multiple organ systems, including but not limited to: the central nervous system (cerebral malaria), haematopoietic system (severe anaemia) as well as systemic metabolic problems (acidosis and hypoglycaemia) (Trampuz *et al.*, 2003b; Bartoloni and Zammarchi, 2012b). Occurring mostly in non-immune patients and children under the age of five infected by *P. falciparum*, these complications can rapidly develop and lead to death within hours or days (Trampuz *et al.*, 2003b).

Enlarged liver and spleen are often observed in young children and non-immune adult patients, whereas acute renal failure is more common in adults (Bartoloni and Zammarchi, 2012b). Pregnant women are particularly prone to develop acute respiratory failure and primigravidae from endemic areas is classified as a high-risk population for pregnancy-associated malaria (PAM).

Cytoadherance and sequestration of infected erythrocytes in the microvascular beds of vital organs such as the brain or the lungs is believed to be one of the key pathogenesis of severe malaria, as observed in *post mortem* brain sections (Mackintosh *et al.*, 2004). Not only does the cytoadhesive parasitized erythrocytes produce physical obstruction to the blood flow, resulting in subsequence tissue hypoxia, the host immune and inflammatory response to the release of parasitic and cell components such as glycosylphosphatidylinositol (GPI), uric acid and haem upon schizont rupture further exacerbates the situation (Mackintosh *et al.*, 2004; Fairhurst *et al.*, 2012). Free haem-induced oxidative damage to the endothelium as well as the decrease in bioavailability of nitric oxide (NO) both contribute to the blood brain barrier (BBB) dysfunction (Figure 1.3) (Yeo *et al.*, 2007; Miller *et al.*, 2013). This could lead to coma, seizures and possible neurological effects (table 1) (Carter *et al.*, 2006; Idro *et al.*, 2006).

Severe anaemia is another complication often associated with severe malaria. Although the increased haemolysis of infected erythrocytes upon merozoite egress as well as immune clearance through phagocytosis and destruction of "by-stander" uninfected erythrocytes due to damages caused by reactive oxygen species (ROS) released by infected RBCs all contribute to the reduction in circulating erythrocytes and thus anaemia, another important contributing factor is the reduced erythropoiesis in infected individuals (Fig 1-3) (Autino *et al.*, 2012; Miller *et al.*, 2013). Studies have shown that accumulation of hemozoin-laden monocytes in the bone marrow can inhibit erythropoiesis through the production of bioactive aldehydes such as 4-hydroxynonenal (HNE), which has been shown to inhibit growth and differentiation of

erythroid cells (Skorokhod *et al.*, 2010). Dysregulation of cytokines as a response to malaria infection can also have a negative effect on erythropoiesis (Table 1)(Haldar and Mohandas, 2009; Perkins *et al.*, 2011). Other factors such as malnutrition and co-infection with HIV, bacteremia or hookworms can also contribute to the pathophysiology (Calis *et al.*, 2008; Autino *et al.*, 2012).

Several factors are likely to contribute to metabolic acidosis found in children with severe malaria, which precipitate clinically as respiratory distress (English *et al.*, 1996). Poor tissue perfusion due to cytoadhesion and occlusion of the microvasculature by the infected erythrocytes increases the production of lactic acid through anaerobic glycolysis. Decrease in hepatic blood flow and thus liver clearance as well as increased lactic acid production by the parasite due to cytokine stimulation and decrease in gluconeogenesis due to circulating tumor necrosis factor all contribute to elevated level of lactate in the blood (Sasi *et al.*, 2007; Miller *et al.*, 2013). Severe anaemia and hypovolaemia also exacerbate the issue (Table 1, Fig 1-3).

Primigravidae living in endemic areas are most at risk of pregnancy-associated malaria (PAM), due to the transient depression of cell-mediated immunity as well as the lack of antibodies against CSA-binding *P. falciparum* multigravidae have developed during their first pregnancy (Meeusen *et al.*, 2001; Uneke, 2007; Autino *et al.*, 2012). PAM is also associated with high morbidity for both mother and child, with the mother at risk of severe anaemia, miscarriage and pre-term delivery and the fetus at risk of low birth weight, intrauterine growth retardation and death (Table 1) (Agan *et al.*, 2010; Falade *et al.*, 2010; Bardaji *et al.*, 2011).

The preferential binding of the VAR2CSA variant of PfEMP1 (*Plasmodium falciparum* erythrocyte membrane protein 1) to low sulfated form of chondroitin-4-sulfate (C4S) found in the placenta causes an accumulation of parasitized erythrocytes in the intervillous space (Fried and Duffy, 1996; Achur *et al.*, 2000) (Salanti *et al.*, 2004; Viebig *et al.*, 2005). The subsequent activation and infiltration of phagocytes as well as the release of pro-inflammatory cytokines and depositions of fibrin and hemozoins contribute to an increased thickness of the trophoblast basement membrane and thus impair the materno-fetal exchange of oxygen and nutrients, leading to poor pregnancy outcomes (Table 1) (Rogerson *et al.*, 2007; Uneke, 2007; Autino *et al.*, 2012).

Table 1 Pathophysiology and pathogenesis of severe and pregnancy-associated malaria.

GPI - glycosylphosphatidylinositol; RBC - red blood cell. Adapted from Mackintosh *et al.*, (2004).

Syndromes	Clinical features	Disease mechanisms
Severe anaemia	Shock; impaired consciousness; respiratory distress	Reduced RBC production (reduced erythropoietin activity, proinflammatory cytokines); increased RBC destruction (parasite-mediated, erythrophagocytosis, antibody and complement-mediated lysis)
Cerebral complications (cerebral malaria)	Impaired consciousness; convulsions; long-term neurological deficits	Microvascular obstruction (parasites, platelets, rosettes, microparticles); proinflammatory cytokines; parasite toxins (e.g. GPI)
Metabolic acidosis	Respiratory distress, hypoxia, tachypnea; acidaemia; reduced central venous pressure	Reduced tissue perfusion (hypovolaemia, reduced cardiac output, anaemia); parasite products; proinflammatory cytokines; pulmonary pathology (airway obstruction, reduced diffusion)
Other	Hypoglycaemia; disseminated intravascular coagulation	Parasite products and/or toxins; proinflammatory cytokines; cytoadherence
Pregnancy-associated Malaria (PAM)	Placental infection; low birth weight and fetal loss; maternal anaemia	Premature delivery and fetal growth restriction; placental mononuclear cell infiltration and inflammation; proinflammatory cytokines

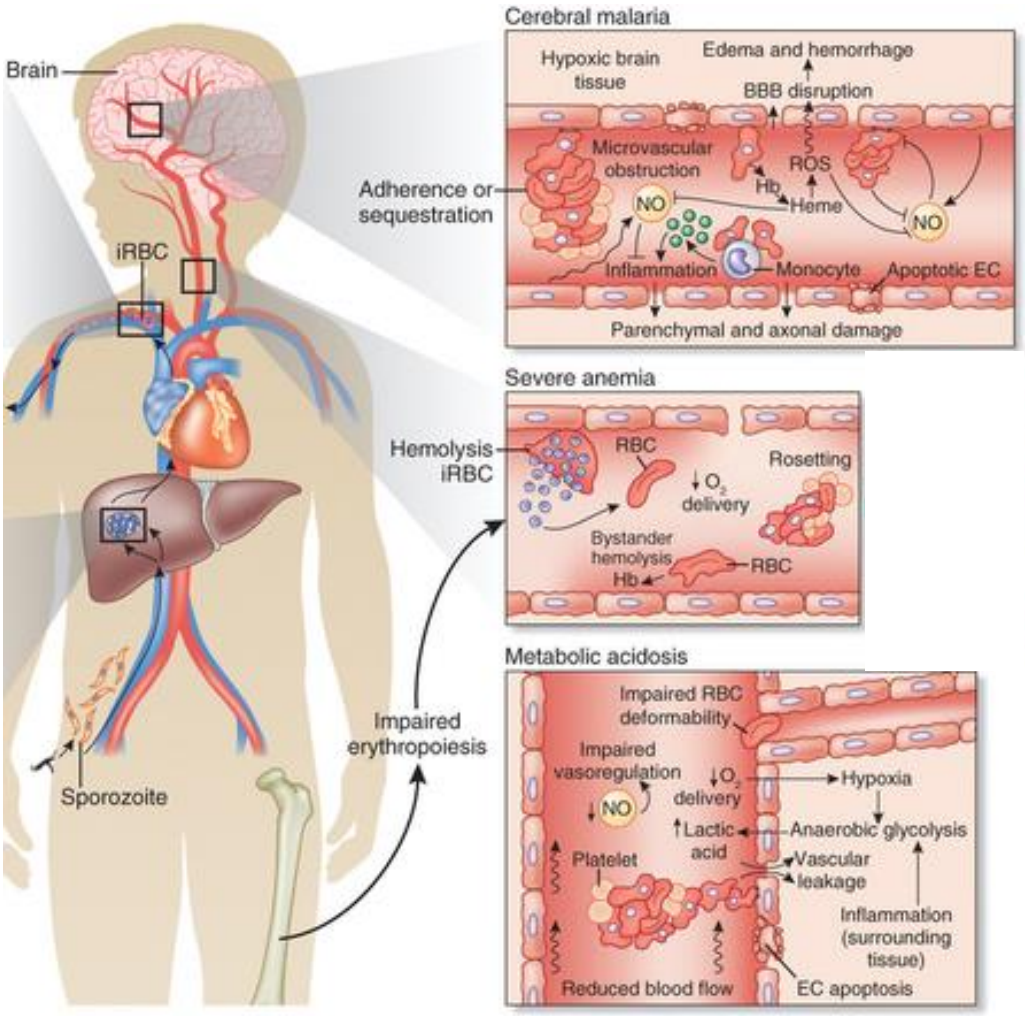

Figure 1-3 Severe malaria pathogenesis

Possible mechanisms of pathogenesis in severe malaria. Cerebral malaria: Cytoadhesion of infected RBCs to endothelial cells as well as resetting of uninfected RBCs causes obstruction to the blood flow, leading to tissue hypoxia and lactic acidosis. Release of free haemoglobin (Hb) from ruptured erythrocytes contributes to endothelial injury and dysfunction as it catalyses oxidative damage to the ECs, through ROS production, and consumes nitric oxide (NO). Without the anti-inflammatory and endothelial regulation action of nitric oxide, the inflammatory reaction to the sequestered iRBC is exacerbated, which causes damage to the blood brain barrier (BBB). Severe anaemia: Haemolysis of infected and bystander (uninfected) RBCs causes anemia that may be exacerbated by impaired erythropoiesis caused by parasitic toxins. Rosetting of both infected and uninfected erythrocytes meant that fewer RBC are available to carry oxygen around the circulation. Oxidative damage to uninfected RBC, caused by parasitic production of ROS, accelerates the senescence and removal of erythrocytes. Metabolic acidosis: Sequestration and rosetting reduce the blood flow. Lowered oxygen delivery causes hypoxia which increases lactic acid production through anaerobic glycolysis. Coupled with the increased metabolism of glucose into lactic acid by the parasites, this causes deep breathing states that lead to respiratory distress and failure. Adapted from Miller *et al.*, (2013).

1.3.2 Recommended treatments and anti-malarial resistance

In order to increase effectiveness and reduce the possibility of drug resistant parasite development, artemisinin-based combination therapies (ACTs) are the current recommended first line treatment for uncomplicated *P. falciparum* malaria. Artemisinin and its derivatives are exceptionally fast-acting drug effective against all stages of the intra-erythrocytic parasite and is shown to reduce severe malaria mortality by approximately 30% compared to quinine (White *et al.*, 2014). However, their *in vivo* half-lives are typically only around 1 h in humans (Dondorp *et al.*, 2009). ACTs combine artemisinins with longer acting partner drugs with a different mode of action to prevent recrudescence as well as delay the emergence of drug resistance (Tilley *et al.*, 2016).

A 3-day regimen of one of these 5 commercially available ACTs are recommended for use for children and adult, except pregnant women in the first trimester: Ariplus® (artesunate-sulfadoxine-pyrimethamine), Artekin® (dihydroartemisinin-piperaquine), Coarsucam® (artesunate-amodiaquine), Coartem® (artemether-lumefantrine) or Mefliam Plus® (artesunate-mefloquine) (WHO, 2015a).

A 7-day regimen of quinine – clindamycin combination therapy is recommended to pregnant women in their first trimester to reduce adverse risks on the developing foetus (WHO, 2015a).

For severe malaria, an intravenous or intramuscular application of artesunate for at least 24 h is recommended. Once the patient can tolerate oral medication, a 3-day regimen of ATC is recommended (WHO, 2015a).

Despite the use of ACTs, reports of artemisinin resistance have emerged from the Greater Mekong Subregion in South East Asia (Imwong *et al.*, 2017). Resistance has now been documented against all classes of anti-malarial drugs currently in use, which proves a great challenge for malaria control and treatment (Wongsrichanalai *et al.*, 2002; WHO, 2015a). This highlights the need for continued basic research in malaria biology, in the hope of finding new avenues for drug development as well as ways to control and eventually eliminate malaria.

1.4 Parasitic remodeling of host erythrocytes

1.4.1 Erythrocytic membrane cytoskeleton

The mature human erythrocyte is a terminally differentiated cell, specialized in oxygen and carbon dioxide transport. It contains no nucleus or other cell organelles and instead, filling 95% of its cytosol with haemoglobin (Haldar and Mohandas, 2007; Kanias and Acker, 2010). It measures 7-8 μm in diameter and is between 1.5 – 2.5 μm thick, with a high surface area to volume ratio and a biconcave discoid shape, both enabling optimal gas exchange (Keohane *et al.*, 2015). However, to withstand large shear stresses in the arteries as well as survive repeated passage though narrow capillaries 2-3 μm in diameter, the erythrocyte requires membrane that is both mechanically stable and deformable (Haldar and Mohandas, 2007; Keohane *et al.*, 2015; Gokhin and Fowler, 2016).

The inner membrane surface of an erythrocyte is lined with a 2D, quasi-hexagonal meshwork containing spectrin, actin and associated proteins such as tropomodulin1, αβ-adducin and tropomyosins (Gokhin and Fowler, 2016). Erythrocyte spectrin is composed of two parallel chains of α- and β-spectrin oriented in opposite directions, with a self-association site at the "head" end (Fig 1-4a). The nucleation site at the "tail" end facilitates electrostatic binding of individual α- and β-spectrin chains, allowing the rest of the molecule to "zip" together into coils (Fig 1-5b) (Lux, 2016). α- spectrin consists of 21 spectrin-type repeats, each formed by three α-helices labelled A-C (Fig 1-4b), plus an α0 partial repeat at the N-terminus, containing only the C-helix. β-spectrin consists of 16 repeats plus a β17 at the C-terminus, containing only A and B helices. The partial repeats α0 and β17 binds together to create a spectrin dimer. Some of these repeats, indicated by stars in figure 1-5a, are reported to be unstable under physiological conditions (An *et al.*, 2006). This may contribute to the molecule's flexibility as the repeats may partially unfold as the erythrocyte deform (Johnson *et al.*, 2007).

A bigger contributor to the ability of erythrocyte membrane to withstand large amounts of distortion may be the weak association between the oligomers. Most of spectrin in the erythrocytes are found as $\alpha_2\beta_2$ tetramers but the weak self-association between oligomers allow tetramers to dissociate and reform when the membrane is distorted by shear forces, thus enabling the erythrocyte to deform as it travels through microcapillaries (An *et al.*, 2002; Salomao *et al.*, 2006).

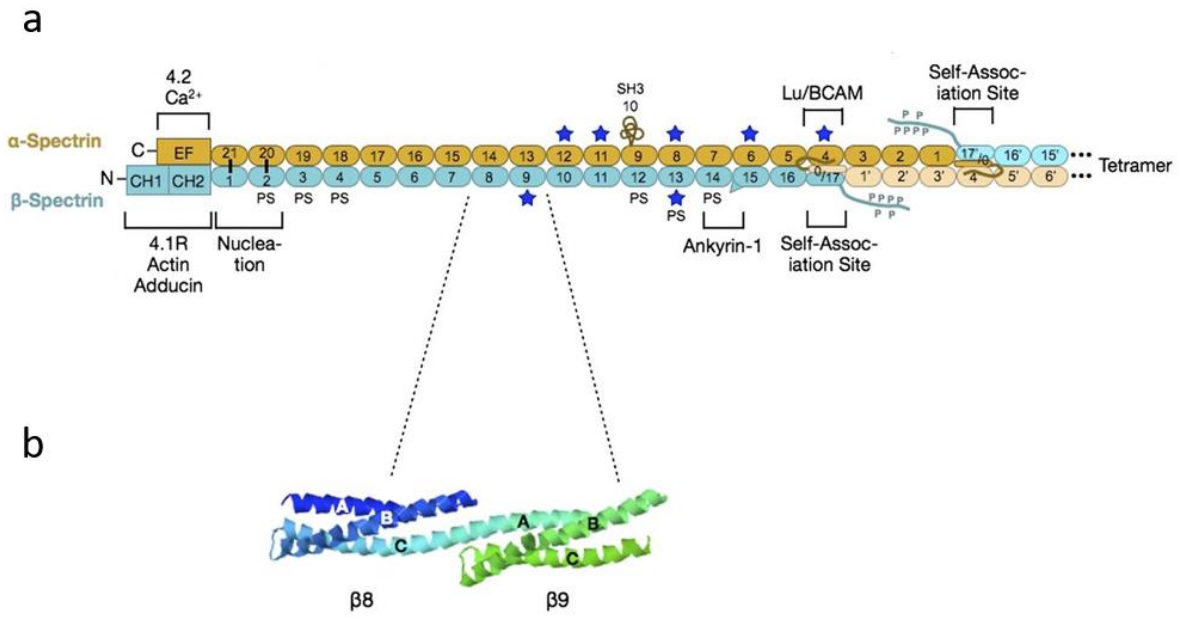

Figure 1-4 Spectrin structure and binding sites.

(a) Schematic diagram showing the orientation of the α- and β- spectrin in a dimer, as well as mapped binding sites for known associated proteins. 4.2 – protein 4.2; Ca^{2+} - calcium ion; CH – calponin homology; 4.1R – protein 4.1R; Lu-BCAM – Lutheran/basal cell adhesion molecule. PS denotes repeats which are able to bind phosphatidyl serine; blue star denotes repeats which are unstable at physiological temperature. (b) Structure of β8 and β9 spectrin repeats, displaying the triple helical structures of helix A, B and C in a Z-configuration (PDB 1S35). The junction between the repeats is formed by helix C from β8 and helix A from β9. Adapted from Lux, (2016)

In native erythrocyte membrane preparations, the spectrin tetramers are said to be in a 'folded' configuration, with an end-to-end distance of between 35 – 100 nm (Fig 1-5a) (Swihart *et al.*, 2001; Nans *et al.*, 2011). However, the tetramers can be extended up to 190 nm when spread *in vitro*, allowing for flexibility and extension during erythrocyte membrane deformation (Fig 1-5a) (Shotton *et al.*, 1979).

The spectrin tetramers are connected to protofilaments of β-actin to form a quasi-hexagonal network of 2D lattices (Fig 1-5a). The length of the F-actin nodes is uniformly kept at approximately 37 nm, suggesting tight regulations by actin binding proteins (Fowler, 2013). These include capping at the pointed end by two tropomodulin 1 (Tmod1) molecules, capping at the barbed end by an αβ-adducin heterodimer and binding along its length by two tropomyosin isoforms, TM5b and TM5NM1, for stabilisation (Fig 1-5a) (Gokhin and Fowler, 2016). These lateral lattices of spectrin-actin and associated proteins are vertically connected to the erythrocyte plasma membrane through interactions with ankyrin-B, which links spectrin tetramers to Band 3, an integral membrane protein (Fig 1-5) (Bennett and Baines, 2001; Gokhin

and Fowler, 2016). Other proteins which can link the actin-spectrin lattice to the lipid bilayer include αβ-adducin, which binds Band 3 as well as actin barbed ends, and protein 4.1R enhances spectrin-actin binding but can also bind to Band 3 and glycophorin-C (Fig 1-5b) (Anderson and Lovrien, 1984; Pasternack *et al.*, 1985; Anong *et al.*, 2009; Gokhin and Fowler, 2016).

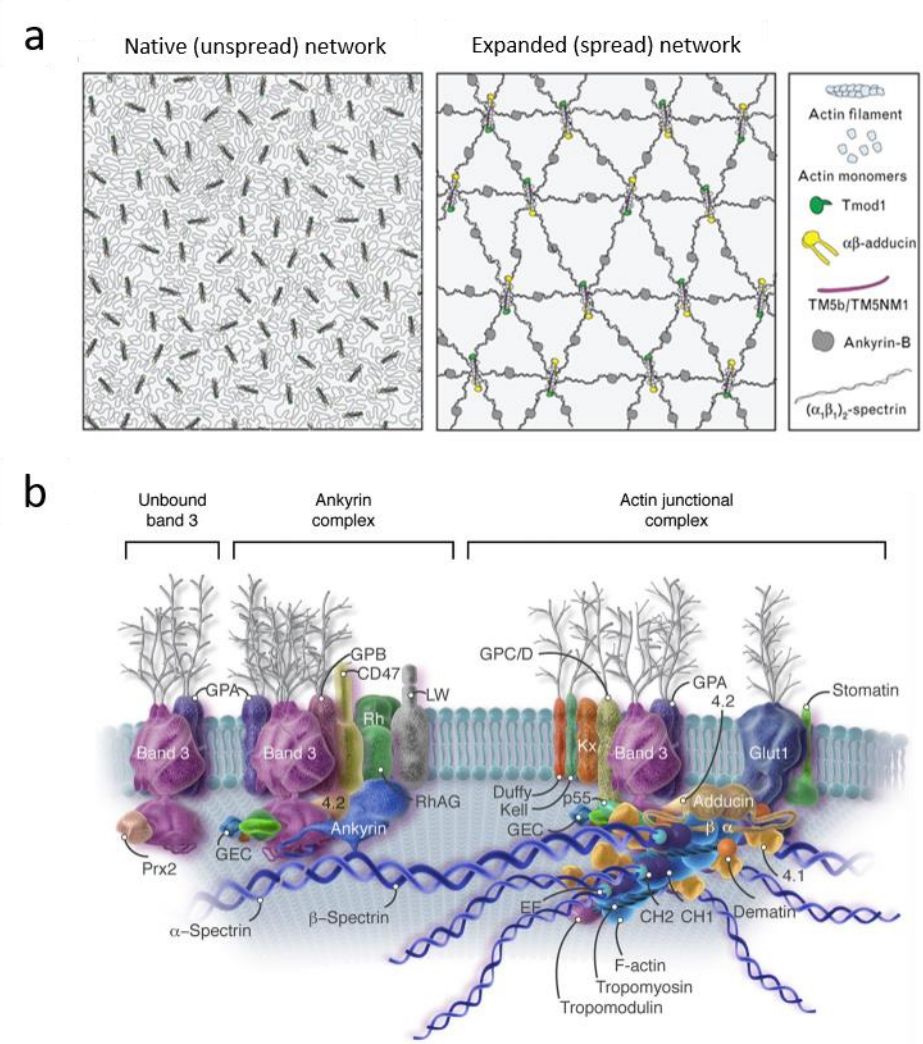

Figure 1-5 Current model of erythrocytic membrane cytoskeleton and associated proteins.

(a) Schematic diagram illustrating cytoskeletal components in native and spread erythrocyte membranes. Spectrin tetramers are found in 'folded' configuration in native membranes, interconnecting with actin 'nodes' and actin binding proteins. The spread network reveals a quasi-hexagonal lattice. Tmod1 – tropomodulin 1; TM5b/TM5NM1 – tropomyosin isoforms. Adapted from Gokhin and Fowler, (2016) (b) A model of a cross-section through the lipid bilayer of the erythrocytic membrane. GPA – glycophorin A; Prx2 – peroxiredoxin 2; GEC – Glycolytic enzyme complex; 4.2 – protein 4.2; GPB – glycophorin B; RhAG – Rh-associated glycoprotein; LW – Landsteiner-Wiener; GPC/D – glycophorin C/D; 4.1 – protein 4.1R; Glut 1 – glucose transporter 1. Reproduced from Lux, (2016).

1.4.2 Parasitic remodelling of host erythrocyte

As the uninfected erythrocyte contains no intracellular organelles or protein export machineries, the *Plasmodium* parasite needs to substantially remodel the host cell in order to acquire the necessary nutrients for growth as well as export parasitic factors necessary for the development and completion of the intra-erythrocytic replication cycle, including immune evasion (Fig 1-6a) (Haldar and Mohandas, 2007).

In order to remodel the host cell to its liking, the parasite first need to establish its own protein export pathway. Now enveloped in a parasitophorous vacuole (PV), the parasite needs to export the protein across the parasitophorous vacuolar membrane (PVM) before it can target the protein to specific locations within the erythrocyte cytoplasm or to the erythrocyte plasma membrane (Przyborski *et al.*, 2016). Protein transport across the PVM is shown to be mediated by a complex of proteins called PTEX (*Plasmodium* translocon of exported proteins) containing at least five members, although the individual components of the complex and their specific roles are still under investigation (Elsworth *et al.*, 2014; Przyborski *et al.*, 2016).

Once the exported protein has successfully crossed the PVM, there is still the question of protein trafficking within the erythrocyte cytosol. Maurer's clefts (MCs) are parasite-derived Golgi-like membranous structures shown to act as a protein sorting station for many proteins exported to the erythrocyte surface, including the PfEMP1 (*Plasmodium falciparum* erythrocyte membrane protein 1) family of adhesins, best known for its role in cytoadhesion and pathogenesis (Fig 1-6c) (Mundwiler-Pachlatko and Beck, 2013). The Maurer's clefts are shown to bud off from the PV shortly after infection, with many of the MC resident proteins being detectable from 2-6 h post invasion (Spycher *et al.*, 2006; Gruring *et al.*, 2011; McMillan *et al.*, 2013). Recent data from Cyrklaff *et al.*, (2011) also reported vesicular trafficking between the MCs and the knobs, electron-dense protrusion on the erythrocytic surface involved in adhesin presentation (Fig 1-6d). The vesicles were shown to travel along elaborate networks of filamentous actin, which the parasite has mined and re-modelled from the erythrocyte cytoskeleton (Cyrklaff *et al.*, 2011; Cyrklaff *et al.*, 2012).

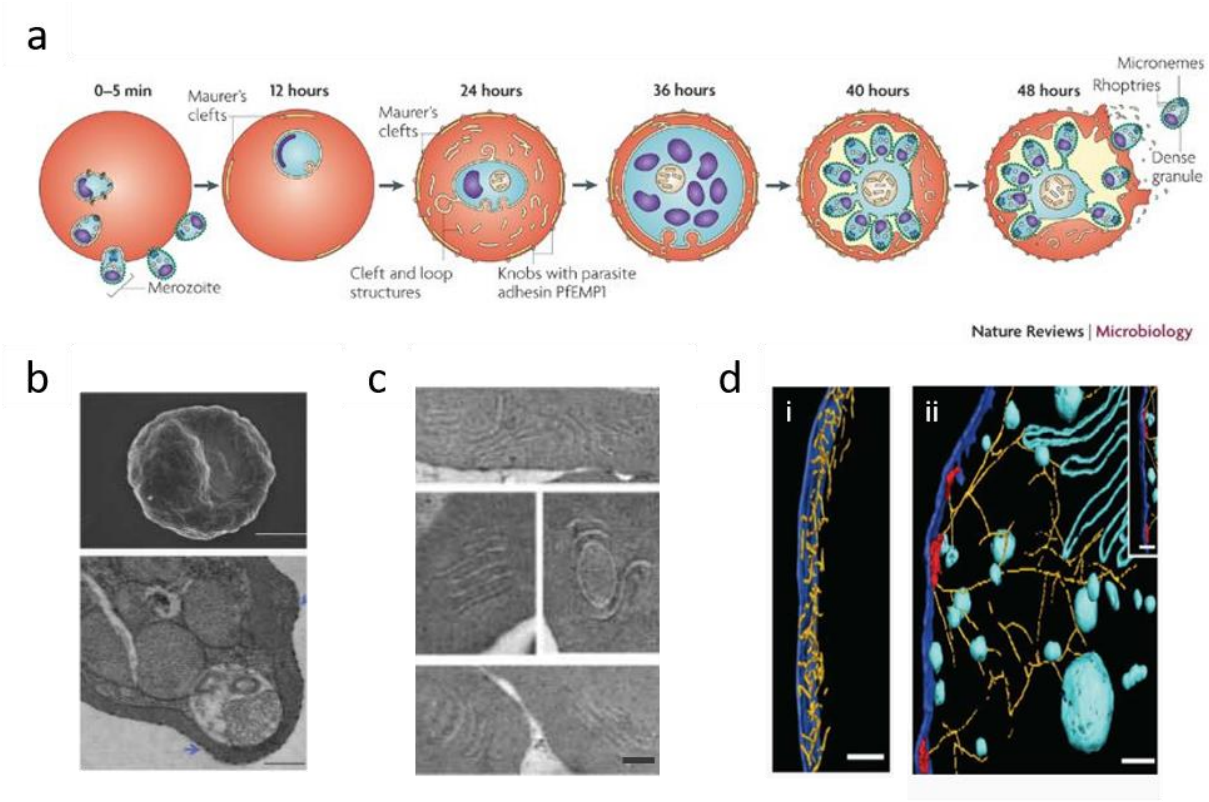

Figure 1-6 *Plasmodium falciparum* remodelling of host erythrocyte during the intra-erythrocytic stage.

(a) Schematic depiction of parasite remodelling of host erythrocyte throughout the 48 h intra-erythrocytic stage. Maurer's clefts are established in the host cytoplasm from approximately 12 h post infection (p.i.) and knobs and surface adhesin presentation are established by 24 h p.i. Adapted from Maier *et al.*, (2009) (b) knob morphologies of infected HbAA erythrocytes as seen by SEM (top) and TEM (bottom). Scale bar 2µM for SEM and 0.5 µm for TEM. Blue arrow in the TEM image indicates an electron-dense knob on the erythrocyte membrane. Adapted from Fairhurst *et al.*, (2012) (c) Adapted from Maurer's cleft morphologies as seen by TEM on high-pressure frozen 100 nm sections. Scale bar 100 nm. Adapted from Cyrklaff *et al.*, (2016) (d) Surface-rendered reconstruction from cryo-electron tomograms of uninfected HbAA erythrocyte (i) and parasitized HbAA erythrocyte (ii). Scale bar 100 nm. Erythrocyte actin cytoskeleton (yellow) in infected erythrocyte have been reorganised from short protofilaments in uninfected erythrocytes (i) into long filamentous network (ii), connecting the Maurer's cleft (light blue) to the knob (red) at the plasma membrane (dark blue). Vesicles are seen to be associated with the actin filaments (light blue). Adapted from Cyrklaff *et al.*, (2011).

1.4.3 Knob, PfEMP1 and Cytoadhesion

As shown in figure 1-6b, knobs are first identified as electron-dense protrusions on the surface of mature parasitized erythrocytes, with heights ranging from 2 – 20 nm and diameter ranging from 50-120 nm (Gruenberg *et al.*, 1983; Quadt *et al.*, 2012; Subramani *et al.*, 2015). The main component of knobs is the aptly named knob-associated histidine rich protein (KAHRP), a 59-72 kDa protein containing a PEXEL (*Plasmodium* export element) motif and an N-terminus

signal sequence (Fig 1-7a) (Triglia *et al.*, 1987; Marti *et al.*, 2004; Watermeyer *et al.*, 2016). KAHRP is shown to interact with components of the host cytoskeleton, including spectrin, actin and ankyrin R (Oh *et al.*, 2000; Pei *et al.*, 2005; Rug *et al.*, 2006; Weng *et al.*, 2014), as well as the parasite adhesin PfEMP1(Ganguly *et al.*, 2015) (Fig1-7a).

KAHRP expression has been shown to be essential for cytoadhesion of parasitized erythrocyte under physiological flow condition, as *kahrp*- parasites were unable to cytoadhere to CD36, despite the presence of PfEMP1 on the erythrocytic surface (Crabb *et al.*, 1997; Rug *et al.*, 2006). This suggests an important role for the correct display and presentation of adhesins in cytoadhesion.

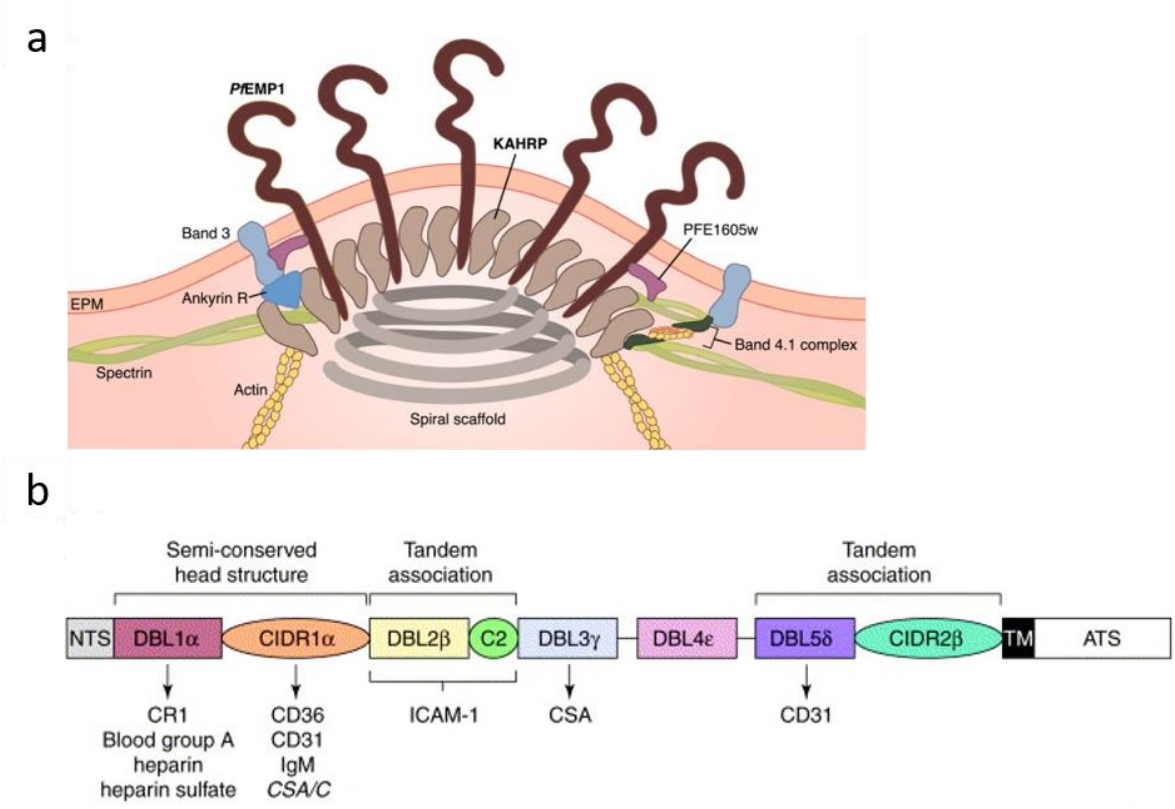

Figure 1-7 Knob architecture and PfEMP1 structure and binding domains.

(a) A model of a cross-section through a "knob", a parasite-derived protrusion on the surface of an infected HbAA erythrocyte. The knobs are shown to be involved in adhesin presentation. EPM – erythrocyte plasma membrane; PfEMP1 – *Plasmodium falciparum* erythrocyte membrane protein 1; KAHRP – knob-associated histidine rich protein. Reproduced from Helms *et al.*, (2016) (b) PfEMP1 is a family of single-pass transmembrane proteins involved in cytoadhesion of infected erythrocytes to various host receptors. A typical structure of PfEMP1 consists of a highly conserved intracellular acidic terminal segment (ATS) and a highly variable extracellular domain, assembled from four basic building blocks in various configurations: N-terminal segment (NTS), Duffy-binding-like domain (DBL), cysteine-rich interdomain region (CIDR) and C2 domains. Known interactions between specific domains and host receptors are shown. TM – transmembrane domain. Adapted from Smith *et al.*, (2001).

The parasite takes up more room in the infected erythrocytes as it develops (Waldecker *et al.*, 2017). The insertion of various proteins and channels into the erythrocytic membrane causes membrane stiffening as well as potential recognition of parasitic proteins by the host immune system (Maier *et al.*, 2009; Watermeyer *et al.*, 2016). Circulating erythrocytes need to be able to pass through the splenic interendothelial slit (IES) in order to avoid clearance - late stage parasitized erythrocytes are simply too stiff to pass this test (Pivkin *et al.*, 2016). In order to avoid detection and elimination in the spleen, the parasite export and display adhesins from the PfEMP1 family, which can interact with host receptors on the endothelial cells and allow the parasitized erythrocyte to sequester in the microvasculature of various organs (Maier *et al.*, 2009; Tilley *et al.*, 2011; Helms *et al.*, 2016). Inadvertently causing obstruction of blood flow, leading to hypoxia and tissue necrosis, as well as endothelial cell activation, cytoadhesion has often been implicated in the pathogenesis of severe malaria (Mackintosh *et al.*, 2004; Miller *et al.*, 2013).

PfEMP1, the parasitic protein responsible for cytoadhesion, is encoded by 60 different members of the *var* gene family. The protein size varies from 200 – 350 kDA but there are some conserved structural features, namely the N-terminal segment (NTA), followed by a semi-conserved head structure containing Duffy Binding Like domains (DBL; α-ε) and cysteine-rich interdomain regions (CIDR; α-γ), a C2 domain, a transmembrane domain (TM) and a conserved intra-cellular acidic terminal segment (ATS) (Fig 1-7b) (Kraemer and Smith, 2006; Pasternak and Dzikowski, 2009). The highly variable extracellular domain allows for interactions with a multitude of host receptors, including CD31, CD36, intercellular adhesion molecule 1 (ICAM 1), P-selectin and chondroitin- 4- sulfate (CSA) (Rowe *et al.*, 2009; Tilley *et al.*, 2011; Helms *et al.*, 2016).

Despite the variation in the extracellular domain and the binding partner, only one variant of PfEMP1 is expressed on each infected erythrocyte at a given time. How the parasite controls the PfEMP1 expression so tightly is still a matter of ongoing investigation, although it has been speculated that epigenetic mechanisms might be involved as the majority of the parasite in each new cycle express the same *var* gene, hinting at possible role of genetic imprinting (Scherf *et al.*, 1998; Craig and Scherf, 2001; Scherf *et al.*, 2008).

Although what causes the parasite to switch the expression from one PfEMP1 variant to another is also still under investigation, the biological advantage of "allelic exclusion" is clear – to

minimise exposure of its antigenic repertoire means more successful immune evasion and thus a higher chance of transmission to a new host (Pasternak and Dzikowski, 2009).

1.5 Haemoglobinopathic erythrocytes and protection against severe malaria

1.5.1 Haemoglobinopathies

Haemoglobin (Hb) is a metalloprotein adapted for oxygen transport, with a heme prosthetic group bound to a pocket in each of the four globin monomers (Hardison, 1996). Adult haemoglobin (HbA – $\alpha_2\beta_2$) is a heterotetramer consisting of two α- and two β-globin chains, which allows the molecule to effectively bind oxygen at high partial pressure in the lungs and then release it in the tissue with lower oxygen partial pressure (Weatherall, 2010).

Haemoglobinopathies are inherited disorders of the globin gene and can be broadly divided into two categories: the thalassemais affect the amount of protein output, while the Hb variants affect the structures of the proteins (Trent, 2006). Table 2 summarises some key features of the most common haemoglobinopathies, including their geographical distributions and genotypes.

In sickle cell haemoglobin (HbS), a single amino acid substitution at position 6 of the β-globin chain causes glutamate to be substituted by valine. This compromises its ability to stay soluble at high concentration, thus resulting in self-aggregation of deoxy HbS molecules under low-oxygen conditions (Weatherall, 2010). The resulting rope-like fibres can distort the cell shape into the distinctive "sickle" or "half-moon" shapes. HbS cells also have decreased elasticity and increased tendency to adhere to endothelial cells, resulting in intermittent vaso-occlusive events (Rees *et al.*, 2010). The shortened lifespan of the cells is also said to contribute to chronic nitric oxide depletion, in addition to anaemia, due to the constant presence of haem released after intravascular haemolysis, resulting in pulmonary hypertension (Gladwin *et al.*, 2004; De Castro *et al.*, 2008).

In parts of sub-Saharan Africa, Middle East and India, the allele frequency of HbS could be as high as 40% (Flint *et al.*, 1998; Bauduer, 2013). This strongly correlates with the geographical distribution of malaria, suggesting a co-evolutionary selective pressure (Williams and Weatherall, 2012).

Comparatively, HbC has emerged much more recently, with its geographical reach only limited to West Africa – the allele frequency is up to 20% but only in central Ghana and Burkina Faso (Serjeant, 2013). A point mutation leading to an amino acid substitution at the same position as found in HbS, position 6 of β-globin gene, caused a negatively charged glutamic acid to be exchanged for a positively charged lysine (Feeling-Taylor *et al.*, 2004). This resulted in formation of intracellular crystals and induced erythrocyte dehydration (Nagel *et al.*, 2003).

Table 2 The Major Haemoglobinopathies at a glance. Reproduced from Taylor *et al.*, (2013)

Hemoglobinopathy	Epidemiology	Genotype	Molecular Pathology	Clinical Phenotype
α-thalassemias				
Trait				
α^{+}-thal trait	Global	Loss of one α-globin gene (αα/α-)		Asymptomatic; normal RBC size, quantity, and peripheral blood smear
α^{0}-thal trait	Global	Loss of two α-globin genes (αα/–)		Mild anemia
Hemoglobin H (HbH) disease	Global	Loss of three α-globin genes (α-/–)	Accumulation of unpaired β-chains that form HbH and precipitate in RBCs	Chronic hemolytic anemia with hepatic, splenic, skeletal, and metabolic sequelae; transfusion support required in 2nd to 3rd decade of life
Hydrops fetalis/ Hb Barts	Global	Loss of all four α-globin genes (–/–)	Accumulation of unpaired γ-chains *in utero*, forming Hb Bart's, which is unable to release oxygen	Incompatible with extra-uterine life
β-thalassemias				
Minor/trait/ heterozygosity	Global	Reduced expression of one β-globin gene		Typically asymptomatic; normal hematocrit, low mean corpuscular volume
Major	Global	Reduced expression of both β-globin genes	Accumulation of unpaired α-chains, leading to oxidant damage to RBCs and erythroid precursors	Profound anemia leading to transfusion dependence, complicated by iron overload
Hemoglobin S	Central, East, and West Africa; Arabian peninsula; South Asia	Glu→Val at position 6 of β-globin	Aggregation of deoxygenated HbS into polymers, leading to RBC deformation, hemolysis, and microcirculatory obstruction	Sickle-cell disease with frequent pain crises, transfusions, and acute chest syndrome when inherited as HbSS; asymptomatic when inherited as HbAS
Hemoglobin C	West Africa, centered on western Burkina Faso and northern Ghana	Glu→Lys at position 6 of β-globin	Formation of hexagonal HbC crystals	Mild hemolysis and anemia when inherited as HbCC; asymptomatic when inherited as HbAC
Hemoglobin E	Southeast Asia, centered on border of Thailand, Laos, and Cambodia	Glu→Lys at position 26 of β-globin	Mildly reduced expression of β-globin due to insertion of splice site and resulting mRNA degradation	Mild anemia, microcytosis, and hypochromia
Hemoglobin F[a]	>50% of hemoglobin at birth, largely absent by 6 months of age	Normal	Tetramer consisting of two α-chains and two γ-chains	Greater oxygen affinity within RBCs than adult hemoglobin A due to attenuated interactions with 2,3-bisphosphoglycerate

The human genome normally contains four copies of α-globin genes (in paired copies on chromosome 16: genotype αα/αα) and two copies of β-globin genes (on chromosome 11). Normal adult hemoglobin (HbAA) is a tetramer of two α-globin and two β-globin proteins.
[a]Not technically a hemoglobinopathy but rather a normal hemoglobin variant of all newborns and infants.
doi:10.1371/journal.ppat.1003327.t001

1.5.2 Epidemiological evidence of protection

The "malaria hypothesis" was hypothesized by J.B.S. Haldane in 1949, stating that infectious diseases could be one of the naturally selective factors driving evolution, using the co-occurrence of β-thalassemia and malaria in Mediterranean countries as an example

(Dronamraju *et al.*, 2006). This was empirically shown in 1954 by Anthony Allison (1954), who was able to demonstrate a decreased malaria incidence in children with sickle cell traits compared to their peers without the traits.

In a meta-analysis of recent publications, Taylor *et al.*, (2012) was able to conclude that HbAS, HbCC, HbAC, homozygous α-thalassaemia and heterozygous α-thalassaemia conferred significant protection against severe malaria – but only HbAS was associated with protection against uncomplicated malaria. These findings do reflect the individual studies reported, where children carrying HbAS was shown to suffer fewer episodes of both severe and uncomplicated malaria, with a 10-fold lower risk of mortality in the former case (Aidoo *et al.*, 2002; Cyrklaff *et al.*, 2012; Fairhurst *et al.*, 2012). HbC is also reported to protect against symptoms of severe malaria but not uncomplicated malaria (Agarwal *et al.*, 2000).

1.5.3 Aberrant ultrastructural morphologies, host actin remodelling and reduced cytoadhesion in parasitized haemoglobinopathic erythrocytes

Regardless of the epidemiological evidence, the molecular mechanisms behind the protection of haemoglobinopathic erythrocytes against severe malaria have yet to be elucidated (Taylor *et al.*, 2013).

Recent studies by Fairhurst *et al.*, (2005), Cholera *et al.*, (2008) and Cyrklaff *et al.*, (2011; 2016) have found that both parasitized HbS and HbC displayed aberrant knobs and Maurer's cleft morphologies, as well as inability to reorganise host actin cytoskeleton (Fig 1-8). The cytoadhesive phenotype as well as levels of PfEMP1 surface presentation were also reduced in infected HbS and HbC, relative to HbAA.

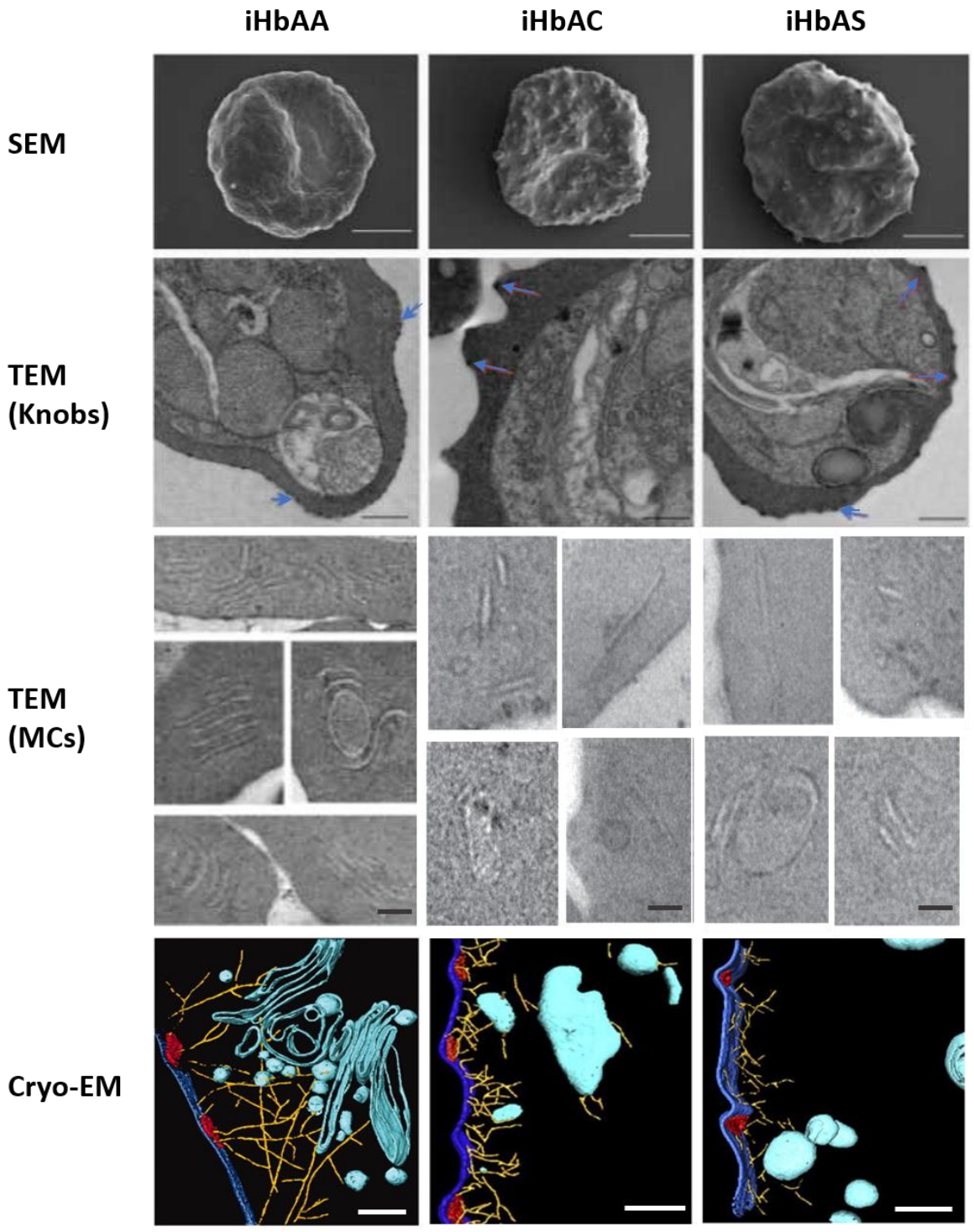

Figure 1-8 Aberrant ultrastructural morphologies in infected HbAC and HbAS erythrocytes

SEM and TEM showing enlarged and irregularly distributed knob morphologies in infected HbAC and HbAS. Blue arrows indicae knobs in the TEM images. The Maurer's clefts (MCs) were malformed and the parasite was unable to reorganise host actin cytoskeleton (yellow) into elaborate filamentous networks as seen in infected HbAA (cryo-EM). The following colours were used for specific ultrastructures in the surface-rendered view of cryo-EM: MCs -light blue, actin cytoskeleton - yellow, knobs – red and plasma membrane – blue. Scale bars – SEM 2 µm, TEM (knobs) 0.5µm, TEM (MCs) 100 nm, Cryo-EM 100 nm. Adapted from Cyrklaff *et al.*, (2011); Fairhurst *et al.*, (2012); Cyrklaff *et al.*, (2016).

In trying to find a common mechanism behind these morphological phenotypes, a hypothesis was generated around the effects of pro-oxidative environment and reactive oxygen species produced by the unstable HbS and HbC, which are prone to auto-oxidation (Hebbel *et al.*, 1982; Macdonald and Charache, 1982; Hebbel *et al.*, 1988; Krause *et al.*, 2012). Actin cytoskeleton has been found to be destabilised in the presence of oxidatively damaged haemoglobin such as irreversible hemichromes (Jarolim *et al.*, 1990; Cyrklaff *et al.*, 2011). This would affect both the Maurer's cleft morphologies as well as the trafficking of PfEMP1 to the erythrocyte surface, resulting in the final phenotypical outcome of reduced cytoadhesion and thus reduced malaria pathogenesis.

1.6 Overall aim

This thesis comprises of three distinct but interrelated projects, aimed to further our understanding of the molecular mechanisms behind the ability of haemoglobinopathic erythrocytes to protect their hosts against severe complications in malaria.

Project I: Visualisation of erythrocyte cytoskeletal proteins by super-resolution microscopy

Project I aims to establish a working protocol for imaging of actin and spectrin in erythrocyte samples using direct stochastic optical reconstruction microscopy (*d*STORM).

Project II: Kinetics of protein export in infected haemoglobinopathic erythrocytes

Project II aims to investigate differential export kinetics of selected parasitic proteins in infected HbAA and haemoglobinopathic erythrocytes.

Project III: Oxidative pre-treatment of uninfected erythrocytes to mimic the protective phenotypes of haemoglobinopathic erythrocytes

Project III aims to investigate the effect of an induced pro-oxidative environment on the parasite morphologies and cytoadhesion phenotype.

By better understanding the molecular mechanisms which underpins the protective phenotype of haemoglobinopathic erythrocytes against severe malaria, we hope to explore new venues of research into novel clinical interventions which could circumvent the rise of drug-resistant parasites.

2 Material and Methods

2.1 Materials

2.1.1 Equipment

Equipment	Model	Company
Analytical balance	ABT 120-5DM	Kern & Sohn, Balingen, Germany
Autoclave	ABT 120-5DM	Kern & Sohn, Balingen, Germany
	2540 EL	Tuttnauer, Breda, The Netherlands
Balance		Sartorius GmbH, Göttingen
Centrifuge	Biofuge fresco	Thermo Fisher Scientific, Dreieich, Germany
	Biofuge pico	Thermo Fisher Scientific, Dreieich, Germany
	Megafuge 1.0 R	Heraeus, Hanau, Germany
	Megafuge 2.0 R	Heraeus, Hanau, Germany
Confocal microscope	LSM510	Zeiss, Jena, Germany
Flow cytometer	FACSCalibur	Becton and Dickinson, Heidelberg, Germany
Syringe pump	55-2316	Harvard Apparatus, Holliston, MA
Freezer -20ºC	LGex 3410 MediLine	Liebherr, Biberach, Germany
Freezer -80ºC	HERAfreeze	Thermo Fisher Scientific, Dreieich, Germany
Fridge	LKexv 3910 MediLine	Liebherr, Biberach, Germany
Heating block	NeoBlock Mono I	NeoLab, Heidelberg, Germany
High precision pump	55-2316	Harvard Apparatus, MA, USA

Equipment	Model	Company
	AL-4000	World precision instruments, Florida,USA
Ice machine		Ziegra, Isernhagen, Germany
Incubator	Heraeus Cytoperm2	Thermo Fisher Scientific, Dreieich, Germany
	HeraCell	Thermo Fisher Scientific, Dreieich, Germany
Inverted microscope	Zeiss Axio Observer Z1	Carl Zeiss, Oberkochen, Germany
	DM IL	Leica, Wetzlar, Germany
Light optical microscope	Axiolab	Zeiss, Jena, Germany
Liquid nitrogen tank	MVE Cryosystem 6000	Thermo Fisher Scientific, Dreieich, Germany
	LS 6000	Taylor-Wharton, Husum, Germany
	RS Series	Taylor-Wharton, Husum, Germany
Magnetic sorter	VarioMACS	Miltenyi Biotec, Bergisch Gladbach, Germany
Magnetic stirrer	RCT	IKA, Staufen, Germany
	COMBIMAG RCH	IKA, Staufen, Germany
MiliQ water system	Purist ultrapure	Rephile, Germany
Particle counter	Z1	Beckman Coulter, Krefeld, Germany
pH meter	pH 7110	WTW, Weilheim, Germany
Pipets	P2, P10, P20, P1000	Gilson, Limburg an der Lahn, Germany
Pipetus	Forty\Standard	Hirschmann, Eberstadt, Germany
Adaptors for silicon tubing	Elbow connector	Ibidi, München, Germany

Equipment	Model	Company
	Luer connector male	Ibidi, München, Germany
	Luer lock connector male	Ibidi, München, Germany
	Luer lock connector female	Ibidi, München, Germany
	Female luer lock coupler	Ibidi, München, Germany
Silicon tubing	1.6 mm	Ibidi, München, Germany
Scanning electron microscope	Leo Gemini 1530	Carl Zeiss Oberkochen, Germany
Shaker	KS 501 digital	IKA, Staufen, Germany
Spectrophotometer	UVIKON 923	Kontron instruments, Munich, Germany
Sputter coatter	EM MED 020	Leica, Wetzlar, Germany
Sterile work bench	Herasafe	Thermo Fisher Scientific, Dreieich, Germany
	SterilGard Class II	The Baker company, Sanford, ME, USA
Thermocycler	Labcycler	Sensoquest, Göttingen, Germany
UV chamber	GS Gene linker	Bio-Rad, München, Germany
UV table	TFX-35M	Vilber Lourmat, Eberhardzell, Germany
Vortex	Genie 2	Scientific Industries, Bohemia, NY, USA
Waterbath	MP	Julabo, Seelbach, Germany

2.1.2 Disposables

Disposable	Company
µ-slide, 8-chamber	Ibidi, München, Germany
96 well cell culture plates	Greiner bio one, Frickenhausen, Germany
Aluminium foil	Carl Roth, Karlsruhe, Germany
Cellstar Tubes	Greiner bio one, Frickenhausen, Germany
Centrifuge bottles Nalgene 500 ml	Thermo Fisher Scientific, Dreieich, Germany
Clingfilm Saran	Dow, Schwalbach, Germany
Cuvettes Gene Pulser	Bio-Rad, München, Germany
Filters Millex GS (0,2 µm)	Merck Millipore, Darmstadt, Germany
Filter systems 500 ml	Corning, Kaiserslautern, Germany
Gloves TouchNTuff	Ansell, München, Germany
MACS CS column	Miltenyi Biotec, Bergisch Gladbach, Germany
Micro tubes 1.5 ml	Saarstedt, Nümbrecht, Germany
Parafilm	Bemis, Londonderry, UK
Petri dishes (10 ml diameter)	Greiner bio one, Frickenhausen, Germany
Petri-dishes (25 ml diameter)	Greiner bio one, Frickenhausen, Germany
Pipette Tipps	Corning, Kaiserslautern, Germany
Plastic pipettes (1 ml; 2 ml; 5 ml; 10 ml; 25 ml)	Corning, Kaiserslautern, Germany
Precision wipes (11x21cm)	Kimberly Clark, Mainz, Germany
Polypropylene tubes (14 ml)	Greiner bio one, Frickenhausen, Germany
PyroMark Q96 Plate Low	QIAGEN, Hilden, Germany
Disposable Scalpel	Feather, Osaka, Japan

Transfer pipettes	Sarstedt, Nümbrecht, Germany

2.1.3 Kits

Kits	**Company**
Ambion DNA-free kit	Invitrogen - Thermo Fisher Scientific, Vilnius, Lithuania
SuperScript III First Strand Synthesis	Invitrogen-Thermo Fisher Scientific, Vilnius, Lithuania
Taq DNA polymerase kit	Qiagen, Düsseldorf, Germany
Gel extraction kit	QIAGEN, Hilden, Germany
PCR purification kit	QIAGEN, Hilden, Germany

2.1.4 Antibodies

Antibodies	**Company**
Anti β-tubulin	Invitrogen - Thermo Fisher Scientific, Vilnius, Lithuania
Anti spectrin	Invitrogen-Thermo Fisher Scientific, Vilnius, Lithuania
Anti-VAR2CSA	Gifted from Ali Salanti

2.1.5 Fluorescent Dyes

Dye	**Ex/Em**	**Company**
Alexa Fluor 488	490/525	Invitrogen-Thermo Fisher Scientific, Vilnius, Lithuania
Alexa Fluor 532	532/554	Invitrogen-Thermo Fisher Scientific, Vilnius, Lithuania

Alexa Fluor 647	650/665	Invitrogen-Thermo Fisher Scientific, Vilnius, Lithuania
SiR Actin	652/674	Invitrogen-Thermo Fisher Scientific, Vilnius, Lithuania
Phalloidin-Alexa Fluor 488	490/525	Invitrogen-Thermo Fisher Scientific, Vilnius, Lithuania
Propidium Iodide	493 / 636	Invitrogen-Thermo Fisher Scientific, Vilnius, Lithuania

2.1.6 Buffers, media and solutions

Buffer / Media / Solution	**Composition / Recipe**
Complete culture medium	RMPI 1640 medium supplemented with 2 mM L-glutamine, 25 mM HEPES, 100 µM hypoxanthine, 20 µg/ml gentamicin and 10% (v/v) human serum.
Freezing solution	6.2 M Glycerol, 140 mM Na-Lactat, 0.5 mM KCl, pH 7.2 adjusted with 0.5 M of $NaHCO_3$ at pH 9.
Thawing solution I	12% (wt/v) sodium chloride.
Thawing solution II	1.8% (wt/v) sodium chloride.
Thawing solution III	0.9% (wt/v) sodium chloride, 0.2% (wt/v) glucose.
Sorbitol lysis solution	280 mM D-sorbitol, 5 mM HEPES, pH 7.4. (300 mOsm). Heat sterilized.
MACS buffer	PBS, 2mM EDTA, 0.05% (wt/v) BSA
Gelatin solution	0.5% (wt/v) gelatin (from porcine skin type A) was dissolved in RPMI 1640 supplemented with 2 mM L-glutamine and 25 mM HEPES for 30 min at 56°C.

Buffer / Media / Solution	**Composition / Recipe**
RMPI incomplete	RMPI 1640, 2 mM L-glutamine and 25 mM HEPES.
Adhesion medium	RMPI 1640, 2 mM L-glutamine and 25 mM HEPES, 0.05% (wt/v) pH 7.2.
Glucose solution for dSTORM	100 mg glucose, 900 µL PBS, 100 µL glycerin
Enzyme solution for dSTORM	1 mg glucose oxidase (Sigma G2133-50KU), 20 µL Tris-HCl pH 7.5 (1M Stock), 25 µL KCL (1M Stock), 2 µL catalase from bovine liver (C100-50MG), 4 µL TCEP/DTT (1M Stock), 0.5 mL glycerine, 0.45 mL water
MEA/PBS for dSTORM	1M stock solution (freshly prepared from salt stock; MEA: cysteamine hydrochloride (Sigma M6500-25G))
*d*STORM imaging buffer (Buffer I)	950 µl PBS, 50 µl freshly prepared MEA/PBS, 15 µl of 1M KOH
*d*STORM imaging buffer (Buffer II)	900 µl PBS, 100 µl freshly prepared MEA/PBS 15 µl of 1M KOH, 50 µl Enzyme solution
*d*STORM imaging buffer (Enzyme solution)	1 mg glucose oxidase (Sigma G2133-50KU) 20 µl Tris-HCl pH 7.5 (1M Stock) 25 µl KCL (1M Stock) 2 µl catalase from bovine liver (C100-50MG) 4 µl DTT (1M Stock) 0.5 ml glycerin 0.45 ml water
Hypotonic solution A	1:10 dilution of RPMI 1640 and distilled water, 20 µg/ml leupeptin, 20 µg/ml pepstatin

Buffer / Media / Solution	Composition / Recipe
Hypotonic solution B	1:5 dilution of RPMI 1640 and distilled water, 20 µg/ml leupeptin, 20 µg/ml pepstatin

2.1.7 Primers

Target	Primers	Sequence
Cyclophilin	PFE0505w_Fwd	5' AAACGGGAGATCCTTCAGGT
	PFE0505w_Rev	5' AAGGACATGGGACAGTGGTT
var2csa	PFL0030c_ex_Fwd	5' GACGCGAAACGAAACCGTAA
	PFL0030c_ex_Rev	5' ACTACTTGGGCCACAATTTTTTG

2.1.8 Software

Program	Company
SigmaPlot 13.0	Systat, San Jose, CA, USA
LSM imaging software	Zeiss, Jena, Germany
FIJI	(Schindelin *et al.*, 2012)
RapidSTORM 3.3	(Wolter *et al.*, 2012)
Andor Solis 4.16	Andor, Belfast, Northern Ireland
SuReSim	(Venkataramani *et al.*, 2016)

2.2 Methods

2.2.1 Ethical Clearance

The text of the following paragraph has been taken from Kilian *et al.*, (2015) and has originally been written by myself:

All studies were approved by both the ethical review boards of Heidelberg University, Germany, and the Biomolecular Research Center (CERBA/Labiogene) at the University of Ouagadougou, Burkina Faso. Written informed consent was given by all blood donors.

2.2.2 Blood collection and genotyping

Haemoglobinopathic erythrocytes (HbAC and HbAS) were donated in Burkina Faso and immediately shipped at 4° C to Heidelberg University for further analysis. Fetal erythrocytes were obtained from the umbilical cord following delivery at Heidelberg University Hospital.

The plasma and buffy coat were removed and discarded after 10 min of centrifugation at 800 g (RT). The erythrocytes were washed three times with three volumes of RPMI-1640 medium and stored at 4°C. Erythrocytes were used within two weeks after collection. Haemoglobin genotypes were performed by the Kooperatives Speziallabor of the Heidelberg University Hospital.

2.2.3 Methods for *Plasmodium falciparum* cell culture

2.2.3.1 In vitro culture of *P. falciparum*

Throughout this study, the *P. falciparum* strains FCR3-CSA and HB3 were kept in continuous cultures as previously described (Trager and Jensen, 1976). The haemoglobin variant of uninfected erythrocytes used in the culture were sometimes varied according to the experimental setup. Briefly, cultures were maintained in a Petri dish of either 10 or 35cm diameter with 3.5% hematocrit. The medium used was RPMI 1640 supplemented with 2 mM L-glutamine, 25 mM HEPES, 100 µM hypoxanthine, 20 µg/ml gentamycin, 5% albumax and 5% human heat-inactivated A-positive serum. AB-positive serum was substituted in case of cultures containing HbS or HbC blood.

Cultures were incubated at 37°C under controlled atmospheric conditions of 5% O_2, 3% CO_2, 92% N_2 and a humidity of 96%. The parasitemia was kept below 5%.

2.2.3.2 Monitoring of parasitemia and intra-erythrocytic developmental stage

2% Giemsa (BDH Laboratory Supplies) and thin blood smears were used to determine the developmental stage and parasitemia of the parasite cultures. A drop of the culture was collected from the bottom of the petri dish and spread onto the glass slide. After 10 sec of fixation in 100% Methanol, the slide was stained in 2% Giemsa solution for 15 minutes and rinsed with deionised water. The stained blood smear was evaluated with a light microscope.

2.2.3.3 Synchronization of Asexual Stages

5% D-sorbitol was used for synchronisation and selection of ring stage parasites as previously described (Lambros and Vanderberg, 1979). Briefly, the resuspended culture is centrifuged at 1900 rpm for 2 min and the supernatant is discarded. The pellet is resuspended in 5 volumes of 5% sorbitol. The suspension is gently mixed and incubated at 37°C for 5 min. The suspension is centrifugated for 2 min at 1900 rpm, the sorbitol solution discarded and the pellet resuspended in 14 ml cell culture medium. The synchronised pellet is re-cultured after another round of washing with the medium.

The activation of the New Permeability Pathway (NPPs) during the trophozoite stage allows uptake of sorbitol, which leads to hypotonic lysis during the washing step. Ring stages younger than 18 h p.i. are retained after the treatment. Tighter synchronisation can be achieved through repeated synchronization after 4–6 h.

2.2.3.4 Gelatin sedimentation

Gelatin sedimentation can be used to separate *P. falciparum* infected erythrocytes according to their densities, in that the schizont and trophozoite-stage have lower densities than ring-infected and uninfected erythrocytes, causing them to take longer to sediment (Goodyer *et al.*, 1994).

The parasite culture is resuspended and centrifuged for 2 min at 1900 rpm at room temperature. After removal of the medium, the pellet is resuspended in 9x volume of 0.5% gelatin for 1 h and kept at 37 °C. After the allotted time, the supernatant containing late-stage parasites was

carefully transferred to a new falcon tube and centrifugated for 2 min at 1900 rpm to pellet the parasitized erythrocytes. The cells were washed with RPMI 1640 and re-cultured.

2.2.3.5 Selection of CSA adhesive P. falciparum infected erythrocytes

Selection and enrichment of CSA binding parasites were carried out as previously described (Alkhalil *et al.*, 2000). Briefly, sterile tissue culture flasks were coated with 30mg/ml CSA in PBS and incubated overnight at 4°C. Mature stage parasites were enriched via gelatin floatation as described above. In parallel, the flask was washed and blocked with 1% BSA for 1 h. The parasites were resuspended in adhesion medium and incubated on the CSA-coated flask for 1 hour at 37°C. Non-adherent cells were gently removed with the supernatant and the flask was washed 5-10 times with adhesion medium using a gentle rocking motion. The last wash should be strong and the supernatant is taken to be centrifuged for 2 min at 1900 rpm to pellet the CSA-adhesive parasites. The pellet is used for inoculum of further parasite culture. As the binding strength is reported to gradually decrease over time, the process was repeated once every 3 weeks to maintain the adhesive phenotype (Achur *et al.*, 2008).

2.2.3.6 Purification of late stages P. falciparum through magnetic column

The Magnetic Activated Cell Sorter (MACS) system was used to purify *P. falciparum* trophozoite and schizont. Briefly, the MACS CS column was washed twice with MACS buffer and inserted into the VarioMACS separator. The culture was resuspended, applied to the top of the column and allowed to flow through with the flow rate of 1 drop every 3 sec. The column was washed with MACS buffer until the flow through was clear. The column was then removed from the separator and the enriched late stages iRBC were eluted using 10 ml of MACS buffer. The cells were centrifuged at 1900 rpm for 2 min and to sediment the pellet and then further processed according to different experimental requirements.

2.2.3.7 Infection of haemoglobinopathic erythrocytes

Tightly synchronized parasites (±6 h) at trophozoite stage were magnetically enriched as described above. The purified iRBCs were washed with RPMI culture medium containing AB

serum and then added to fresh HbAS or HbAC erythrocytes to a parasitemia of 1-2% and 3.5% haematocrit for cell culture. Parasite invasion and development were monitored with thin blood smears. Paired and parallel infection of haemoglobin AA erythrocytes were used as control.

2.2.3.8 Cryopreservation of *P. falciparum*

The parasite culture was resuspended and centrifuged at 1900 rpm for 2 min and the supernatant discarded. Slowly, 1/3 pellet volume of freezing solution was added drop by drop and mixed carefully with the infected erythrocytes. The mixture was incubated at room temperature for 5 min and then a further 4/3 volume of freezing solution were slowly added to the sample. The sample was transferred to 2 cryogenic vials that were kept at -80ºC for short term storage. The vials were transferred to liquid nitrogen tanks for long term storage of the samples.

2.2.3.9 Thawing of *P. falciparum*

The frozen cryovial was gently thawed and 5-7 drops of 12% NaCl solution was added over 5 min while thoroughly mixing the suspension after every drop. The mixture was then transferred to a 15 ml falcon tube and 4.5 ml of 1.6% NaCl solution was slowly added over 5 minutes while mixing. After centrifugation at 1900 rpm for 4 minutes, the supernatant was removed and the pellet was resuspended in 4.5 ml of 0.9% NaCl + 0.2% Dextrose solution. After centrifugation for 4 minutes at 1900 rpm, the supernatant was removed and the pellet was resuspended in 13 ml cell culture medium for cultivation.

2.2.4 Microscopy

2.2.4.1 Direct Stochastic Optical Reconstruction Microscopy (*d*STORM)

2.2.4.1.1 Cleaning and functionalisation of glass surface

2M NaOH was pipetted into the imaging chamber and incubated for 20 minutes. After washing with PBS (3 x 5 min), the chamber was then incubated with 0.01% Poly-L-Lysine for 1 h, followed by 200µg/µl concanavalin A for 1 h before sample application. The chamber was kept moist at all times.

2.2.4.1.2 Sample preparation

Uninfected and MACS-purified, infected trophozoite-stage HbAA erythrocytes were fixed with 4% PFA and 0.0075% GA for 30 min, washed with PBS and briefly perforated with 5AU of activated streptolysin-O (SLO) in order to release some haemoglobin content and reduce background fluorescence. The samples were then labelled with primary mouse anti-spectrin antibody and anti-mouse Alexa Fluor 647 secondary antibody, immobilised on pre-coated glass-bottom ibidi µ-slides and imaged at 63x magnification with Buffer II as blinking buffer.

For actin imaging, the same sample preparation protocol was followed but Phalloidin-conjugated Alexa Flour 488 was used instead of the primary and secondary antibodies.

2.2.4.1.3 Image acquisition

2D-STORM imaging was carried out on a custom-built set up, as described by Flottmann (2014). A minimum of 5000 frames were recorded with Andor Solis software at an integration time of 100 ms, a preamplifier gain of 1, EM-gain of 200 and in frame transfer mode. The excitation was performed under TIR illumination to only excite and observe molecules within a short distance from the glass bottom.

2.2.4.1.4 Data analysis

RapidSTORM software and theoretical PSF was used to reconstruct the localisation from the video files.

2.2.4.2 Stimulated Emission Depletion (STED) Microscopy

2.2.4.2.1 Ghost membrane preparation

The ghost membrane preparations were prepared as previously described (Blisnick *et al.*, 2000). Briefly, uninfected erythrocytes were incubated in 40 volumes of hypotonic solution A for 15 min at 4°C. The lysate was centrifuged for 30 min at 15 000×g, 4°C and the ghosts were collected and washed extensively before resuspension in 9 volumes of hypotonic solution A at 4°C.

Infected red blood cells were incubated in 40 volumes of hypotonic solution B for 15 min at 4°C. The lysate was centrifuged for 30 min at 15 000×g, 4°C and the ghosts were collected at

the surface of the free parasite pellet, washed extensively and finally resuspended in 9 volumes of hypotonic solution B and stored at 4°C.

2.2.4.2.2 Sample preparation and imaging

Samples of uninfected and MACS-purified infected erythrocytes/ghost preparations were fixed with 4% PFA and 0.0075% GA for 30 min then washed with PBS and incubated with 5 µm of SiR actin for 30 min. The samples were mounted on a coverslip and first a confocal image was taken with the 642 nm excitation laser. Subsequently, the 775 nm laser was used to quench the fluorophores outside of the focal area through STED and an image was acquired. This work was carried out in collaboration with Dr. Janina Hahn, AG Hell.

2.2.4.3 Transmission Electron Microscopy (TEM)

Infected erythrocytes were high-pressure frozen using Balzers HPM010 (BAL-TECH AG, Lichtenstein) at 2100 bar (COS, University of Heidelberg). The vitreous samples were perfused, with slow exchange of bound water using organic solvents (anhydrous acetone) containing 0.1% glutaraldehyde, 0.25% uranyl acetate, and 0.01% osmium tetroxide. Substitution with Lowicryl HM20 resins was initiated at –90°C and the temperature was increased by 10°C/h, as previously described (Hillmer *et al.*, 2012). 100 nm sections were cut at room temperature and examined using a Zeiss EM900 transmission electron microscope at 80kV (BioQuant EM Core Facility, University of Heidelberg).

2.2.4.4 Scanning Electron Microscopy (SEM)

P. falciparum-infected erythrocytes were washed in phosphate buffered saline (pH 7.2) and fixed in 2% glutaraldehyde and 4% paraformaldehyde for at least 30 min. Samples were spread onto poly-lysine coated glass cover slips and sequentially dehydrated using ethanol series and HMDS as a final chemical dehydration step. After mounting onto SEM pin and sputter-coating the sample with a 10 nm layer gold particles, samples were photographed at 5 kV using a Hitachi S-4500 field emission scanning electron microscope.

2.2.5 Adhesion Assay

Adhesion assay of parasitized RBC to CSA bound on plastic Petri dish was carried out as previously described (Beeson *et al.*, 1999; Buffet *et al.*, 1999; Viebig *et al.*, 2005). Briefly, circles of approximately 0.5 cm diameter were marked on the underside of a plastic Petri dish for each receptor, all in triplicates. 1mg/ml purified CSA or 1% BSA was dissolved in PBS and 20 µl of each solution were applied to indicated spots. The receptor plates were incubated overnight at 4°C in a humid box. Trophozoites were purified using Magnetic Activated Cell Sorter (MACS) column as described by Staalsoe *et al.*, (1999) and parasitemia after purification calculated. Meanwhile, the receptor spots were washed 3 times with PBS and blocking with 1% BSA for at least 30 minutes. After washing the spots with adhesion medium, $5*10^6$ infected erythrocytes were applied to each spot and incubated for 1 h at room temperature. After gently washing off unbound cells, the remaining cells were fixed with 2% glutaraldehyde in PBS for at least 2 h. After staining for 10 minutes with 10% Giemsa and allowing the plates to dry, the spots were imaged using Zeiss Axiovert 200M, 10x objective. 3 areas from each spots were randomly selected and imaged. All results shown are averages of triplicate spots of binding above levels recorded for the BSA control. Statistical analysis was carried out using Sigma Plot.

2.2.6 Flow cytometry

The text of the following paragraph has been taken from Cyrklaff *et al.*, (2016) and has originally been written by myself:

The levels of VAR2CSA present was determined using flow cytometry, as previously described (Barfod *et al.*, 2006). Briefly, samples of highly synchronised trophozoite-stage parasite cultures were collected and washed with PBS, supplemented with 2% fetal calf serum (FCS). A rabbit antiserum against baculovirus-produced recombinant domains of VAR2CSA was used as the primary antibody. 3ml of the sera was used to label the samples for 30 min in a final volume of 50 ml PBS/FCS. After several washing steps, the samples were then labelled with 1:100 Alexa 488 goat anti-rabbit IgG (HþL) (Life Technologies) and 1:100 propidium iodide for 30 min in a final volume of 50ml PBS/FCS. Uninfected erythrocytes were treated concurrently throughout as a negative control. The fluorescence was finally determined using a FACScalibur (Becton Dickinson) and the CellQuest Pro Software 6.0.4 BD (Franklin Lakes).

2.2.7 Quantification of haemoglobin content by spectroscopy (NPPs activation

Highly synchronized infected red blood cells were evaluated for hemolytic capability as an indirect measurement of NPPs activation over the entire intraerythrocytic life cycle. Briefly, samples of $1x10^7$ iRBC were collected every 4 h, washed in PBS and then suspended in 800 µl of isosmotic sorbitol lysis solution for 10 min at 37°C. After 2 min centrifugation at 500 g, 700 µl of the supernatant were collected and the absorbance at 540 nm was measured in order to estimate the haemoglobin concentration released from the lysed cells. Hemolysis of uninfected erythrocytes was assessed in parallel as negative control. Duplicates of at least two independent samples were carried out.

2.2.8 Oxidative pre-treatment of erythrocytes

Erythrocytes were incubated with the candidate oxidative agents at indicated concentration for 1 hour RT. For treatments with H_2O_2 and tBOOH, an equimolar concentration of DTT was applied to the erythrocyte after 3 PBS washings to try and restore the oxidative balance. For treatments with menadione sodium bisulfate and diamide, the number of washing steps was increased to 5. 3-4ml of medium was added on top of the blood pellet after discarding the supernatant from the last wash. Store at 4°C.

2.2.9 Hemozoin Quantification

The text of the following paragraph has been taken from Cyrklaff *et al.*, (2016) and has originally been written by myself:

The amount of hemozoin was determined as previously described (Schwarzer *et al.*, 1992). Briefly, infected erythrocytes at trophozoite and schizont stages were collected by centrifugation and washed twice with PBS. The pellet was then osmotically lysed by adding 50 ml of ice-cold distilled water (dH_2O) before centrifugation at 4,000 rpm at 4° C for 30 min to precipitate the hemozoin and the membrane ghosts. After the centrifugation, the white layer of RBC membrane ghosts was aspirated and the sticky black hemozoin pellet underneath washed twice with ice-cold dH_2O. These were then dissolved in 1 ml of 0.1M NaOH and incubated at 50 °C for 10 min. The absorbance at 400 nm was used to determine the amount of hemozoin present; 100 ml of each sample was added to 96-well plates and a serial dilution of 0.1M haemin

chloride (Sigma Aldrich) was used to plot a standard curve. The concentration of hemozoin present in each sample was extrapolated from said graph.

2.2.10 RNA purification and cDNA synthesis

Synchronized trophozoite/schizont-stage iRBC were isolated by MACS, as previously described (Staalsoe et al., 1999). Briefly, 50 µl of packed erythrocytes with ~50% parasitaemia was dissolved in 1 ml of TRIzol (Invitrogen) and RNA was prepared according to the manufacturer's instruction. RNA pellets were dissolved in 10 µl of RNase-free water and treated with DNaseI (Sigma-Aldrich) for 25 min at room temperature, followed by 10 min heat inactivation at 65°C. DNA-free RNA samples were used for synthesis of cDNA by reverse transcriptase (Superscript II, Invitrogen) and random hexamer primers as described by the manufacturer. cDNA synthesis was performed with assistance from Sophie Adjelley, EMBL Heidelberg.

2.2.11 Quantitative real-time polymerase chain reaction (qRT-PCR)

All q-PCR measurements were performed using the LightCycler 96 system (Roche). Reactions were prepared in volumes of 20µl using SYBR Green PCR master mix (Applied Biosystems) and a primer concentration of 1µM. The following PCR cycling conditions were used: initial heat activation step at 95°C for 15 min, followed by 40 cycles of 95°C for 30 s, 55°C for 30 s and 68°C for 40s with a final extension at 68°C for 40 s. The amplification specificity for each primer pair was determined by melting-curve analysis of each PCR product.

Gene specific standard curves were generated by determining the 'amplification efficiency' relative to the single copy endogeneous control gene (cyclophilin), based on real-time measurements of 10-fold dilutions of genomic DNA. Transcript abundance was determined according to the ΔCt (cycle threshold) method, in which the Ct value for each specific gene was compared with that of the endogeneous control. Both qPCR measurement and analysis was performed with assistance by Sophie Adjelley, EMBL Heidelberg. Primer sequences used are shown in section 2.1.7 (Duffy *et al.*, 2002; Salanti *et al.*, 2003).

2.2.12 Sample preparation for Mössbauer spectroscopy

5ml aliquots of uninfected pre-treated HbAA, fetal and haemoglobionpathic erythrocytes were shipped from Heidelberg to Krakow with dry ice, keeping the temperature within range of 4°

C. Further sample processing and measurement of Mössbauer spectroscopy was carried out as described (Cyrklaff *et al.*, 2016).

3 Project I: Visualisation of erythrocyte cytoskeletal proteins by super-resolution microscopy

Impaired actin reorganisation in infected haemoglobinopathic erythrocytes has been implicated as one of the possible machanisms by which these hereditry conditions protect the host against life-threatening complications of severe malaria (Cyrklaff *et al.*, 2012). Previous studies have utilised electron microscopy (EM), more specifically cryo-electron tomography, in visualising the actin reorganisation in infected erythrocytes (Cyrklaff *et al.*, 2011). However, cryo-electron tomography as a technique is known to require great expertise in both image acquisition and data processing, with low throughput and high time investments required. Electron microscopy, in general, is also incompatible with live-cell imaging, as water molecules in the samples need to either be removed, as in classical EM, or immobilised, in the case of cryo-EM, to render the sample compatible with imaging under high vacumm.

Classical confocal/light microscopy, although compatible with live cell imaging and requires less time and expertise, is faced with the lateral resolution limit of 200 nm and axial resolution limit of 500 nm, restricting it from the visualisation of small, intricate structures such as filamentous actin in erytrocytic membrane, which is approximately 37 nm in length (Henriques *et al.*, 2011; Gokhin and Fowler, 2016). The recent development of different methods in super-resolution microscopy, also refered to as single molecule localisation microscopy (SMLM), have enabled scientists to overcome the diffraction limit and gained deeper understanding of various cellular dynamics and protein complexes, with a lateral resolution of up to 20 nm, a spatial resolution of up to 50 nm and a temporal resolution of 0.5-1 s (Endesfelder *et al.*, 2010; Jones *et al.*, 2011; Sauer and Heilemann, 2017).

3.1 Aim of the study

In this project, our aim was to establish a working protocol for direct stochastic optical reconstruction microscopy (*d*STORM) in uninfected and infected erythrocytes as a higher throughput method of nanoscale visualization, complementary to cryo-EM. Imaging of differential actin reorganization in infected haemoglobinopathic and HbAA erythrocytes would

be used as benchmark experiments to evaluate the applicability of *d*STORM for the stated purpose.

3.2 Alexa Fluor 647 is a suitable fluorophore for *d*STORM visualisation

As proof of principle, fixed HeLa cells were stained with anti-tubulin and Alexa Fluor 647 antibodies (kindly provided by Dr. Benjamin Flottman) and imaged with the total internal reflection (TIRF)-*d*STORM set-up as well as the traditional widefield illumination for comparison (Fig 3-1).

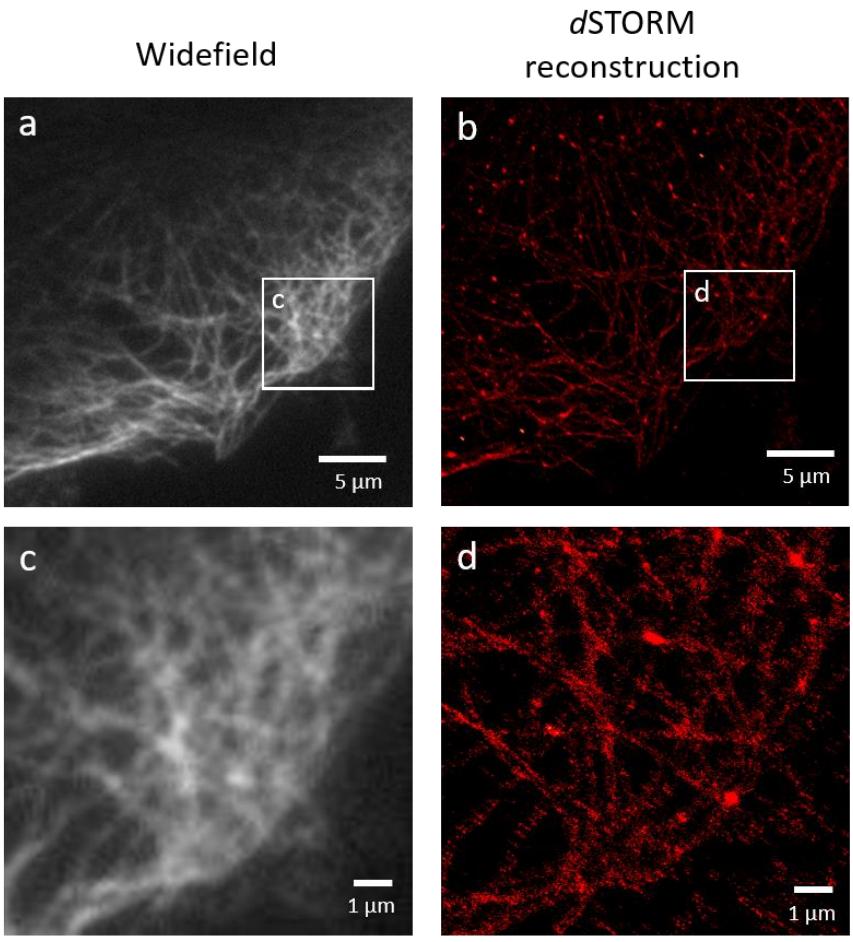

Figure 3-1 Enhanced resolution of *d*STORM imaging as compared to traditional widefield microscopy.

(a) A widefield image of a fixed HeLa cell stained with anti β-tubulin antibody and Alexa Fluor 647 was taken prior to *d*STORM image acquisition. (b) A *d*STORM reconstruction of the same sample using RapidSTORM software. (c) and (d) A section of the widefield image and *d*STORM reconstruction were magnified to illustrate the higher resolution provided by *d*STORM imaging.

As shown in panel c and d (Fig 3-1), the *d*STORM reconstruction was able to more distinctly resolve the tubulin filaments than traditional widefield microscopy. However, areas of over-saturation were also present, especially at the junctions where several tubulin filaments seemed to cross, and if one would like to further investigate these junctions, adjustments in laser intensity and/or antibody concentrations would need to be considered.

Although Alexa Fluor 647 worked well in the established system of HeLa cells, two additional fluorophores were tested for *d*STORM imaging in the erythrocytes: Alexa Fluor 488 and Alexa Fluor 532. As there were several key differences between imaging tubulin in HeLa cells and actin and spectrin in infected and uninfected erythrocytes, we thought it prudent to test and select the optimal fluorophore in the target system.

Alexa Fluor 488 was selected for its ability to exhibit blinking behaviour in PBS, circumventing the need for toxic blinking buffers containing mercaptoethalamine (MEA) (Dempsey *et al.*, 2011). However, we found that the haemoglobin autofluorescence (Khandelwal and Saxena, 2007; Zhurova et al., 2014), even after sample perforation with streptolysin-O to release the haemoglobin content, as well as the low blinking rate rendered this particular fluorophore unsuitable for use due to low signal to noise ratio (data not shown). Alexa Fluor 532 also exhibited high background and low blinking rate, so much so that a reconstruction was not possible due to low photon count (data not shown). Alexa Flour 647 performed better than the previous two fluorophore, although it still exhibited signs of bleaching. However, the conditions were able to be marginally improved by adapting the imaging buffer to include an enzymatic oxygen scavenging system (Buffer II) (van de Linde *et al.*, 2011). Although signs of bleaching still occurred, the photon count were sufficient for reconstructions, albeit the high background autofluorescence still remained (Fig 3-2a and d).

One of key difference between the test sample of HeLa cells and our erythrocyte samples was the fact that HeLa cells were adherent cells. This is of a significant importance in *d*STORM as adherent cells greatly reduce the problem of ‘drifting’ caused by movements of sample during the image acquisition. Several immobilisation methods were tested, including Matrigel, poly-L-Lysine coated slides as well as varying concentrations of concanavalin-A. A sequential coating of 0.01% Poly-L-Lysine followed by 200µg/µl concanavalin A was selected as the final immobilisation protocol.

3.3 Differences between the cytoskeletal network of uninfected and infected RBCs cannot be resolve with *d*STORM

3.3.1 Spectrin

In uninfected HbAA erythrocytes, spectrin tetramers are known to form a quasi-hexagonal meshwork connecting to junctional complexes containing short F-actin filaments of approximately 37 nm in length as well as actin-binding proteins such as tropomyosin, tropomodulin and protein 4.1R (Gokhin and Fowler, 2016) (Lux, 2016). This lends the erythrocytic membrane its characteristic flexibility and tensile strength. This network is said to be altered by the *Plasmodium* parasite upon infection (Shi *et al.*, 2013). We began our experiments with spectrin rather than actin because we hypothesised that the regularity of the meshwork structures in uninfected erythrocytes might lend itself better to visualisation.

Uninfected and magnetically-purified, infected trophozoite-stage HbAA erythrocytes were fixed with 4% PFA and 0.0075% GA for 30 min, washed with PBS and briefly perforated with 5AU of activated streptolysin-O (SLO) in order to release some haemoglobin content and reduce background fluorescence. The samples were then labelled with primary mouse anti-spectrin antibody and anti-mouse Alexa Fluor 647 secondary antibody, immobilised on pre-coated glass-bottom ibidi µ-slides and imaged at 63x magnification with Buffer II as blinking buffer. A minimum of 5000 frames were taken for *d*STORM reconstruction using RapidSTORM software.

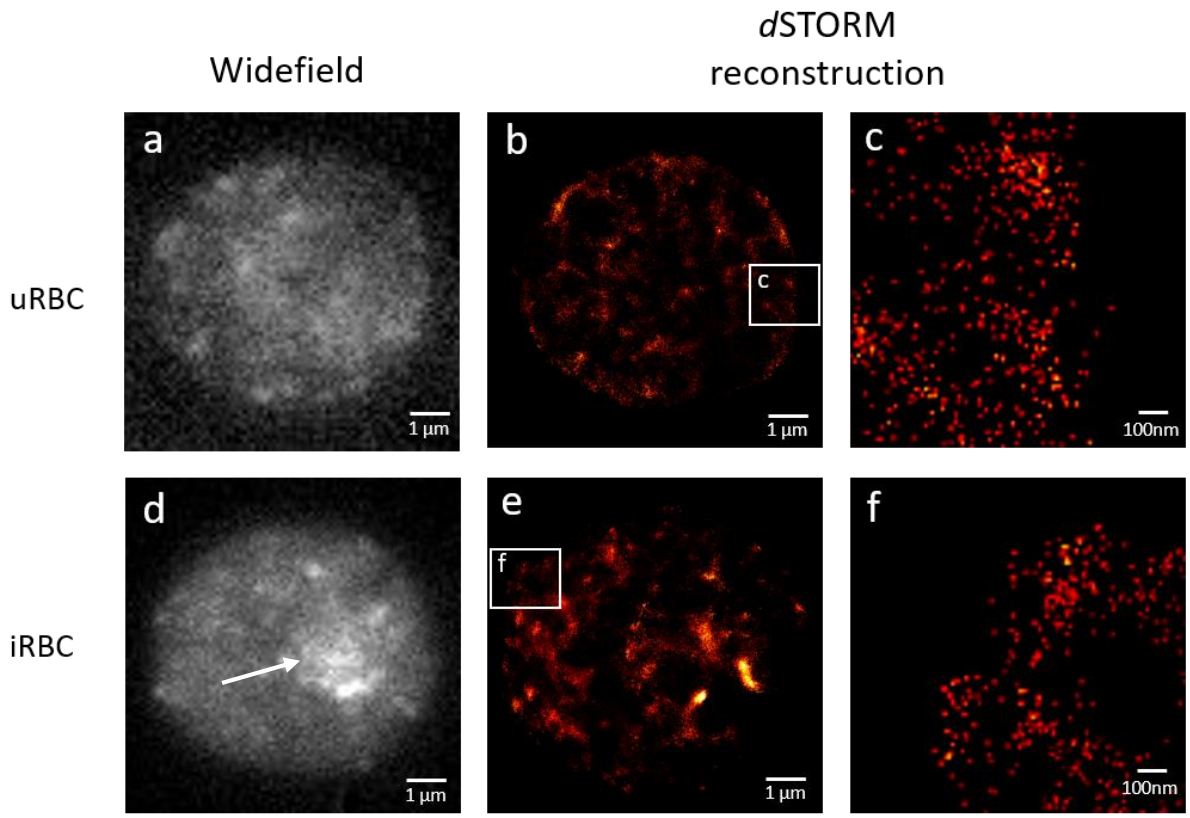

Figure 3-2 Visualisation of spectrin network in uninfected and infected HbAA erythrocytes using *d*STORM

Uninfected (a-c) and infected (d-f) HbAA erythrocytes were labelled with anti-spectrin antibody and visualized using Alexa Fluor 647 and *d*STORM imaging. The white arrow in (d) indicates the position of the parasite in the infected cell. Selected sections of the *d*STORM reconstructions from (b) and (d) were magnified and displayed in (c) and (f) to allow for more direct comparison between the two samples. Images shown are representative of at least five different independent biological replicates. uRBC – uninfected erythrocyte; iRBC – infected erythrocyte.

As shown in figure 3-2c and f, there were no distinguishable differences in the apparent spectrin network of uninfected and infected erythrocytes. Unlike the microtubule filaments seen in figure 3-1b and d, it is difficult to visualise any filamentous or mesh-like structure in this case. Figure 3-2a and d also showed a high degree of background fluorescence regardless of the SLO-treatment. The parasite itself also seemed to acquire an especially intense fluorescence staining (Fig 3-2 d).

3.3.2 Actin

Although we could not visualise the hexagonal meshwork structures in uninfected samples and no discernible differences between spectrin network of uninfected and trophozoite-infected erythrocytes were detected, we continued with our attempt at actin visualisation. Since the filamentous actin reorganised by the parasite were reported to be, on average, 150 nm in length

(Cyrklaff *et al.*, 2011), we expected that the longer length may increase the resolution, compared to the folded spectrin network at approximately 45 nm in length (Nans *et al.*, 2011; Shi *et al.*, 2013). The fact that the phalloidin-conjugate of Alexa Flour 647 is also commercially available also allowed us to expect a higher labelling efficiency, leading to a higher signal-to-noise ratio, relative to secondary antibody labelling.

Following the same sample preparation technique, fixed uninfected and infected HbAA erythrocytes were stained with phalloidin-conjugated Alexa Fluor 647 and imaged using TIRF-*d*STORM.

Although a comparison between panels a-b and d-e from figure 3-3 suggest a more uniform, intense staining of F-actin around the rim of the uninfected erythrocytes, a closer look at the *d*STORM reconstructions in panels c and f showed no visible differences between F-actin staining in the two samples. Unlike the images of the tubulin network in HeLa cells, the reconstructed images of F-actin staining in infected HbAA erythrocyte did not produce clear, filamentous structures. Instead, the individually localised fluorophores - seen as dots in the images - were spread out, making it difficult to judge whether the underlying structures could be arranged in any form of filaments.

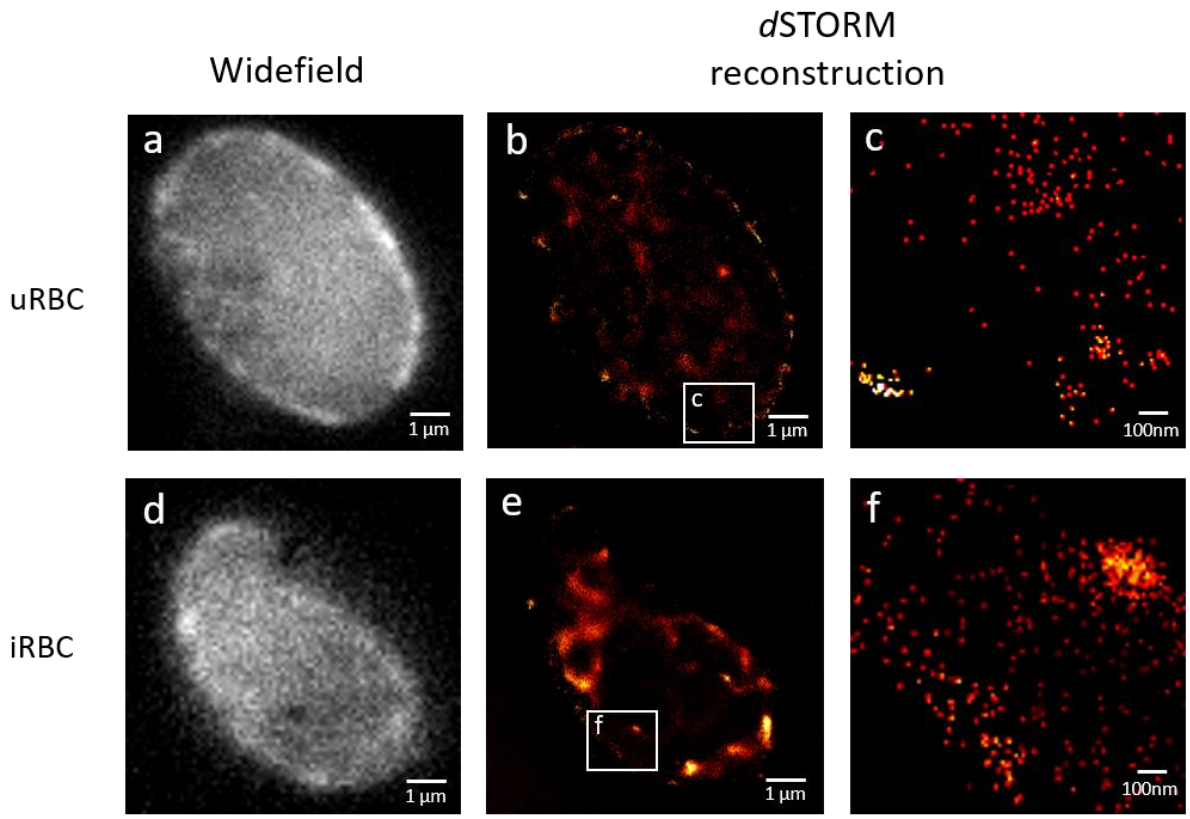

Figure 3-3 Visualisation of actin network in uninfected and infected HbAA erythrocytes using *d*STORM

Uninfected (a-c) and infected (d-f) HbAA erythrocytes were labelled with phalloidin-Alexa 647 and imaged using *d*STORM. The white arrow in (d) indicates the position of the parasite in the infected sample. Selected sections of the *d*STORM reconstructions from (b) and (d) were magnified and displayed in (c) and (f) to allow for more direct comparison between the two samples. Images shown are representative of at least five different independent biological replicates. uRBC – uninfected erythrocyte; iRBC – infected erythrocyte.

3.3.3 *d*STORM Simulation Software (SuReSim)

We consulted Dr. Varun Ventrankamani and Dr. Frank Herrmandörfer, both of whom were more experienced in *d*STORM imaging, regarding our results. At the time, they were involved in the development of the "SuReSim", a software which would allow users to simulate *d*STORM reconstructions based on 'ground truth models' of the structure of interest with variable experimental parameters such as labelling intensities, epitope densities, average blinking number and background signal (Venkataramani *et al.*, 2016). Data regarding the length, branching angles and density of F-actin in uninfected and infected erythrocytes were extracted from previously publish electron microscopy experiments and used as 'ground truth models' – underlying structures of interest to be imaged by *d*STORM (Fig 3-4c and d). For the simulated *d*STORM reconstruction of F-actin in uninfected erythrocytes (Fig 3-4b), a 10%

labelling efficiency and an epitope density of 0.015 epitopes/nm^2 for phalloidin-conjugated Alexa Flour 647 were assumed (Faulstich *et al.*, 1993; Venkataramani *et al.*, 2016). The outcome of the SuReSim simulation was consistent with the experimental reconstruction (Fig 3-4a) performed by Varun and Frank, as well as those performed prior to our consultation (Fig 3-3b and c). The SuReSim output of F-actin labelling in infected erythrocytes (Fig 3-4e) also showed similar images to those seen in our previous experimental reconstructions (Fig 3-3e and f).

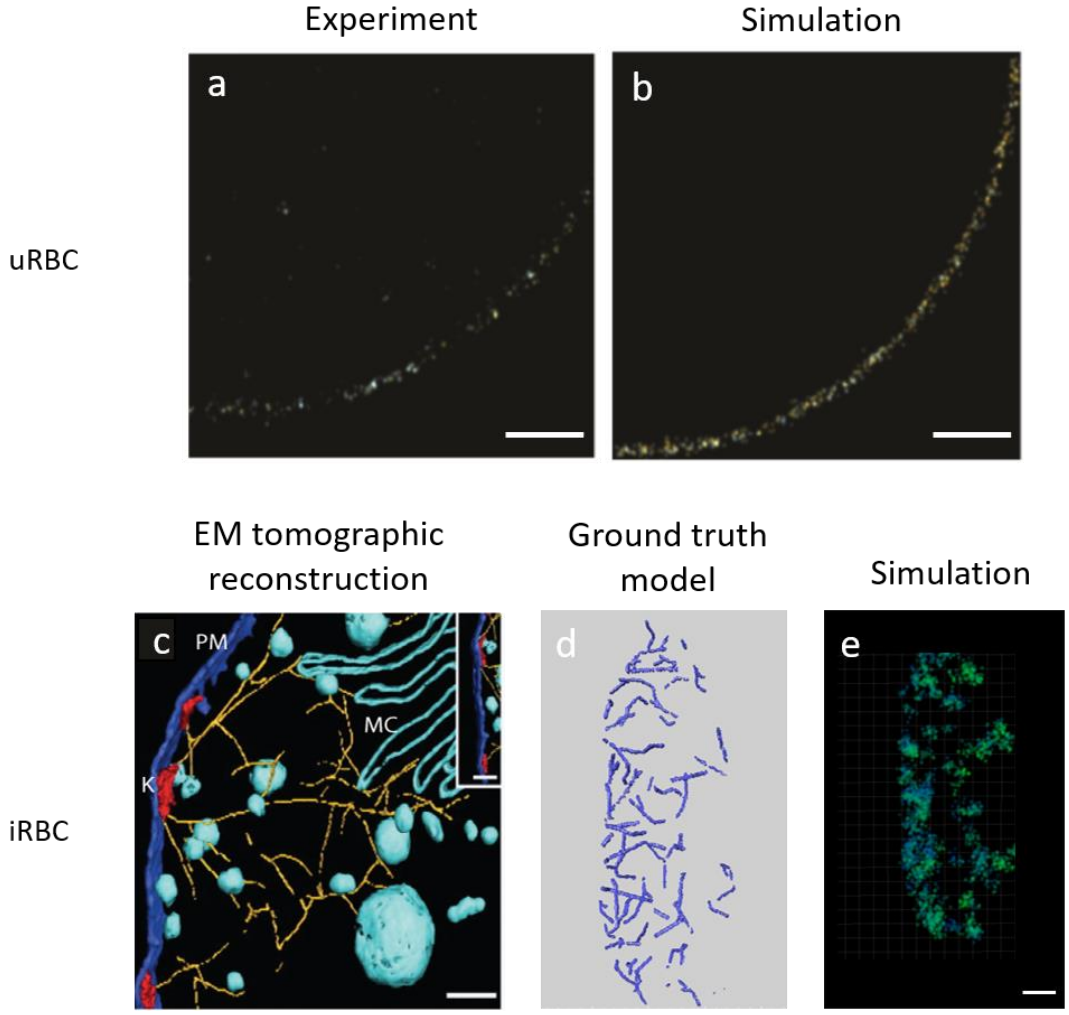

Figure 3-4 Simulation of likely dSTORM imaging outcomes based on ground-truth models by the software SuReSim.

(a) and (b) cortical actin in uninfected erythrocytes (uRBC), visualized by *d*STORM imaging and SuReSim simulation respectively. Adapted from Venkataramani *et al.*, (2016) Scale bar 500 nm. (c) surface-rendered view of infected trophozoite stage HbAA erythrocyte, reconstructed from cryo-tomographic tilt series. Actin filaments seen in yellow. MC – maurer's cleft; PM – plasma membrane; k – knob. Scale bar 100 nm. Adapted from Cyrklaff *et al.*, (2012). (d) extraction of actin filament coordinates from (c) to apply as 'ground truth model' – a basis for SuReSim simulation for actin in infected erythrocytes. (e) simulated dSTORM reconstruction, assuming 10% labelling efficiency, 20 nm axial resolution and 30 nm lateral resolution. Scale bar 500 nm. uRBC – uninfected erythrocyte; iRBC – infected erythrocyte.

3.4 Differences between the actin network of uninfected and infected RBCs cannot be resolve with STED

As both our experimental results and the SuReSim simulations showed that it was unlikely for *d*STORM to be able to resolve the differences in actin re-arrangement between uninfected and infected erythrocytes, we attempted another method of super-resolution imaging – namely, stimulated emission depletion (STED) microscopy. SiR-Actin, a far-red fluorophore developed by Lukinavičius *et al.*, (2014), was an attractive option as it would further minimize the autofluorescence of haemoglobin in the green spectrum. This work was carried out in collaboration with Dr. Janina Hahn, AG Hell, University of Heidelberg.

3.4.1 Infected erythrocytes could not be imaged with STED microscopy

Samples of uninfected and magnetically-purified infected erythrocytes were fixed with 4% PFA and 0.0075% GA for 30 min, washed with PBS and incubated with 5 µm of SiR actin for 30 min. The samples were mounted on a coverslip and first a confocal image was taken with the 642 nm excitation laser (Fig 3-5a and c). Subsequently, the 775 nm laser was used to quench the fluorophores outside of the focal area through STED and an image was acquired (Fig 3-5b and d).

While STED images showed an improved resolution of the cortical actin in uninfected red blood cell relative to confocal images, infected erythrocytes entirely failed to be imaged with STED (Fig 3-5). The initial confocal imaging of the infected sample could be performed as expected, but once the STED laser reached the position where the parasite resided in the infected red blood cell, the cell seemed to simply burst (Fig 3-5c and d). This was observed in all repeats of infected trophozoite-stage erythrocyte samples from at least three independent biological replicates.

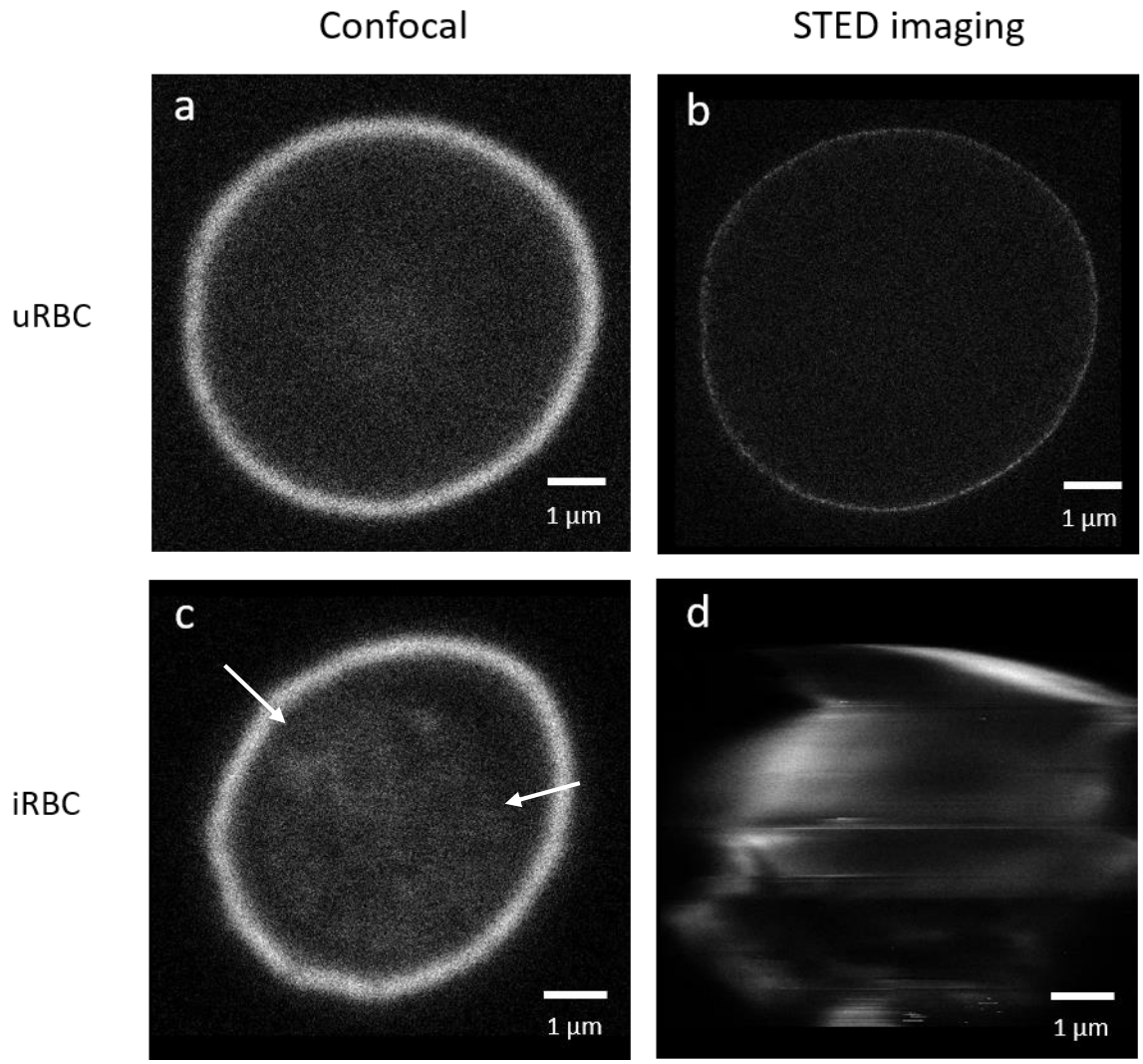

Figure 3-5 STED imaging of uninfected and infected HbAA erythrocytes.

Uninfected (a-b) and infected (c-d) HbAA erythrocytes were fixed and stained with 5 µM SiR-Actin for 30 min. The sample slide was then loaded onto a Leica DMI6000B microscope and confocal image was taken with 645 nm laser, followed by STED imaging with 775nm laser (performed by Dr. Janina Hann). White arrows in (c) point towards the position of the parasite in the infected sample. Images shown are representative of at least three independent biological replicates. uRBC – uninfected erythrocyte; iRBC – infected erythrocyte.

3.4.2 STED imaging cannot resolve actin on ghost membrane preparations

To circumvent the problem of "exploding" infected erythrocytes, ghost membrane preparations from both uninfected and infected erythrocytes were prepared using hypotonic solutions and protease inhibitors (Blisnick *et al.*, 2000). These samples were then fixed, labelled and imaged in the same way as the previous attempt. The ghost membrane preparations from infected erythrocytes were able to be imaged with STED without further problems (Fig 3-6e and f).

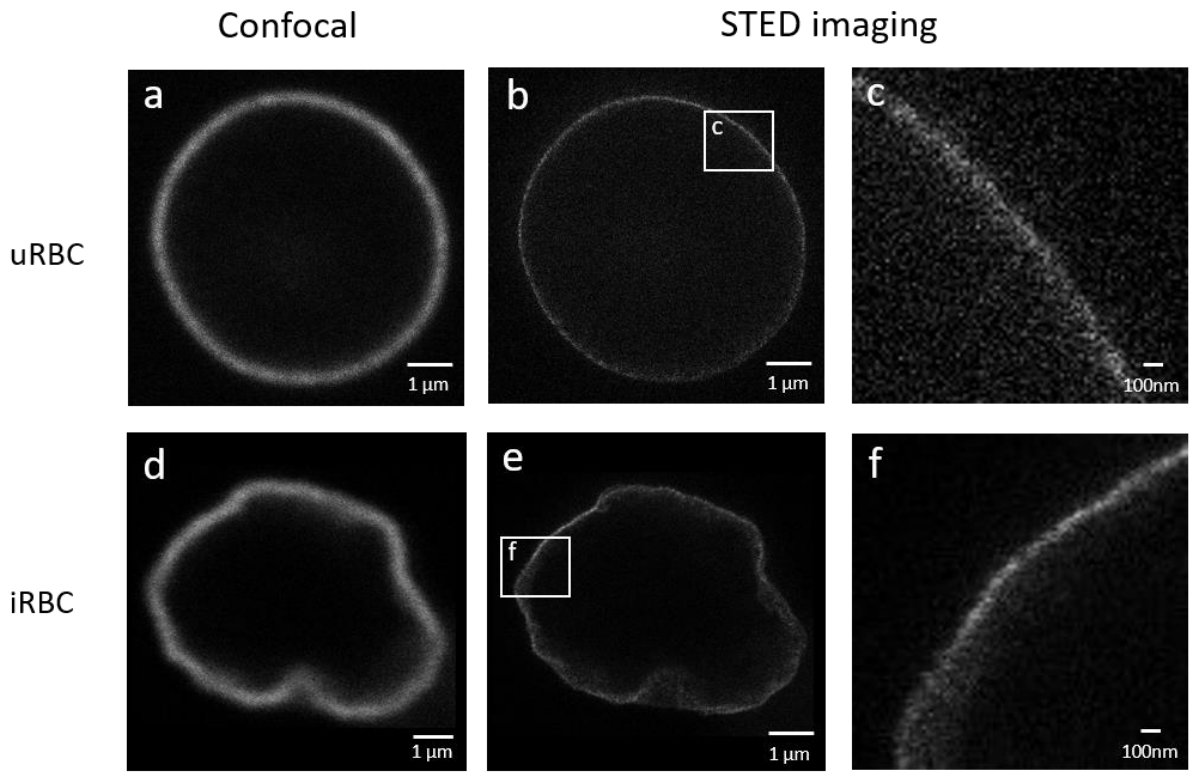

Figure 3-6 STED imaging of ghost preparations from uninfected and infected HbAA erythrocytes.

Erythrocyte membrane ghosts were prepared according to stated protocol (Blisnick *et al.*, 2000). Ghost preparations from uninfected (a-c) and infected (d-f) HbAA erythrocytes were fixed and stained with 5 µM SiR-Actin for 30 min. The sample slide was then loaded onto a Leica DMI6000B microscope and confocal image was taken with 645 nm laser, followed by STED imaging with 775 nm laser (performed by Dr. Janina Hann). White arrows in (c) point towards the position of the parasite in the infected sample. Images shown are representative of at least three independent biological replicates. uRBC – uninfected erythrocyte; iRBC – infected erythrocyte.

Although cortical F-actin from both infected and uninfected ghost preparations were now able to be imaged with STED, a closer look at the resolved images in panel c and f (fig 3-5) did not reveal any significant differences in the arrangement of actin filaments in uninfected versus infected samples.

3.5 Discussion

Unfortunately, both *d*STORM and STED microscopy failed to visualize the differential arrangements of cortical F-actin in uninfected and infected HbAA erythrocytes. In the case of *d*STORM, the experimental findings were also supported by the simulations from the software SuReSim (Venkataramani *et al.*, 2016). Although the length of F-actin in uninfected erythrocytes is reported to be approximately 37 nm, technically within the axial resolution limit of super-resolution microscopy (Gokhin and Fowler, 2016), we could not visualize individual actin filaments. One of the possible reasons could be due to the high density of actin in the cortical membrane of the uninfected erythrocytes (Lux, 2016; Venkataramani *et al.*, 2016). Kudryashev *et al.*, (2010) also discussed the impact of actin length and orientation and the subsequent effects thereof on its detection by cryo-electron tomography. Although different in the imaging modality and system, the paper points to several factors effecting actin visualization that could also play a role in our super-resolution imaging. Cortical F-actin in erythrocytes are reported to lie at approximately 20° to the membrane plane and have random orientations (Picart and Discher, 1999; Lux, 2016). As we were using 2D TIRF-*d*STORM to image the cortical actin, the lack of information regarding the 3D arrangement of the filaments could contribute to the "crowding effect" of the localized fluorophore, making it more difficult to distinguish individual filamentous structures in the reconstructed images.

Increasing evidence have emerged that erythrocytic F-actin is more dynamic than previously believed: Gokhin *et al.*, (2015) has reported that between 25-30% of erythrocytic F-actin are mobile and able to undergo both lateral movements and subunit assembly/disassembly (Gokhin *et al.*, 2015; Gokhin and Fowler, 2016). In HbAA parasitized erythrocytes, surface-rendered views of cryo-electron tomographic tilt series have previously shown elaborate actin networks of filaments between 40 – 600 nm in length, with some filaments branching at 70° and 110° angles (Cyrklaff *et al.*, 2011; Cyrklaff *et al.*, 2012; Rug *et al.*, 2014). These dynamic processes and transient structures could be affected by the process of sample fixation. This could explain why we could not visualize the longer actin filaments in infected erythrocytes, even though the average length were reported to be over 170 nm (Cyrklaff *et al.*, 2016). Several recent studies have tried to investigate the effect of fixatives such as paraformaldehyde (PFA) and glutaldehyde (GA) on actin filaments in super-resolution imaging more systematically (Whelan and Bell, 2015; Bachmann *et al.*, 2016; Leyton-Puig *et al.*, 2016). While both Bachmann *et al.*, (2016) and Whelan and Bell, (2015) found GA to be more efficient at preserving thin and short actin filaments, Leyton-Puig *et al.*, (2016) argued that under optimal conditions, PFA performed

just as well as GA in structural preservation. However, these studies were performed in adherent cells such as HeLa or COS-7, whose actin filaments were longer and much more visible. The same systematic approach should also be carried out in our erythrocyte samples – but the dense arrangements and much shorter filaments would most likely prove problematic for visualization, as we have found.

One could argue for live-cell imaging, which would remove potential artifacts that would arise from fixatives currently used in the sample preparation. However, the current imaging protocols for *d*STORM and STED microscopy need to be substantially adapted first. In the case of *d*STORM, the imaging buffer requires oxygen scavenging, which is not conducive to keeping cells alive (Dempsey *et al.*, 2011). There should also be minimal movement of the cell during image acquisition to prevent 'drift' – an artifact where a photon cannot be accurately localized and appears elongated due to sample movement. This is of special concern with erythrocytes as they are non-adherent cells and the live parasite in infected samples could cause substantial vibration during imaging. As for STED microscopy, the high laser intensity required would result in phototoxicity in live cell – one must then consider a compromise between the resolution, size of area of interest and speed (Cox, 2015).

The fact that STED microscopy of infected erythrocyte was only possible with ghost membrane preparation is another point to consider. Although the cause of the sample disruption during STED image acquisition of infected erythrocytes was not experimentally determined, one possible explanation could be the interaction between hemozoin crystal and the 775 nm STED laser. Lukianova-Hleb *et al.*, (2014) reported that nanobubbles could be generated by aiming a short pulse of laser at the hemozoin. The absorption of the optical energy and conversion to heat by the crystal causes rapid evaporation of the surrounding liquid, creating nanobubbles. The mechanical force generated by the collapse of these nanobubbles was sufficient to destroy the infected erythrocyte within nanoseconds (Hleb and Lapotko, 2014). Although a 532 nm laser was used in the excitation pulse, one could imagine a similar scenario occurring in our case. Unfortunately, no absorption spectra for hemozoin above 700 nm has been reported (Lee *et al.*, 2012).

At the time of writing, Pan *et al.*, (2018) was able to image spectrin and actin in uninfected erythrocyte with 3D-STORM by letting the cells adhere to poly-lysine coated coverslip before fixation to create a flat surface for optimal imaging. Both the spectrin and actin images reported had much more regular labelling than ours, most likely due to the flattened surface of the cell. However, the images still fail to show filamentous structures as would be seen by the

reconstructions from cryo-EM (Cyrklaff *et al.*, 2011). This is not to say that STORM is inferior to cryo-EM – only that the extraction of relevant information such as filament length, orientation or branching from pointillistic reconstructions would need much more careful analysis of the data and one cannot rely simply on the visual information of the images as one may have been accustomed to in confocal microscopy.

Despite the advances in super-resolution microscopy, cryo-EM is still a very important tool in imaging transient and fragile ultrastructures. Although incompatible with live cell imaging, the plunge-frozen sample could give us a snapshot into a cell which has been preserved at close-to-life state. Both techniques have their own limitations but with the emergence of super-resolution microscopy, scientists now have more options than ever in their toolbox to help investigate the inner workings of cells and proteins.

3.6 Outlook

Although both *d*STORM and STED microscopy failed to distinguish the differences in actin filaments in uninfected vs HbAA-infected erythrocytes, there are still several potential experiments that could be attempted.

Gokhin *et al.*, (2015) reported a 60% decrease in soluble G-actin after treatment of the erythrocyte with Jasplakinolide, a drug which enhances actin nucleation. However, the corresponding TIRF image of F-actin shows no visible differences when compared to non-treated samples. The differences in cortical F-actin may become more apparent at higher resolution.

Cortical actin in uninfected erythrocytes are also bound by tropomyosin, tropomodulin and adducin. What happen to these molecules as the parasite remodels the host actin cytoskeleton is as yet unknown. Super-resolution microscopy may be able to help clarify the fates of these proteins.

Alternatively, there are still a lot of unanswered questions with regards to parasitic protein export pathway, knob assembly and adhesin clustering, to name a few. Putting aside the problems associated with visualisation of actin and spectrin, using super-resolution microscopy to localise other proteins of interest might reveal some interesting paradigm – especially now that we are able to first use SuReSim to determine if *d*STORM experiments would yield meaningful outcomes or not (Venkataramani *et al.*, 2016).

4 Project II: Kinetics of protein export in infected haemoglobinopathic erythrocytes

Cytoadhesion of infected erythrocytes to the microvasculature of vital organs is one of the key hallmarks of severe malaria pathogenesis. Both the levels of cytoadhesion and the amount of surface adhesin, PfEMP1, are reduced in infected haemoglobinopathic erythrocytes, relative to infected HbAA erythrocytes (Fairhurst *et al.*, 2005; Cholera *et al.*, 2008). Cyrklaff *et al.*, (2011) have previously reported that *Plasmodium falciparum* is able to reorganise host actin cytoskeleton into long filamentous structures that seemed to be involved in the trafficking and display of PfEMP1 on knobs. This process is also found to be impaired in haemoglobinopathic erythrocytes (Cyrklaff *et al.*, 2011). Coupled with the aberrant knob structures and distribution, these findings indicate possible disruptions in the parasitic export pathway of infected haemoglobinopathic erythrocytes.

Previous studies have mostly performed experiments with infected HbAA erythrocytes or infected haemoglobinopathic erythrocytes at particular stages in the intra-erythrocytic life cycle; for instance, most adhesion assays are performed with trophozoites or schizonts, where the level of surface adhesin expressions are highest (Fairhurst *et al.*, 2005; Cholera *et al.*, 2008). Madhunapantula *et al.*, (2007) characterised the adhesion phenotype of infected HbAA erythrocytes to placental CSPG between 6 – 46 h post infection. However, the kinetics of placental adhesion phenotype during the entire intraerythrocytic cycle has never been described for infected haemoglobinopathic erythrocytes before.

4.1 Aim of the study

In this project, we aim to investigate the kinetics of adhesion phenotype and protein export in infected HbAA and haemoglobinopathic erythrocytes over the course of the 48 h intra-erythrocytic cycle. This would help to further investigate the impact of haemoglobinopathic erythrocytes on the parasitic protein export system and quantitatively describe the dynamics of reduced cytoadhesion in more detail.

4.2 Infected haemoglobinopathic erythrocytes exhibited delayed and reduced adherence and surface antigen presentation

Tightly synchronized FCR3-CSA parasites, pre-selected for their CSA-adhesive phenotype, were cultured in erythrocytes containing either HbAA, HbAS or HbCC, henceforth referred to only by their haemoglobin variants, for two replication cycles before the start of the experiments. Purified chondroitin sulfate A (CSA) was used as a surrogate receptor for placental malaria. The number of infected erythrocytes used for the static adhesion assay was kept constant between all timepoints and haemoglobin variants. All experiments were performed as paired and parallel assays, with infected HbAA erythrocytes as a control.

The number of adherent cells at each timepoint was quantified and a sigmoidal function was fitted to the dataset for each haemoglobin variant (Fig 4-1a). Both HbAA and HbAS first exhibited signs of adherence around 14 h post infection (p.i.) and reached a plateau of maximal adherence around 26 h p.i. However, infected HbAS showed an approximately 40% reduction in the final number of adherent cells/mm^2 relative to infected HbAA (513±102 cells/mm^2 for HbAS and 876±211 cells/mm^2 for HbAA, respectively, $p < 0.01$).

A slower increase in the kinetics of adherence was also observed in infected HbAS. Linear functions fitted to the slope of each dataset revealed that in infected HbAS, adherence rose at a rate of 20±2 cells per hour, compared to 61±4 cells per hour in infected HbAA (Fig 4-1a, $p < 0.01$). Infected HbCC showed no adhesive phenotype at all.

We then went on to investigate the temporal appearance of parasitic adhesins on the erythrocytic surface in both HbAA and haemoglobinopathic erythrocytes (Fig 4-1b). Samples were taken at specified time points and fixed with 0.05% glutaldehyde (GA). Quantification of surface adhesins was carried out by flow cytometry, using pooled sera from individuals living in malaria holoendemic regions from Burkina Faso as the primary antibody.

Similar to the trend seen in the adhesive phenotypes, surface adhesins were detected in infected HbAA and HbAS from 16 h p.i. onwards, with the temporal increase of 30±4 arbitrary fluorescence units per hour in HbAA and 10±4 arbitrary fluorescence units per hour in HbAS (Fig 4-1b, $p < 0.01$). The final plateau value for infected HbAS was also approximately 50% less than those for infected HbAA erythrocytes (157±20 units and 373±52 units, respectively) (Fig 4-1b, $p < 0.01$). No surface antigen was detected for infected HbCC until 36 h p.i. and the maximum value detected was even lower than those in infected HbAS at 94±8 arbitrary fluorescence units (Fig 4-1b).

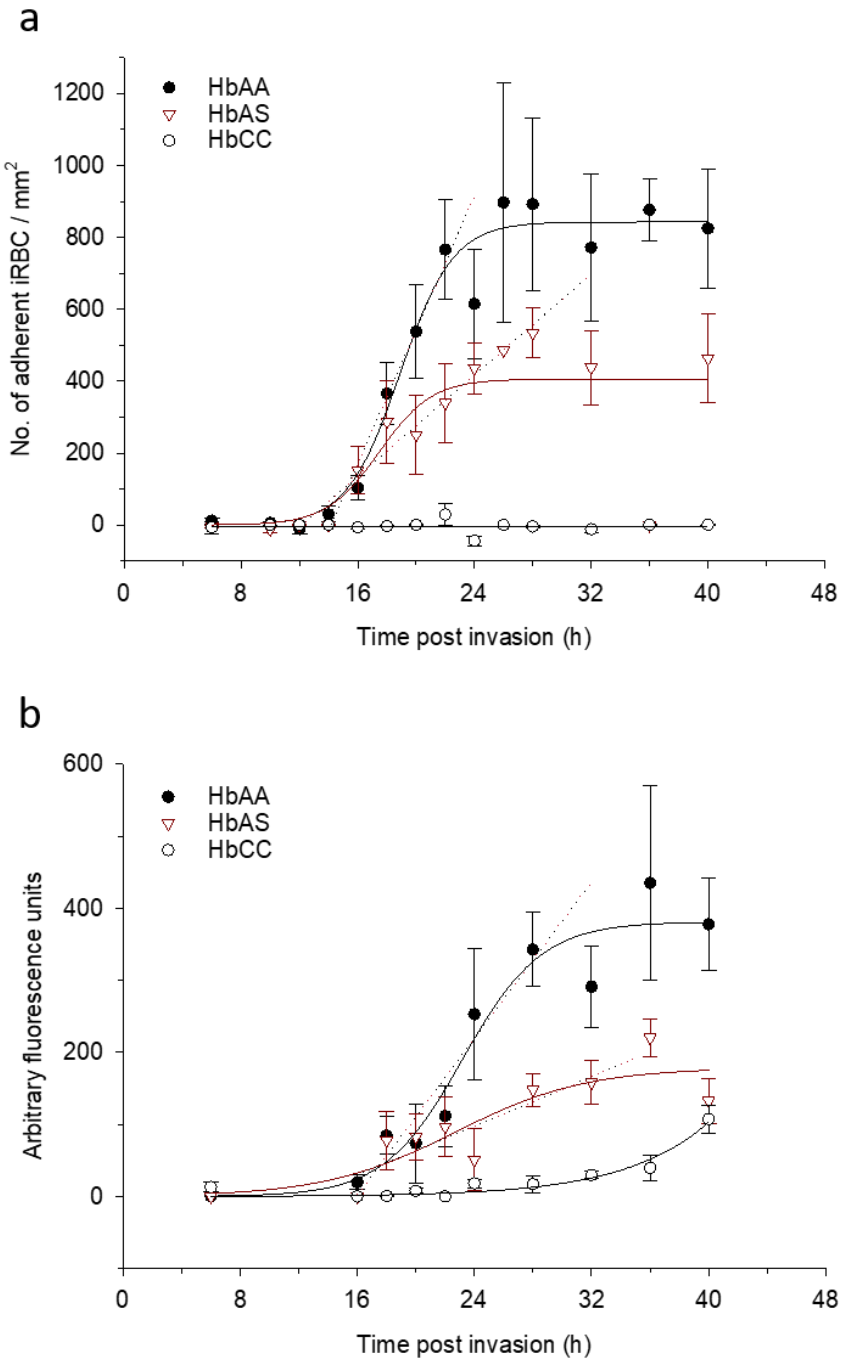

Figure 4-1 Kinetics of adhesion and surface antigen presentation in infected HbAA and haemoglobinopathic erythrocytes.

(a) Static adhesion assay was performed on tightly synchronized FCR3-CSA parasite cultures at specified time points between 6-40 hrs post infection. The number of CSA-adherent cells were quantified by Giemsa staining and image analysis with FIJI. All experiments were performed as paired and parallel assays with infected HbAA samples as control. Each data point represents the mean of at least three independent biological replicates with blood donated from at least three different donors ± standard error of the mean. (b) Surface antigen presentation of each Hb variant was assessed using FACS and pooled sera from residents of malaria endemic regions in Burkina Faso. Samples were taken at specified time points and fixed with 0.05% GA. Further steps were carried out as stated in the protocol. All experiments were performed in paired and parallel assays with infected HbAA samples as control and each data point represents the mean of at least three independent biological replicates with blood donated from at least three different donors ± standard error of the mean. Figures adapted from Kilian *et al.*, (2015)

4.3 Infected haemoglobinopathic erythrocytes exhibited delayed onset and activation of the New Permeability Pathway

As infected HbAS showed delayed kinetics in both surface adhesin presentation and adherent phenotype, we wondered if this phenomenon could also be seen in other pathways unrelated to cytoadhesion. The New Permeability Pathway (NPP), first described in 1983 by Ginsburg *et al.*, (1983), is responsible for the increase in permeability of the erythrocytic membrane to a wide range of solutes, including amino acids, peptides, sugars and different organic and inorganic ions (Kirk and Lehane, 2014). The molecular components of the NPP as well as its physiological functions are still currently under investigation and is a matter of some debate (Ginsburg and Stein, 2004; Staines *et al.*, 2004; Thomas and Lew, 2004; Kirk and Lehane, 2014). The NPP has been hypothesised to be involved in uptake of essential nutrients from the plasma, excretion of parasitic waste product and the swelling of late-stages infected erythrocytes due to the dissipation of the Na^+/K^+ gradient and the subsequent influx of water (Mauritz *et al.*, 2009; Kirk and Lehane, 2014).

In order to investigate the kinetics of NPP development in parasitized HbAA and haemoglobinopathic erythrocytes, sorbitol-induced haemolysis was used as a read-out. Samples of highly synchronised parasites were taken every 4 h throughout the 48 h intra-erythrocytic cycle and lysed in iso-osmotic sorbitol lysis buffer as previously described (Kirk *et al.*, 1994). Spectroscopic absorbance at 540 nm wavelength (A_{540}) is correlated to the amount of haemoglobin released due to cell lysis. This was used to semi-quantitatively describe the establishment and functionality of the NPP as the osmosis of water into the cell would increase after influx of sorbitol through the NPP, driving cell lysis. All experiments were performed in a paired and parallel assay with infected HbAA erythrocytes as control. The mean of at least three independent experiments ± standard error of mean for each timepoint and each haemoglobin variant was plotted, and a three parameter Hill function fitted to each dataset (Fig 4-2). For ease of visual comparison, a dotted line indicating 50% induction of the NPP in infected HbAA erythrocyte was also shown. This corresponded to 26 h p.i. in infected HbAA and 30 h p.i. in both infected HbAS and HbAC erythrocytes (Fig 4-2). F-statistic also showed a significant difference between the timecourses of NPP induction and development between infected HbAA and HbAS and HbAA and HbAC (Fig 4-2, $p < 0.001$ in both cases) but no significant difference between infected HbAS and HbAC samples (Fig 4-2, $p < 0.77$).

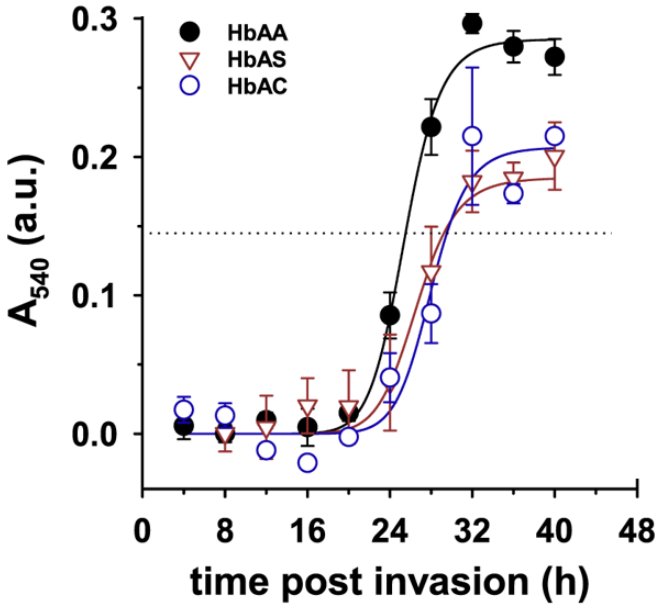

Figure 4-2 Induction of the new permeability pathways (NPP) in infected HbAA and haemoglobinopathic erythrocytes.

Samples of infected erythrocytes were taken at specified timepoints throughout the 48 h intra-erythrocytic cycle. Onset and development of the NPP were assessed through sorbital-induced hemolysis. Absorption spectroscopy at 540 nm wavelength (A_{540}) was used to quantify the amount of haemoglobin released. Dotted line designates a 50% NPP induction in infected HbAA erythrocytes. All experiments were performed in paired and parallel assays with infected HbAA samples as control and each data point represents the mean of at least three independent biological replicates with blood donated from at least three different donors ± standard error of the mean. Statistical significance between each dataset was calculated using F-statistics ($p < 0.001$ between HbAA and HbAS, $p < 0.001$ between HbAA and HbAC and $p < 0.77$ between HbAS and HbAC). a.u. – arbitrary units. Figure adapted from Waldecker *et al.*, (2017). Data generated in a collaboration with Dr. Christine Lansche.

4.4 Discussion

Our timecourse for CSA-adhesion in infected HbAA erythrocytes agreed well with previously publish result for adherence to Cluster of Differentiation 36 (CD36), intercellular adhesion molecule-1 (ICAM-1) and thrombospondin (TSP) (Gardner *et al.*, 1996). In contrast, Madhunapantula *et al.*, (2007) showed that adhesion to isolated placental chondroitin sulfate proteoglycan (CSPG) exhibits a peak adhesion at 22 to 26 h p.i. then the binding capacity gradually decreased during trophozoite maturation instead of remaining constant. They have argued that this could be due to the increase in apperance of other parasitic export proteins on the surface of the infected erythrocytes, which could sterically mask the chondroitin-4-sulfate (C4S) binding protein(s). They hypothesised that the parasite could utilize this mechanism to limit exposure of the adhesin to the host immune system. However, this seems somewhat self-contradictory since the reduction in binding capability at the late trophozoite/schizont stage

would also result in many parasitized erythrocytes being unable to escape splenic clearance and thus enable the host to generate of parasite-specific adaptive immune response, to the detriment of the remaining parasites (Engwerda *et al.*, 2005; Del Portillo *et al.*, 2012).

One possible explaination for the discrepancy between our result and those published by Madhunapantula *et al.*, (2007) could be the difference in the ligand used for the adhesion assays: bovine chondroitin sulfate A (CSA) was used in our experiment while low-sulfated CSPG isolated from the placenta was used in theirs. Although many studies have previously used CSA-coated petri dishes to investigate the binding characteristics of CSA-adherent iRBCs (Beeson *et al.*, 1999; Achur *et al.*, 2000; Alkhalil *et al.*, 2000), new methodologies have emerged which attempt to mimic *in vivo* settings more closely. Placental cryosections have previously been used (Flick *et al.*, 2001; Avril *et al.*, 2004; Muthusamy *et al.*, 2004) but one could argue that the fixation and cryopreservation may cause some damage to the receptors and epitopes present, despite attempts otherwise. The fixation and cryopreservation also prevented studies of signalling pathways and downstream consequnces of the binding on the trophoblasts (Lucchi *et al.*, 2006). For such studies, as well as further cytoadhesion studies, the human syncytiotrophoblast and the choriocarcinoma cell line (BeWo) has been adopted (Haase *et al.*, 2006; Lucchi *et al.*, 2006; Viebig *et al.*, 2006). Most recently, Pehrson *et al.*, (2016) described a method to profuse freshly donated placenta for *ex vivo* studies of adherent phenotypes under physiological flow conditions in the villous trees. Although this is by far the method with conditions nearest to the *in vivo* placental tissue, it does require access to the labor ward and prompt delievery of freshly donated placenta, so it remains to be seen if this method could become more widely used in the field.

With regards to the adherence phenotype of infected haemoglobinopathic erythrocytes (Fig 4-1a), our results are in good agreement with previously published data, even though the receptors under investigation were different: infected HbCC erythrocytes show no adhesion to both human dermal microvascular endothelial cells (HDMECs) and human microvascular endothelial cells (HMVECs) (Fairhurst *et al.*, 2005; Cholera *et al.*, 2008) and infected HbAS show approximately 50% reduction in adhesion to HMVECs relative to infected HbAA erythrocytes (Cholera *et al.*, 2008).

The detection of surface antigen at 16 h p.i. (Fig 4-1b) is also supported by both Kriek *et al.*, (2003) and Dahlbäck *et al.*, (2007) for parasitized HbAA erythrocytes. The timing is consistant with the results published by Kyes *et al.*, (2000), demonstrating that transcription of *var* genes begins as early as 3 h p.i. and peaks at approximately 10-12 h p.i. Cholera *et al.*, (2008) showed

that the reduction in surface PfEMP1 signal for parasitised HbAS erythrocytes is approximately 14% relative to parasitized HbAA, which is much lower than our 50% reduction. However, this maybe explained by the fact that pooled sera was used in our experiments while PfEMP1-specific antibody was used in the other study. For parasitized HbCC erythrocytes, our result of approximately 75% reduction in surface antigen presentation relative to parasitized HbAA erythrocytes is also in agreement with previously published data (Fairhurst *et al.*, 2005).

The delayed onset of the NPPs seen in infected haemoglobinopathic erythrocytes are also in agreement with other reports of delayed protein export in infected haemoglobinopathic erythrocytes (Kilian *et al.*, 2015). No significant reduction in the replication rates and hemozoin digestion in infected haemoglobinopathic erythrocytes were observed in our experiments (Waldecker *et al.*, 2017), also in agreement with previously published report (Kilian *et al.*, 2015). NPP impacts the volumetric changes of the infected erythrocyte over the course of the intra-erythrocytic life cycle through the pertubation of the Na^+/K^+ gradient. The delay in its establishment would account for the delay in volume expansion seen in infected HbAC erythrocytes as well as infected HbAS, although to a lesser extent (Waldecker *et al.*, 2017). Not only does the change in cell shape affects its cytoadhesive properties such as contact area as well as its behaviour in flow, it also affects endothelial cell activation and host immune responses (Lansche *et al*., manuscript under preparation). This would most likely contribute to the molecular mechanism by which haemoglobinopathic erythrocytes protect its carrier against the severe complications of malaria.

4.5 Outlook

Our results contribute to the growing collection of evidence that delayed protein export, reduced surface adhesin presentation and reduced cytoadhesive phenotype are involved in the protection of haemoglobinopathic carriers against severe malaria. However, more molecular detail behind this protection remains to be elucidated.

Previous reports suggest that the parasite's inability to reorganise host actin cytoskeleton in infected haemoglobinopathic erythrocytes leads to the impaired presentation of PfEMP1 adhesin at the erythrocytic surface as actin is believed to be involved in vesicular transport of proteins between the Maurer's clefts and the knobs (Cyrklaff *et al.*, 2011; Cyrklaff *et al.*, 2012; Rug *et al.*, 2014). Our result with the delayed establishment of NPP in infected

haemoglobinopathic erythrocyte suggests a wider range of affected proteins and processes. It would be interesting to investigate the fates of proteins involved in both the export pathway between the parasitophorous vacuole (PVM) and the erythrocyte cytoplasm such as components of the PTEX (Chisholm Scott *et al.*, 2018). In addition, the involvement of chaperones and other proteins in transporting the parasitic protein through the host cytoplasm to the Maurer's clefts such as PfTRiC (Mbengue *et al.*, 2015) remains to be investigated for infected haemoglobinopathic erythrocytes.

Kilian *et al.*, (2013) also reported that in infected haemoglobinopathic erythrocytes, the movements of the Maurer's clefts were faster compared to infected HbAA erythrocytes. Additionally, the malformed Maurer's cleft ultrastructures seen in electron micrographs of infected haemoglobinopathic erythrocytes (Cyrklaff *et al.*, 2011; Cyrklaff *et al.*, 2016) strongly suggest that both the formation and the function of the Maurer's clefts have been adversely affected. Insights into the protein sorting machinery and the establishment and maintenance of the Maurer's clefts, as well as the fates of its resident proteins, would also be of great benefit to our understanding of the molecular mechanism of protection against severe malaria conferred by haemoglobinopathic erythrocytes.

5 Project III: Oxidative pre-treatment of uninfected erythrocytes to mimic the protective phenotypes of haemoglobinopathic erythrocytes

As previously mentioned, there have been many reports describing the differences between infected HbAA and haemoglobinopathic erythrocytes in cytoadhesion, protein transport kinetics, host actin remodelling as well as knobs and Maurer's clefts morphologies (Fairhurst *et al.*, 2005; Cholera *et al.*, 2008; Cyrklaff *et al.*, 2011; Cyrklaff *et al.*, 2012; Kilian *et al.*, 2013; Kilian *et al.*, 2015; Waldecker *et al.*, 2017). Fetal haemoglobin (HbF) is also believed to be one of the key contributing factors to the protection against severe malaria in the first six months of life, with reported impaired cytoadhesion and abnormal display of PfEMP1 on the erythrocytic surface (Amaratunga *et al.*, 2011). Although the precise molecular mechanisms underlying these changes have yet to be elucidated, some features appear to be common to the haemoglobinopathies conferring protective phenotypes. These include abnormal accumulation of heme and hemichromes on the erythrocytic membranes as well as an abundance of reactive oxygen species (ROS) such as superoxide radicals generated from accelerated heme autooxidation (Hebbel *et al.*, 1982; Hebbel *et al.*, 1988; Chaves *et al.*, 2008). Oxidised forms of haemoglobin also interfere with the parasite's ability to remodel host actin into long filamentous network (Cyrklaff *et al.*, 2011). However, the involvement of oxidative stress and oxidised haemoglobin products as parts of the mechanisms of protection against severe malaria by haemoglobinopathic erythrocytes has yet to be investigated.

5.1 Aim of the study

In order to examine the involvement of oxidative stress and irreversibly oxidised haemoglobin as a mechanism of protection against severe malaria, the pro-oxidative environment of uninfected haemoglobinopathic erythrocytes will be experimentally replicated.

Uninfected HbAA erythrocytes were transiently exposed to various oxidative agents prior to infection with *Plasmodium falciparum* parasites. Various parameters associated with pathogenicity such as cytoadhesion, levels of surface PfEMP1, and knobs and Maurer's cleft morphologies were investigated to determine the degree to which the oxidative pre-treatments were able to replicate the effects seen in infected haemoglobinopathic or fetal erythrocytes.

5.2 Transient oxidative insult to uninfected HbAA erythrocytes reduces cytoadhesion and surface VAR2CSA expression, phenotypes characteristic of infected haemoglobinopathic and fetal erythrocytes

Uninfected HbAA erythrocytes were subjected to transient oxidative stress through incubation with 1 mM of either hydrogen peroxide (H_2O_2), tert-butyl hydroperoxide (tBOOH) or menadione sodium bisulfite (MD). Both H_2O_2 and tBOOH have been widely used as oxidising agents in various *in vitro* systems (Srivastava *et al.*, 1974; Caprari *et al.*, 1995; Zou *et al.*, 2001) and are able to diffuse freely across the plasma membrane due to their small size and lipophilic nature, respectively. Menadione sodium bisulfite, also used as a water-soluble form of vitamin K_3 precursor in animal feeds, has likewise been widely used to study oxidative stress (Chiou and Tzeng, 2000; Criddle *et al.*, 2006; Heart *et al.*, 2012). It generates intracellular ROS through redox-cycling in the presence of molecular oxygen (Thor *et al.*, 1982; Desagher *et al.*, 1997; Criddle *et al.*, 2006). This would more closely reflect the physiological conditions found in haemoglobinopathic erythrocytes, where ROS are constantly generated, in contrast to direct exposure to H_2O_2, which has a more transient effect (Heart *et al.*, 2012).

The irreversibly oxidised ferryl haemoglobin and hemichromes have been shown to inhibit *in vitro* actin polymerisation and destabilise interactions between actin, spectrin and protein 4.1 (Jarolim *et al.*, 1990; Cyrklaff *et al.*, 2011). Reversible oxidative damage caused by the transient oxidative pre-treatment was alleviated by incubating the freshly pre-treated erythrocytes with 1 mM dithiothreitol (DTT) (Caprari *et al.*, 1995) before storage and use in cell culture of *Plasmodium falciparum*. We also treated uninfected HbAA erythrocytes with DTT alone to control for possible effects that may arise from the reducing agent. The treatment of HbCC with DTT would serve as a control to distinguish between possible effects of reversible and irreversible oxidative damage on the aberrant morphologies and cytoadhesive phenotypes seen in infected HbCC erythrocytes.

The fitness of the parasites grown in pre-treated, haemoglobinopathic or fetal erythrocytes were monitored through replication rates and hemozoin quantification. The replication rates of parasites grown in all Hb variants and pre-treated HbAA were recorded over at least eight replication cycles and the mean ± SEM is summarised in Table 5-1. As indicated, both the parasitized pre-treated erythrocytes and those cultivated in haemoglobinopathic or fetal

erythrocytes have comparable replication rates to infected HbAA erythrocytes, similar to previous reports (Kilian *et al.*, 2013; Kilian *et al.*, 2015).

While the replication rates demonstrated that the parasites were able to complete their asexual replication cycle regardless of the haemoglobin variant or the pre-treatments of HbAA erythrocytes that they have been cultured in, the comparable amount of hemozoin incorporation suggests that the parasites cultured in all conditions were equally metabolically active during their intra-erythrocytic life cycle (table 5-1).

Table 5-1 Replication rate and hemozoin digestion levels of parasites in haemoglobinopathic and pre-treated HbAA erythrocytes.

FCR3-CSA parasites were cultured in indicated haemoglobin variant or pre-treated HbAA erythrocytes and the replication rates documented over at least eight replication cycles. The mean replication rates ± standard error of mean is displayed below. The amount of hemozoin digested by schizont-stage parasite cultivated in designated haemoglobin variant or pre-treated HbAA erythrocytes for at least two replication cycles was quantified according to stated protocol (Schwarzer *et al.*, 1992). All experiments were done as paired and parallel assays with infected HbAA as positive control. The value is the mean of at least three independent biological replicates ± standard error of mean. H_2O_2 – hydrogen peroxide; tBOOH – tert-butyl peroxide; MD – menadione; DTT – dithiothreitol.

Hb variant	Replication Rate (per cycle)	Normalised amount of hemozoin (%)
HbAA	**11.5 ± 0.7**	**100**
HbAS	**10.8 ± 0.5**	**108 ± 5**
HbAC	**12.1 ± 0.4**	**98 ± 19**
HbF	**11.8 ± 0.4**	**106 ± 4**
HbAA – H_2O_2	**11.7 ± 0.5**	**104 ± 2**
HbAA – tBOOH	**10.9 ± 0.6**	**107 ± 4**
HbAA – MD	**11.1 ± 0.3**	**113 ± 13**
HbAC – DTT	**10.6 ± 0.5**	**97 ± 8**
HbAA – DTT	**12.1 ± 0.4**	**106 ± 3**

After at least two replication cycles in specified Hb variant or pre-treated HbAA, tightly synchronised trophozoite stage parasitized erythrocytes were taken as samples to investigate their CSA-adhesion phenotype and the amount of surface-presented VAR2CSA (Fig 5-1a and b). To measure the CSA-adhesive phenotype, 1 mg/ml of purified bovine CSA were used as a

surrogate receptor for parasite adhesion in placental intervillous space. The amount of adhesive parasites were stained with Giemsa and quantified microscopically. All experiments were performed in paired and parallel assays and normalised to their respective infected HbAA control sample (Fig 5-1a). Each dot on the graph represents an independent experiment and the mean for each Hb variant is indicated by the red line.

Relative to infected HbAA control, all infected haemoglobinopathic, fetal or pre-treated Hb AA erythrocytes exhibited significantly reduced CSA adhesion ($P < 0.001$ according to Kruskal-Wallis one-way analysis of variance test). The level of CSA adhesion seen in pre-treated HbAA erythrocytes was also of comparable range to those seen in parasitized haemoglobinopathic and fetal erythrocytes: iHbAS 53%, iHbAC 27%, iHbF 45%, iHbAA-H_2O_2 25%, iHbAA-tBOOH 33%, iHbAA-MD 16% (Fig 5-1a). Pre-treatment of uninfected HbAA with DTT alone had no effect on the adhesion phenotype (Fig 5-1a, iHbAA-DTT) while pre-treatment of HbAC with DTT could not rescue the reduced adherence phenotype (Fig 5-1a, iHbAC-DTT).

A similar trend was observed for the amount of surface VAR2CSA detected by flow cytometry (Fig 5-1b). The amount of VAR2CSA detected on the erythrocytic surface was significantly reduced in infected fetal and haemoglobinopathic erythrocytes as well as in infected pre-treated HbAA erythrocytes, relative to infected HbAA erythrocytes ($P < 0.001$ according to Kruskal-Wallis one-way analysis of variance test). Pre-treatment of HbAC with DTT still resulted in the same level of VAR2CSA as those seen in infected HbAC erythrocytes.

To investigate the cause of the reduction in cytoadherence and surface adhesin presentation in more detail, the mRNA expression level of *var2csa* was quantified with quantitative reverse transcription PCR (qRT-PCR). Instead of collecting the samples at trophozoite stage as we've done for the previous two assays, the samples were collected at ring stage, approximately 12 h p.i., as it was shown to be the peak of *var* transcription level (Kyes *et al.*, 2000; Dahlbäck *et al.*, 2007). The mRNA level of *cyclophilin* was used as internal control and the result for each condition was normalised to the paired infected HbAA control sample. The mean of at least three independent biological replicates and three independent blood donors ± SEM for each condition was plotted (Fig 5-1c). There were no statically significant differences between the *var2csa* mRNA levels of all infected Hb variants and pre-treatments.

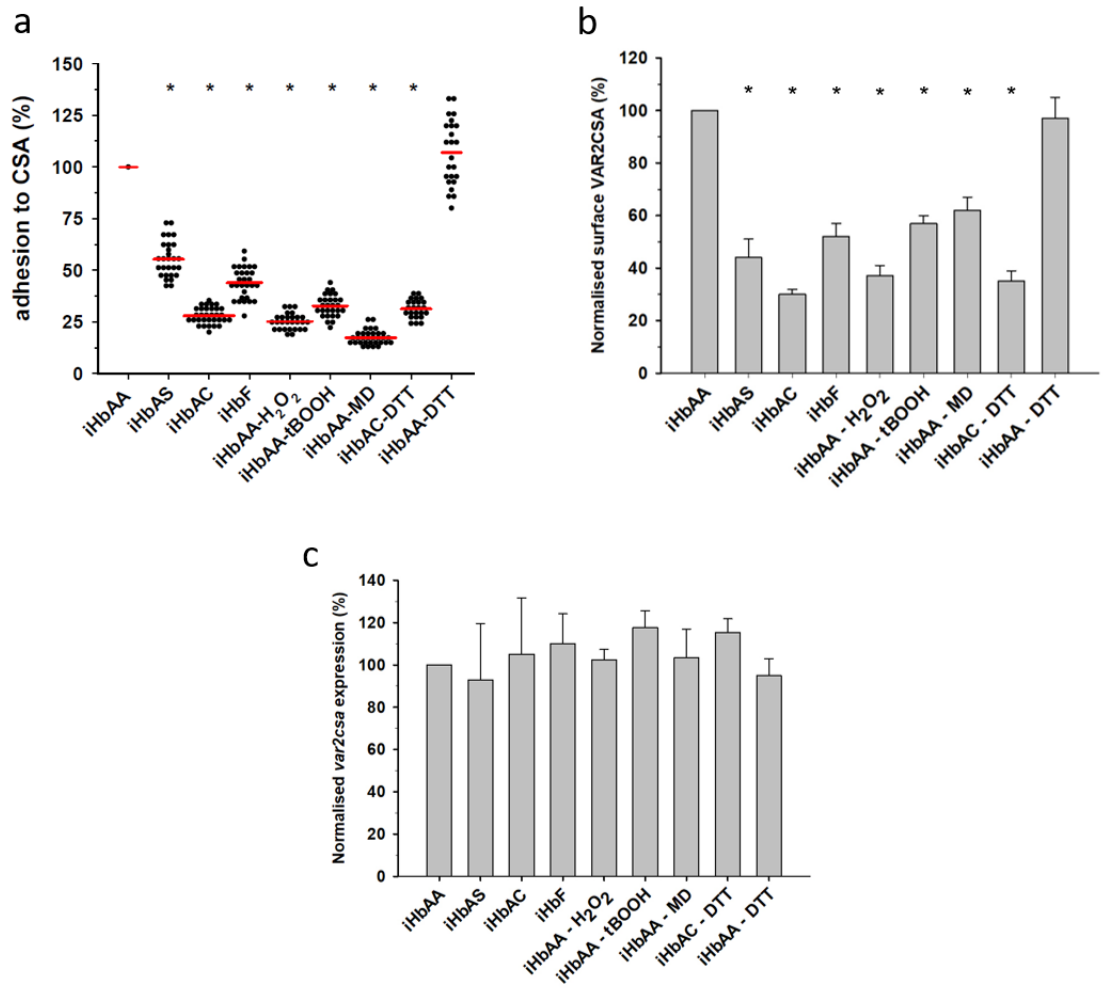

Figure 5-1 Effects of oxidative pre-treatments of HbAA erythrocytes on CSA adhesion, surface PfEMP1 levels and mRNA expression level, relative to infected haemoglobinopathic and fetal erythrocytes.

Prior to infection with the CSA adhesive strain of *Plasmodium falciparum* (FCR3-CSA), uninfected HbAA erythrocytes were transiently exposed to 1 mM of different oxidative agents; either hydrogen peroxide (H_2O_2), tert-butyl peroxide (tBOOH) or menadione (MD). 1 mM of dithiothreitol (DTT) was used to restore the redox balance of the uninfected HbAA erythrocytes after the oxidative pre-treatment. The prefix "i" indicates infected erythrocytes. All experiments were performed in paired and parallel assays with infected HbAA erythrocytes as control. (a) After at least two replication cycles in pre-treated, haemoglobinopathic or fetal erythrocytes, the level of CSA-adhesiveness at trophozoite stage (20 – 30 h p.i.) was measured. Each dot in the graph represents a mean value for an independent experiment, normalised to its paired HbAA values. The red line indicates the mean values for each Hb variant or pre-treatments. **P* < 0.001 compared with parasitized HbAA erythrocytes (Kruskal-Wallis one-way analysis of variance test). (b) Amount of surface VAR2CSA presented was detected by flow cytometry with rabbit antiserum against recombinant domains of VAR2CSA. Samples were harvested at trophozoite stage (24-26 h p.i.) and prepared according to previously published protocol (Barfod *et al.*, 2006). The mean fluorescence was normalised to infected HbAA readouts in each paired experiment. Error bars indicate SEM. **P* < 0.001 compared with parasitized HbAA erythrocytes (Kruskal-Wallis one-way analysis of variance test). (c) *var2csa* mRNA levels in parasitized Hb variants and pre-treated HbAA erythrocytes as detected by qRT-PCR. Samples were harvested at ring stages (12 h p.i.) and prepared according to established protocol (Cyrklaff *et al.*, 2016). The qPCR results were normalised against levels of *cyclophilin* transcripts in each sample as internal controls. The result for each conditions was normalised to its paired HbAA value and the mean plotted. Error bars indicate SEM. Figure adapted from Cyrklaff *et al.*, (2016).

5.3 Infected pre-treated HbAA erythrocytes exhibited knob and Maurer's cleft morphologies comparable to infected haemoglobinopathic erythrocytes

The morphologies of the Maurer's clefts and knobs in infected haemoglobinopathic and fetal erythrocytes have previously been reported by Cholera *et al.*, (2008), Fairhurst *et al.*, (2005) and Amaratunga *et al.*, (2011). However, the TEM sample preparations were done through chemical fixation and Epon embedding. In order to minimize possible artifacts and ultrastructural damages, we perserved our samples with high pressure freezing/freeze substitution (HFP/FS) for TEM examinations. As opposed to chemical fixation, where the rate at which the sample can be preserved is limited by the diffusion of fixatives or cross linkers through the sample, HPF repidly freezes the sample at very low temperatures in a nanoseconds timescale. This allows preservation of the ultrastructures as well as other processes in the cell, whereby the water inside and around the cell turns to vitreous ice and prevents formation of ice crystals that would damage the structures (Griffiths *et al.*, 1984; Müller and Moor, 1984; Griffiths *et al.*, 1993).

In order to avoid possible artifacts and discrepancies that may arise due to differences in sample preparation techniques, we chose to prepare all samples by HPF instead of relying on previously published images for the knobs and Maurer's cleft morphologies. Transmission electron micrograph of 100 nm thick sections are shown in figure 5-2, first column (TEM). Magnified images of knobs and Maurer's clefts can be seen to the right of the images. We did not detect any distinguishable morphological differences in the developing parasites grown in haemoglobinopathic, fetal or oxidatively pre-treated erythrocytes (Fig 5-2). However, both oxidatively pre-treated samples and DTT-treated HbAC sample exhibited ulterations in their ultrastructures such as enlarged and dispersed knobs as well as malformed Maurer's clefts. The aberrant knob distribution and phenotypes could be more clearly observed in scanning electron micrograph (Fig 5-2, right column); only infected HbAA erythrocytes exhibited small, regular, and numerous knobs on the surface of the infected erythrocyte.

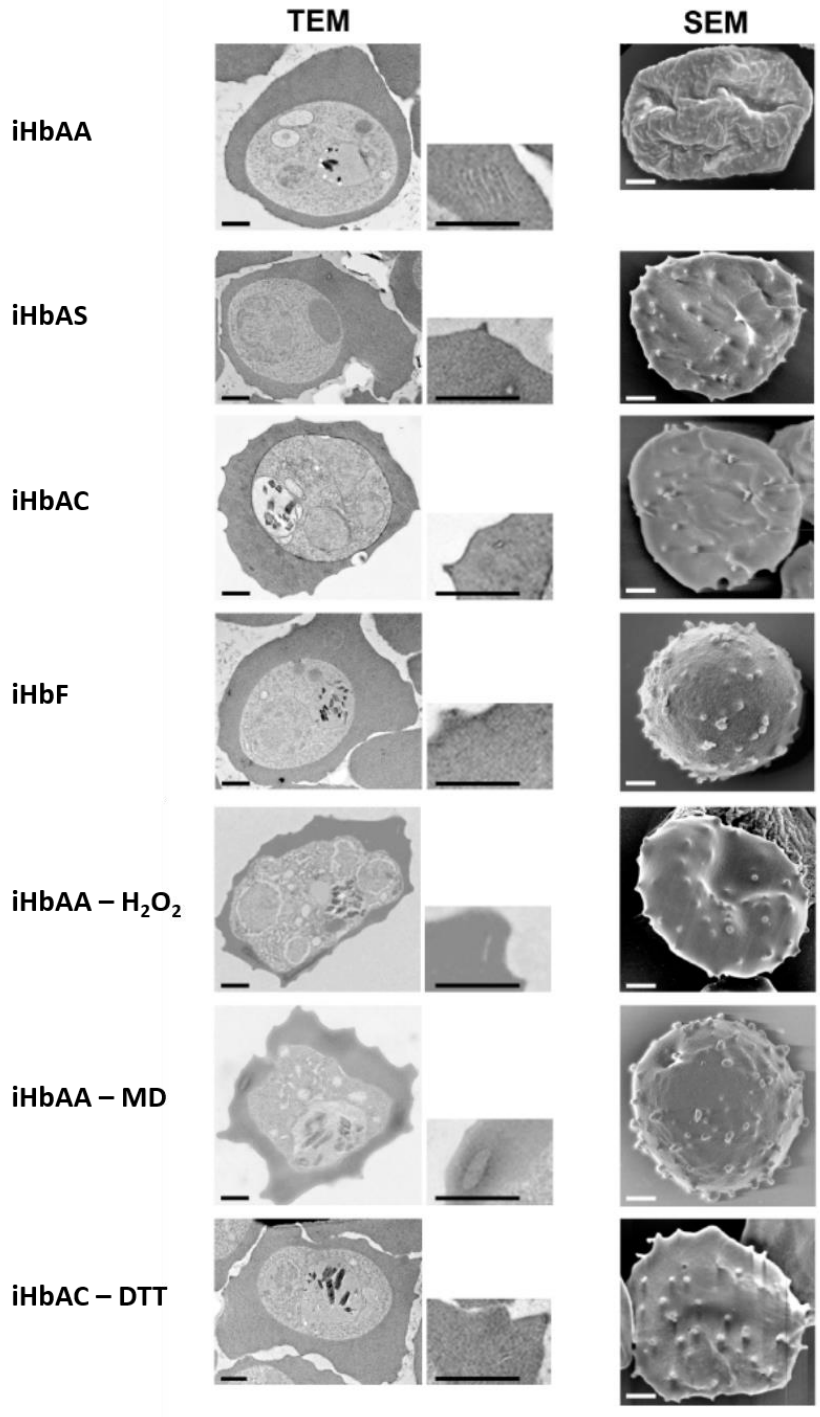

Figure 5-2 Ultrastructural morphologies in infected Hb variants and pre-treated HbAA erythrocytes.

Parasitized trophozoite-stage erythrocytes cultured for at least two replication cycles in haemoglobinopathic, fetal or pre-treated HbAA erythrocytes were taken for imaging with transmission and scanning electron microscopy (TEM and SEM, respectively) to examine the knob and Maurer's clefts morphologies. Samples for TEM were prepared by high-pressure freezing and freeze-substitution, as previously described (McDonald, 2007). A representative from at least 25 images was selected for display in each condition. A zoomed in section of knobs and Maurer's clefts are shown in the inset. SEM samples were prepared according to previously published protocol (Cyrklaff *et al.*, 2016). After chemical dehydration through ethanol series and hexamethyldisalzan, samples were sputter-coated with 5 nm gold and imaged with SEM. Images displayed are representative of at least 25 images in each condition. Scale bar 2 µm. H_2O_2 - hydrogen peroxide; MD – menadione; DTT – dithiothreitol. Figure adapted from Cyrklaff *et al.*, (2016).

5.4 Pre-treatment of uninfected HbAA erythrocytes elevated the levels of irreversibly oxidized haemoglobin to those comparable with haemoglobinopathic and fetal erythrocytes

The pre-treatment of uninfected HbAC with the reducing agent DTT prior to infection was unable to rescue the aberrant knobs and Maurer's cleft morphologies as well as the reduced adhesion phenotype. This strongly suggests the involvement of irreversible oxidized haemoglobin species in the molecular mechanisms behind the observe phenomena. In order to more precisely quantify the levels of irreversibly oxidized hemoglobin in differently treated erythrocytes, Mössbauer spectroscopy was used. This was performed in collaboration with the group of Kvestoslava Burda in Krakow, where we shipped our samples of the uninfected haemoglobinopathic, fetal or oxidatively pre-treated erythrocytes. The samples were from three independent pre-treatments or donors and were all examined by Mössbauer spectroscopy within one week of pre-treatment or acquisition, to avoid the confounding effects of erythrocyte aging. The mean values of oxy-haemoglobin, met-haemoglobin and irreversibly oxidised haemoglobin species found in each haemoglobin variant/ pre-treatment are summarised in Table 5-2.

Table 5-2 Levels of oxidized haemoglobin species found in different variants of uninfected erythrocytes.

Mössbauer spectroscopy was used to measure the levels of various species of oxidized haemoglobin in uninfected haemoglobinopathic and pre-treated HbAA erythrocytes. The results are an average between at least three different independent biological replicates ± standard error of mean. H_2O_2 – hydrogen peroxide; tBOOH – tert-butyl peroxide; MD – menadione; Hb – haemoglobin; Oxy-Hb – oxy-haemoglobin; Met-Hb – met-haemoglobin. Table adapted from Cyrklaff *et al.*, (2016).

Hb variant	Oxy-Hb (%)	Met-Hb (%)	Irreversibly oxidized Hb (%)
HbAA	**94.0**	**1.0**	**5.0**
HbAS	**85.6**	**2.3**	**12.2**
HbAC	**83.5**	**3.9**	**12.6**
HbF	**84.7**	**3.1**	**12.2**
HbAA – H_2O_2	**78.1**	**1.3**	**20.6**
HbAA – tBOOH	**77.7**	**5.4**	**16.9**
HbAA – MD	**70.1**	**7.3**	**22.0**

In all haemoglobinopathic, fetal or pre-treated samples, the levels of irreversibly oxidised haemoglobin were markedly higher than those seen in uninfected HbAA. Interestingly, the level

of met haemoglobin in the H_2O_2 pre-treated sample was comparable to those seen in uninfected HbAA erythrocytes. Pre-treatment with menadione, on the other hand, seems to elevate the level of met-haemoglobin even higher than those found in haemoglobinopathic erythrocytes.

5.5 Discussion

Haemoglobinopathic erythrocytes such as HbS and HbC are known to have reduced lifespan in circulation as well as higher accumulation of hydroxyl radicals due to haemoglobin instability and auto-oxidation (Hebbel *et al.*, 1982; Hebbel *et al.*, 1988; Rees *et al.*, 2010; Hannemann *et al.*, 2011). Previous reports have shown that parasitized HbS, HbC and HbF exhibit reduced cytoadhesion, reduced surface PfEMP1 levels and enlarged and dispersed knobs (Fairhurst *et al.*, 2005; Cholera *et al.*, 2008; Amaratunga *et al.*, 2011). Here, we were able to implicate irreversibly oxidized haemoglobin species as possible causative agents of the aforementioned protective phenotypes through the pre-treatment of HbAA erythrocytes with oxidative agents.

The comparable replication rates and hemozoin digestion levels between parasitized pre-treated HbAA erythrocytes and untreated HbAA control showed that the parasites had no problems growing in the pre-treated HbAA erythrocytes. This was also the case for infected haemoglobinopathic and fetal erythrocytes, both in our experiment and previously published studies (Fairhurst *et al.*, 2005; Cholera *et al.*, 2008; Amaratunga *et al.*, 2011). Moreover, the aberrant knobs sizes and distribution, as well as the malformed Maurer's clefts previously seen in infected haemoglobinopathic and fetal erythrocytes were also observed in our pre-treated samples, along with comparable reduction in cytoadhesion and surface adhesin levels.

The fact that pre-treatment of uninfected HbAC erythrocytes with a reducing agent (DTT) could not restore the cytoadhesion, surface adhesin levels and Maurer's cleft and knob morphologies to those seen in infected HbAA erythrocytes points to the involvement of irreversibly oxidized molecules in these processes. Surface rendered views of cryo-electron tomographic tilt series also showed that parasites in pre-treated HbAA erythrocytes were unable to reorganize host actin into long filamentous network, similar to those seen in infected haemoglobinopathic and fetal erythrocytes (Cyrklaff *et al.*, 2016). Although all of the oxidative agents used in our study have been shown to interact with actin in various ways (Bellomo *et al.*, 1990; Caprari *et al.*, 1995; DalleDonne *et al.*, 1995; DalleDonne *et al.*, 1999), this would not have been the cause of the aberrant host actin remodelling seen in the infected pre-treated erythrocytes as the H_2O_2, tBOOH and menadione were only transiently applied to the uninfected erythrocytes and were subsequently removed through washing steps and incubation with equimolar concentration of

DTT. What could be of interest, however, are the molecular mechanisms through which these oxidising agents exert their effects. H_2O_2 is able to rapidly generate ferryl (Fe^{4+}) haemoglobin and can form the highly reactive hydroxyl radical (OH·) through the ferrous iron-dependent reaction (Fenton, 1894; van den Berg *et al.*, 1992). tBOOH is found to rapidly generate radicals after reacting with cellular haemoglobin and also readily oxidized glutathione (Van der Zee *et al.*, 1989; Caprari *et al.*, 1995; Rossi *et al.*, 2001; Domanski *et al.*, 2005). Menadione is reported to undergo redox-cycling in the presence of molecular oxygen, thereby generating intracellular ROS, including H_2O_2 (Thor *et al.*, 1982; Desagher *et al.*, 1997; Criddle *et al.*, 2006; Loor *et al.*, 2010). It is also reported to oxidise the haem groups of oxy-hemoglobin to met-hemoglobin and, to a smaller extent, hemichrome (Winterbourn *et al.*, 1979). This would explain the highly elevated level of met-haemoglobin found in the MD-treated sample, according to our Mössbauer spectroscopy results (Table 5-2).

As previous studies have suggested that actin is involved in proper formation and establishment of Maurer's clefts, vesicular trafficking of parasitic proteins to the erythrocytic surface and knob formation, it is tempting to attribute the functional outcome of reduced surface adhesin presentation and cytoadhesion to disruption in the protein export pathway due to interference of irreversible oxidized haemoglobin products and other ROS with actin (Rug *et al.*, 2006; Kilian *et al.*, 2013; Cyrklaff *et al.*, 2016). However, both the delayed establishment of NPPs seen in our experiment and a previously published paper by Kilian *et al.*, (2015) suggest a broader effect of the oxidative stress in haemoglobinopathic erythrocytes on the parasitic processes and transport system, not just actin. The delayed and reduced amounts of protein translocation across the parasitophorous vacuole in infected haemoglobinopathic erythrocytes, relative to infected HbAA erythrocytes, begs the question of which other components may have been adversely affected by the oxidative milieu found in haemoglobinopathic erythrocytes.

Although the results from the pre-treated infected erythrocytes seem promising, confirmation with *ex vivo* field isolates would also be ideal as long-term parasite cultures have been shown to lower the adherence as well as knob densities of the lab strains, compared to field isolates (Achur *et al.*, 2008; Quadt *et al.*, 2012). The fact that alterations to the knob morphologies and reduced cytoadhesion observed in haemoglobinopathic erythrocytes infected with lab-strains and *ex vivo* field isolates were reported to be comparable suggests that our findings could also be representative of field isolates (Fairhurst *et al.*, 2005; Cholera *et al.*, 2008).

As pre-treatment with menadione was able to mimic the phenotypes seen in infected haemoglobinopathic and fetal erythrocytes and menadione as a drug is approved for use in

human, Cyrklaff *et al.*, (2016) further extended this research to the malaria mouse model with *Plasmodium berghei* and C57BL/6 mice. Although the mice model system remains controversial in many aspects, including an altered pathogenesis of cerebral malaria compared to those found in humans and the lack of PfEMP1 orthologues (Cabrales *et al.*, 2010; White *et al.*, 2010; Craig *et al.*, 2012), the fact that the mice pre-treated with intraperitoneal injection of menadione before challenge with *Plasmodium berghei* ANKA infected erythrocytes develop significantly less brain damage, microhaemorrhage and blood-brain barrier disruption than the untreated control remains promising. After all, one of the proposed mechanisms of action of artesunate, the current drug of choice for treatment of severe malaria, is through increased intracellular ROS and subsequent DNA damage to the parasite (Gopalakrishnan and Kumar, 2015; WHO, 2015a).

Taken together, our results suggest a key role for inherent oxidative stress and irreversibly oxidised haemoglobin as a starting point in a cascade of events, including delayed protein export and aberrant actin remodelling, which eventually lead to reduced cytoadhesion of haemoglobinopathic erythrocytes, protecting its carrier from severe complications of malaria. However, the overall picture is still far from complete. Previously published studies suggest a more complex, multifactorial mechanisms of protection against severe malaria, including disruption of parasitic protein translation by host microRNAs (LaMonte *et al.*, 2012), increased phagocytosis of infected HbAS erythrocyte by monocytes (Ayi *et al.*, 2004; Lang *et al.*, 2009) and host immune modulation (Ferreira *et al.*, 2011). There is also emerging evidence suggesting that infected haemoglobinopathic erythrocytes have reduced endothelial cell activation upon binding (Lansche *et al*., manuscript in preparation), adding another piece to the complex puzzle that is the molecular mechanisms underlying the protection against severe malaria by haemoglobinopathic erythrocytes.

5.6 Outlook

Further characterisation of the parasitized pre-treated HbAA erythrocytes would be of great interest, especially to investigate how far the induced similarities between the parasitized pre-treated erythrocytes and the haemoglobinopathic erythrocytes runs. For example, whether the parasitized pre-treated HbAA erythrocytes are able to induce endothelial cell activation or whether parasitic protein transport would also be delayed at the parasitophorous vacuole (Kilian *et al.*, 2015).

Along the same line, it would also be interesting to investigate how individual components of the *Plasmodium* translocon of exported proteins (PTEX) are affected in both haemoglobinopathic and pre-treated erythrocytes (Przyborski *et al.*, 2016). Other proteins of interest might include PfTRiC as well as human TRiC, where conflicting reports claimed either one or the other is involved in chaperoning parasitic proteins through the host cytoplasm to the Maurer's cleft (Mbengue *et al.*, 2015; Batinovic *et al.*, 2017). This may help to narrow down which section(s) of the parasitic protein export pathway are particularly adversely affected.

Glucose-6-phosphate dehydrogenase (G6PD) is a key enzyme involved in the erythrocyte's antioxidant response, as it catalyses the reduction of nicotinamide adenine dinucleotide phosphate (NADP+) into NADPH (Peters and Van Noorden, 2009). G6PD-deficiency is widespread in Africa, Asia, the Middle East and the Mediterranean, with allele frequencies of up to 30%, giving rise to the hypothesis that this is due to the selective pressure exerted by the malaria parasite (Ruwende and Hill, 1998; Uyoga *et al.*, 2015). However, the epidemiological evidence for the protection of G6PD-deficiency against malaria is found to be confusing and often contradictory (Mbanefo *et al.*, 2017). As we have pointed to pro-oxidative environments and irreversibly oxidised haemoglobin products as one of the key factors in the protective roles of haemoglobinopathic erythrocytes against severe malaria, further investigation into G6PD-deficient erythrocytes could prove insightful.

6 Conclusion

Despite many epidemiological studies linking haemoglobinopathies to protection against severe malaria, the molecular mechanisms behind the protective traits have yet to be elucidated.

In project I, we attempted to establish a working protocol for visualisation of actin and spectrin in uninfected and infected erythrocytes using 2D TIRF-*d*STORM. Unfortunately, we were not able to distinguish between the short F-actin in uninfected erythrocytes and long filamentous actin remodelled by the parasite upon infection. STED imaging also yielded similar results.

Kinetics of cytoadhesive phenotype, surface adhesin presentation and induction and establishment of the new permeation pathways (NPPs) were investigated in project II. Infected haemoglobinopathic erythrocytes showed delayed and reduced levels of cytoadhesion, surface adhesin presentation and NPPs development, compared to infected HbAA erythrocytes. These results suggest an impaired parasitic protein export pathway in parasitized haemoglobinopathic erythrocytes.

In order to determine the effects of irreversibly oxidised haemoglobin products and elevated levels of reactive oxygen species (ROS) inherent in uninfected haemoglobinopathic erythrocytes on the parasite's ability to remodel the host cell, uninfected HbAA erythrocytes were transiently oxidised prior to infection by *Plasmodium falciparum* in project III. The pre-treated samples exhibited reduced cytoadhesion and surface PfEMP1 levels, comparable to infected haemoglobinopathic and fetal erythrocytes. Maurer's clefts and knob morphologies, as investigated by transmission and scanning electron microscopy, were also visually similar to those seen in infected fetal and haemoglobinopathic erythrocytes, namely enlarged and dispersed knobs as well as malformed Maurer's clefts.

Based on the studies described above, we hypothesise that one of the molecular mechanisms by which haemoglobinopathic and fetal erythrocytes protect their carriers against severe malaria is due to their inherent oxidative imbalance as well as elevated levels of reactive oxygen species (ROS) and irreversibly oxidised haemoglobin products such as ferryl-haemoglobin and hemichromes. These interfere with the parasite's ability to establish functional Maurer's clefts, knobs and long filamentous actin networks in the host cytoplasm, resulting in reduced export of PfEMP1 to the erythrocytic surface, reduced cytoadhesion and, consequently, a reduced risk of severe malaria for their carriers (Fig 6-1).

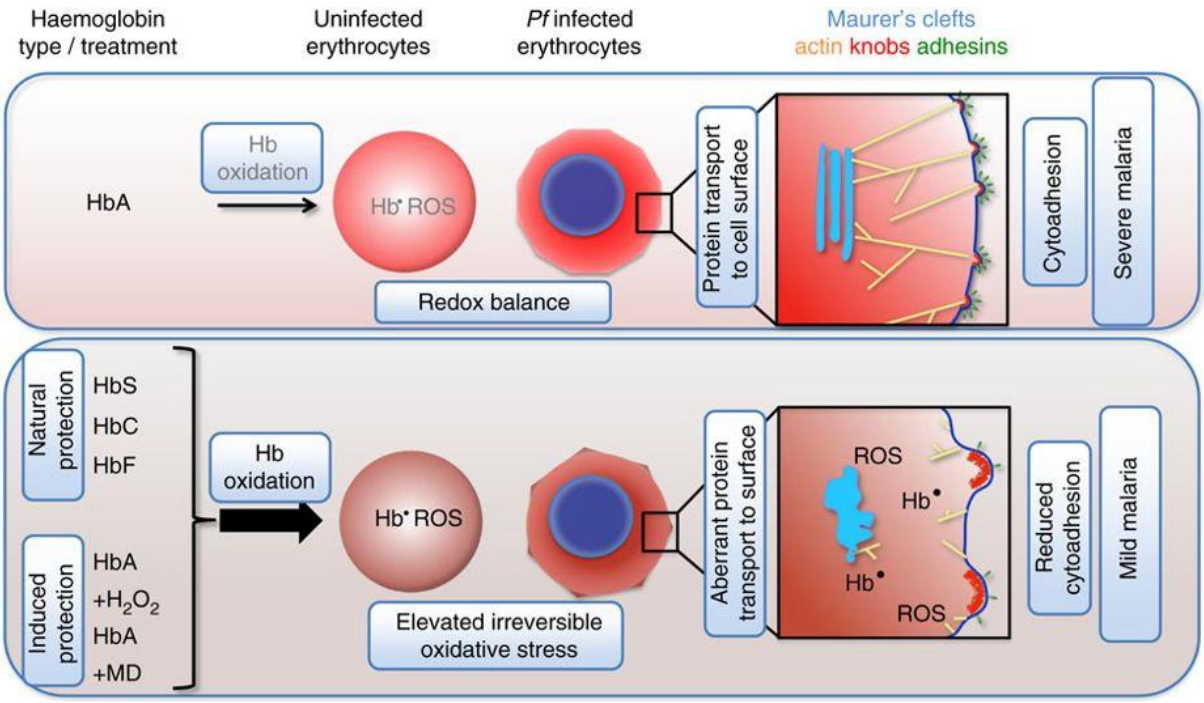

Figure 6-1 Current model for one of the molecular mechanisms of protection against severe malaria by haemoglobinopathic and fetal erythrocytes.

Top panel: Under normal circumstances, HbA-containing erythrocytes are able to mitigate and reverse possible damages from haemoglobin oxidation associated reactive oxygen species (ROS), including globin-based radicals (Hb·). Once infected with *Plasmodium falciparum*, the parasite carries out several changes in its host cell, including: establishing parasitic membranous structures termed Maurer's clefts in the erythrocytic cytosol, displaying parasitic adhesins on membrane protrusions termed knobs and reorganising host actin into long filamentous structures connecting the Maurer's clefts and the knobs. These modifications allow the parasitized erythrocyte to cytoadhere in microvascular beds of vital organs and causes severe complications in malaria which could lead to coma and death. Bottom panel: In haemoglobinopathic and fetal erythrocytes, the elevated levels of oxidative stress and ROS interfere with the Maurer's clefts and knobs morphologies as well as the host actin remodelling, leading to reduced cytoadhesion and less likelihood of developing severe malaria for their carriers. Transient oxidative treatment of HbAA erythrocytes is able to replicate the morphologies and phenotypical outcomes of infected haemoglobinopathic or fetal erythrocytes. Figure adapted from Cyrklaff *et al.*, (2016)

7 References

Acharya, P., Garg, M., Kumar, P., Munjal, A. & Raja, K. D. (2017). ***Host–Parasite Interactions in Human Malaria: Clinical Implications of Basic Research.*** Frontiers in Microbiology, 8**,** 889.

Achur, R. N., Muthusamy, A., Madhunapantula, S. V. & Gowda, D. C. (2008). ***Binding affinity of Plasmodium falciparum-infected erythrocytes from infected placentas and laboratory selected strains to chondroitin 4-sulfate.*** Molecular and Biochemical Parasitology, 159**,** 79-84.

Achur, R. N., Valiyaveettil, M., Alkhalil, A., Ockenhouse, C. F. & Gowda, D. C. (2000). ***Characterization of Proteoglycans of Human Placenta and Identification of Unique Chondroitin Sulfate Proteoglycans of the Intervillous Spaces That Mediate the Adherence ofPlasmodium falciparum-infected Erythrocytes to the Placenta.*** Journal of Biological Chemistry, 275**,** 40344-40356.

Adini, A. & Warburg, A. (1999). ***Interaction of Plasmodium gallinaceum ookinetes and oocysts with extracellular matrix proteins.*** Parasitology, 119 (Pt 4)**,** 331-6.

Agan, T., Ekabua, J., Udoh, A., Ekanem, E., Efiok, E. & Mgbekem, M. (2010). ***Prevalence of anemia in women with asymptomatic malaria parasitemia at first antenatal care visit at the University of Calabar Teaching Hospital, Calabar, Nigeria.*** Int J Womens Health, 2**,** 229-33.

Agarwal, A., Guindo, A., Cissoko, Y., Taylor, J. G., Coulibaly, D., Kone, A., Kayentao, K., Djimde, A., Plowe, C. V., Doumbo, O., Wellems, T. E. & Diallo, D. (2000). ***Hemoglobin C associated with protection from severe malaria in the Dogon of Mali, a West African population with a low prevalence of hemoglobin S.*** Blood, 96**,** 2358-63.

Aidoo, M., Terlouw, D. J., Kolczak, M. S., McElroy, P. D., ter Kuile, F. O., Kariuki, S., Nahlen, B. L., Lal, A. A. & Udhayakumar, V. (2002). ***Protective effects of the sickle cell gene against malaria morbidity and mortality.*** The Lancet, 359**,** 1311-1312.

Alkhalil, A., Achur, R. N., Valiyaveettil, M., Ockenhouse, C. F. & Gowda, D. C. (2000). ***Structural requirements for the adherence of Plasmodium falciparum-infected erythrocytes to chondroitin sulfate proteoglycans of human placenta.*** J Biol Chem, 275**,** 40357-64.

Allison, A. C. (1954). ***Protection afforded by sickle-cell trait against subtertian malarial infection.*** British medical journal, 1**,** 290.

Aly, A. S. & Matuschewski, K. (2005). ***A malarial cysteine protease is necessary for Plasmodium sporozoite egress from oocysts.*** J Exp Med, 202**,** 225-30.

Aly, A. S., Vaughan, A. M. & Kappe, S. H. (2009). ***Malaria parasite development in the mosquito and infection of the mammalian host.*** Annu Rev Microbiol, 63**,** 195-221.

Amaratunga, C., Lopera-Mesa, T. M., Brittain, N. J., Cholera, R., Arie, T., Fujioka, H., Keefer, J. R. & Fairhurst, R. M. (2011). ***A Role for Fetal Hemoglobin and Maternal Immune IgG in Infant Resistance to <italic>Plasmodium falciparum</italic> Malaria.*** PLoS ONE, 6**,** e14798.

Amino, R., Giovannini, D., Thiberge, S., Gueirard, P., Boisson, B., Dubremetz, J.-F., Prévost, M.-C., Ishino, T., Yuda, M. & Ménard, R. (2008). ***Host Cell Traversal Is Important for Progression of the Malaria Parasite through the Dermis to the Liver.*** Cell Host & Microbe, 3**,** 88-96.

Amino, R., Thiberge, S., Martin, B., Celli, S., Shorte, S., Frischknecht, F. & Ménard, R. (2006). ***Quantitative imaging of Plasmodium transmission from mosquito to mammal.*** Nature Medicine, 12**,** 220.

An, X., Guo, X., Zhang, X., Baines, A. J., Debnath, G., Moyo, D., Salomao, M., Bhasin, N., Johnson, C., Discher, D., Gratzer, W. B. & Mohandas, N. (2006). ***Conformational Stabilities of the Structural Repeats of Erythroid Spectrin and Their Functional Implications.*** Journal of Biological Chemistry, 281**,** 10527-10532.

An, X., Lecomte, M. C., Chasis, J. A., Mohandas, N. & Gratzer, W. (2002). ***Shear-Response of the Spectrin Dimer-Tetramer Equilibrium in the Red Blood Cell Membrane.*** Journal of Biological Chemistry, 277**,** 31796-31800.

Anderson, R. A. & Lovrien, R. E. (1984). ***Glycophorin is linked by band 4.1 protein to the human erythrocyte membrane skeleton.*** Nature, 307**,** 655-8.

Anong, W. A., Franco, T., Chu, H., Weis, T. L., Devlin, E. E., Bodine, D. M., An, X., Mohandas, N. & Low, P. S. (2009). ***Adducin forms a bridge between the erythrocyte membrane and its cytoskeleton and regulates membrane cohesion.*** Blood, 114**,** 1904-12.

Autino, B., Corbett, Y., Castelli, F. & Taramelli, D. (2012). ***Pathogenesis of Malaria in Tissues and Blood.*** Mediterranean Journal of Hematology and Infectious Diseases, 4**,** e2012061.

Avril, M., Traoré, B., Costa, F. T. M., Lépolard, C. & Gysin, J. (2004). ***Placenta cryosections for study of the adhesion of Plasmodium falciparum-infected erythrocytes to chondroitin sulfate A in flow conditions.*** Microbes and Infection, 6**,** 249-255.

Ayi, K., Turrini, F., Piga, A. & Arese, P. (2004). ***Enhanced phagocytosis of ring-parasitized mutant erythrocytes: a common mechanism that may explain protection against falciparum malaria in sickle trait and beta-thalassemia trait.*** Blood, 104**,** 3364-71.

Bachmann, M., Fiederling, F. & Bastmeyer, M. (2016). ***Practical limitations of superresolution imaging due to conventional sample preparation revealed by a direct comparison of CLSM, SIM and dSTORM.*** J Microsc, 262**,** 306-15.

Bardaji, A., Sigauque, B., Sanz, S., Maixenchs, M., Ordi, J., Aponte, J. J., Mabunda, S., Alonso, P. L. & Menendez, C. (2011). ***Impact of malaria at the end of pregnancy on infant mortality and morbidity.*** J Infect Dis, 203**,** 691-9.

Barfod, L., Nielsen, M. A., Turner, L., Dahlback, M., Jensen, A. T., Hviid, L., Theander, T. G. & Salanti, A. (2006). ***Baculovirus-expressed constructs induce immunoglobulin G that recognizes VAR2CSA on Plasmodium falciparum-infected erythrocytes.*** Infect Immun, 74**,** 4357-60.

Bartoloni, A. & Zammarchi, L. (2012a). ***Clinical aspects of uncomplicated and severe malaria.*** Mediterr J Hematol Infect Dis, 4**,** e2012026.

Bartoloni, A. & Zammarchi, L. (2012b). ***Clinical Aspects of Uncomplicated and Severe Malaria.*** Mediterranean Journal of Hematology and Infectious Diseases, 4**,** e2012026.

Batinovic, S., McHugh, E., Chisholm, S. A., Matthews, K., Liu, B., Dumont, L., Charnaud, S. C., Schneider, M. P., Gilson, P. R., de Koning-Ward, T. F., Dixon, M. W. A. & Tilley, L. (2017). ***An exported protein-interacting complex involved in the trafficking of virulence determinants in Plasmodium-infected erythrocytes.*** Nature Communications, 8**,** 16044.

Bauduer, F. (2013). ***Red cell polymorphisms and malaria: an evolutionary approach.*** Bulletins et mémoires de la Société d'anthropologie de Paris, 25**,** 55-64.

Beeson, J. G., Brown, G. V., Molyneux, M. E., Mhango, C., Dzinjalamala, F. & Rogerson, S. J. (1999). ***Plasmodium falciparum Isolates from Infected Pregnant Women and Children Are Associated with Distinct Adhesive and Antigenic Properties.*** Journal of Infectious Diseases, 180**,** 464-472.

Bellomo, G., Mirabelli, F., Vairetti, M., Iosi, F. & Malorni, W. (1990). ***Cytoskeleton as a target in menadione-induced oxidative stress in cultured mammalian cells. I. Biochemical and immunocytochemical features.*** J Cell Physiol, 143**,** 118-28.

Bennett, V. & Baines, A. J. (2001). ***Spectrin and ankyrin-based pathways: metazoan inventions for integrating cells into tissues.*** Physiol Rev, 81**,** 1353-92.

Bennink, S., Kiesow, M. J. & Pradel, G. (2016). ***The development of malaria parasites in the mosquito midgut.*** Cellular Microbiology, 18**,** 905-918.

Billker, O., Lindo, V., Panico, M., Etienne, A. E., Paxton, T., Dell, A., Rogers, M., Sinden, R. E. & Morris, H. R. (1998). ***Identification of xanthurenic acid as the putative inducer of malaria development in the mosquito.*** Nature, 392**,** 289-92.

Billker, O., Shaw, M. K., Margos, G. & Sinden, R. E. (1997). ***The roles of temperature, pH and mosquito factors as triggers of male and female gametogenesis of Plasmodium berghei in vitro.*** Parasitology, 115 (Pt 1)**,** 1-7.

Blisnick, T., Morales Betoulle, M. E., Barale, J. C., Uzureau, P., Berry, L., Desroses, S., Fujioka, H., Mattei, D. & Braun Breton, C. (2000). ***Pfsbp1, a Maurer's cleft Plasmodium falciparum protein, is associated with the erythrocyte skeleton.*** Molecular and biochemical parasitology, 111**,** 107-121.

Buffet, P. A., Gamain, B., Scheidig, C., Baruch, D., Smith, J. D., Hernandez-Rivas, R., Pouvelle, B., Oishi, S., Fujii, N., Fusai, T., Parzy, D., Miller, L. H., Gysin, J. & Scherf, A. (1999). ***Plasmodium falciparum domain mediating adhesion to chondroitin sulfate A: a receptor for human placental infection.*** Proc Natl Acad Sci U S A, 96**,** 12743-8.

Cabrales, P., Zanini, G. M., Meays, D., Frangos, J. A. & Carvalho, L. J. M. (2010). ***Murine Cerebral Malaria Is Associated with a Vasospasm-Like Microcirculatory Dysfunction, and Survival upon Rescue Treatment Is Markedly Increased by Nimodipine.*** The American Journal of Pathology, 176**,** 1306-1315.

Calis, J. C., Phiri, K. S., Faragher, E. B., Brabin, B. J., Bates, I., Cuevas, L. E., de Haan, R. J., Phiri, A. I., Malange, P., Khoka, M., Hulshof, P. J., van Lieshout, L., Beld, M. G., Teo, Y. Y., Rockett, K. A., Richardson, A., Kwiatkowski, D. P., Molyneux, M. E. & van Hensbroek, M. B. (2008). ***Severe anemia in Malawian children.*** N Engl J Med, 358**,** 888-99.

Caminade, C., Kovats, S., Rocklov, J., Tompkins, A. M., Morse, A. P., Colón-González, F. J., Stenlund, H., Martens, P. & Lloyd, S. J. (2014). ***Impact of climate change on global malaria distribution.*** Proceedings of the National Academy of Sciences of the United States of America, 111**,** 3286-3291.

Campo, B., Vandal, O., Wesche, D. L. & Burrows, J. N. (2015). ***Killing the hypnozoite – drug discovery approaches to prevent relapse in Plasmodium vivax.*** Pathogens and Global Health, 109**,** 107-122.

Caprari, P., Bozzi, A., Malorni, W., Bottini, A., Iosi, F., Santini, M. T. & Salvati, A. M. (1995). ***Junctional sites of erythrocyte skeletal proteins are specific targets of tert-butylhydroperoxide oxidative damage.*** Chem Biol Interact, 94**,** 243-58.

Carrolo, M., Giordano, S., Cabrita-Santos, L., Corso, S., Vigario, A. M., Silva, S., Leiriao, P., Carapau, D., Armas-Portela, R., Comoglio, P. M., Rodriguez, A. & Mota, M. M. (2003). ***Hepatocyte growth factor and its receptor are required for malaria infection.*** Nat Med, 9**,** 1363-9.

Carter, J. A., A, L. J., K, G. J., Gladys, M., Kenneth, R., R., N. B. G. & C, N. C. R. J. (2006). ***Severe falciparum malaria and acquired childhood language disorder.*** Developmental Medicine & Child Neurology, 48**,** 51-57.

Carter, R. & Mendis, K. N. (2002). ***Evolutionary and historical aspects of the burden of malaria.*** Clin Microbiol Rev, 15**,** 564-94.

Chaves, M. A., Leonart, M. S. & do Nascimento, A. J. (2008). ***Oxidative process in erythrocytes of individuals with hemoglobin S.*** Hematology, 13**,** 187-92.

Chiou, T.-J. & Tzeng, W.-F. (2000). ***The roles of glutathione and antioxidant enzymes in menadione-induced oxidative stress.*** Toxicology, 154**,** 75-84.

Chisholm Scott, A., Kalanon, M., Nebl, T., Sanders Paul, R., Matthews Kathryn, M., Dickerman Benjamin, K., Gilson Paul, R. & Koning-Ward Tania, F. (2018). ***The malaria PTEX component PTEX88 interacts most closely with HSP101 at the host–parasite interface.*** The FEBS Journal, 285**,** 2037-2055.

Cholera, R., Brittain, N. J., Gillrie, M. R., Lopera-Mesa, T. M., Diakite, S. A. S., Arie, T., Krause, M. A., Guindo, A., Tubman, A., Fujioka, H., Diallo, D. A., Doumbo, O. K., Ho, M., Wellems, T. E. & Fairhurst, R. M. (2008). ***Impaired cytoadherence of Plasmodium falciparum-infected erythrocytes containing sickle hemoglobin.*** Proceedings of the National Academy of Sciences, 105**,** 991-996.

Church, J. & Maitland, K. (2014). ***Invasive bacterial co-infection in African children with Plasmodium falciparum malaria: a systematic review.*** BMC Med, 12**,** 31.

Coppi, A., Tewari, R., Bishop, J. R., Bennett, B. L., Lawrence, R., Esko, J. D., Billker, O. & Sinnis, P. (2007). ***Heparan Sulfate Proteoglycans Provide a Signal to Plasmodium Sporozoites to Stop Migrating and Productively Invade Host Cells.*** Cell Host & Microbe, 2**,** 316-327.

Cowman, A. F., Healer, J., Marapana, D. & Marsh, K. (2016). ***Malaria: Biology and Disease.*** Cell, 167**,** 610-624.

Cox, F. E. (2010). ***History of the discovery of the malaria parasites and their vectors.*** Parasit Vectors, 3**,** 5.

Cox, S. (2015). ***Super-resolution imaging in live cells.*** Developmental Biology, 401**,** 175-181.

Crabb, B. S., Cooke, B. M., Reeder, J. C., Waller, R. F., Caruana, S. R., Davern, K. M., Wickham, M. E., Brown, G. V., Coppel, R. L. & Cowman, A. F. (1997). ***Targeted gene disruption shows that knobs enable malaria-infected red cells to cytoadhere under physiological shear stress.*** Cell, 89**,** 287-96.

Craig, A. & Scherf, A. (2001). ***Molecules on the surface of the Plasmodium falciparum infected erythrocyte and their role in malaria pathogenesis and immune evasion.*** Molecular and Biochemical Parasitology, 115**,** 129-143.

Craig, A. G., Grau, G. E., Janse, C., Kazura, J. W., Milner, D., Barnwell, J. W., Turner, G. & Langhorne, J. (2012). ***The role of animal models for research on severe malaria.*** PLoS Pathog, 8**,** e1002401.

Criddle, D. N., Gillies, S., Baumgartner-Wilson, H. K., Jaffar, M., Chinje, E. C., Passmore, S., Chvanov, M., Barrow, S., Gerasimenko, O. V., Tepikin, A. V., Sutton, R. & Petersen, O. H. (2006). ***Menadione-induced Reactive Oxygen Species Generation via Redox Cycling Promotes Apoptosis of Murine Pancreatic Acinar Cells.*** Journal of Biological Chemistry, 281**,** 40485-40492.

Cyrklaff, M., Sanchez, C. P., Frischknecht, F. & Lanzer, M. (2012). ***Host actin remodeling and protection from malaria by hemoglobinopathies.*** Trends in Parasitology, 28**,** 479-485.

Cyrklaff, M., Sanchez, C. P., Kilian, N., Bisseye, C., Simpore, J., Frischknecht, F. & Lanzer, M. (2011). ***Hemoglobins S and C Interfere with Actin Remodeling in Plasmodium falciparum-Infected Erythrocytes.*** Science, 334**,** 1283-1286.

Cyrklaff, M., Srismith, S., Nyboer, B., Burda, K., Hoffmann, A., Lasitschka, F., Adjalley, S., Bisseye, C., Simpore, J., Mueller, A. K., Sanchez, C. P., Frischknecht, F. & Lanzer, M. (2016). ***Oxidative insult can induce malaria-protective trait of sickle and fetal erythrocytes.*** Nat Commun, 7**,** 13401.

Dahlbäck, M., Lavstsen, T., Salanti, A., Hviid, L., Arnot, D. E., Theander, T. G. & Nielsen, M. A. (2007). ***Changes in var gene mRNA levels during erythrocytic development in two phenotypically distinct Plasmodium falciparum parasites.*** Malaria Journal, 6**,** 78.

DalleDonne, I., Milzani, A. & Colombo, R. (1995). ***H2O2-treated actin: assembly and polymer interactions with cross-linking proteins.*** Biophys J, 69**,** 2710-9.

DalleDonne, I., Milzani, A. & Colombo, R. (1999). ***The tert-Butyl Hydroperoxide-Induced Oxidation of Actin Cys-374 Is Coupled with Structural Changes in Distant Regions of the Protein†.*** Biochemistry, 38**,** 12471-12480.

De Castro, L. M., Jonassaint, J. C., Graham, F. L., Ashley-Koch, A. & Telen, M. J. (2008). ***Pulmonary hypertension associated with sickle cell disease: Clinical and laboratory endpoints and disease outcomes.*** American Journal of Hematology, 83**,** 19-25.

Del Portillo, H. A., Ferrer, M., Brugat, T., Martin-Jaular, L., Langhorne, J. & Lacerda, M. V. (2012). ***The role of the spleen in malaria.*** Cell Microbiol, 14**,** 343-55.

Delgadillo, R. F., Parker, M. L., Lebrun, M., Boulanger, M. J. & Douguet, D. (2016). ***Stability of the Plasmodium falciparum AMA1-RON2 Complex Is Governed by the Domain II (DII) Loop.*** PLoS One, 11**,** e0144764.

Dempsey, G. T., Vaughan, J. C., Chen, K. H., Bates, M. & Zhuang, X. (2011). ***Evaluation of fluorophores for optimal performance in localization-based super-resolution imaging.*** Nature Methods, 8**,** 1027-1036.

Desagher, S., Glowinski, J. & Prémont, J. (1997). ***Pyruvate Protects Neurons against Hydrogen Peroxide-Induced Toxicity.*** The Journal of Neuroscience, 17**,** 9060-9067.

Domanski, A. V., Lapshina, E. A. & Zavodnik, I. B. (2005). ***Oxidative processes induced by tert-butyl hydroperoxide in human red blood cells: chemiluminescence studies.*** Biochemistry (Mosc), 70**,** 761-9.

Dondorp, A. M., Nosten, F., Yi, P., Das, D., Phyo, A. P., Tarning, J., Lwin, K. M., Ariey, F., Hanpithakpong, W., Lee, S. J., Ringwald, P., Silamut, K., Imwong, M., Chotivanich, K., Lim, P., Herdman, T., An, S. S., Yeung, S., Singhasivanon, P., Day, N. P., Lindegardh, N., Socheat, D. & White, N. J. (2009). ***Artemisinin resistance in Plasmodium falciparum malaria.*** N Engl J Med, 361**,** 455-67.

Donne, J. (1624). ***Devotions upon emergent occasions***, Cambridge, [Eng.] : The University press, 1923.

Dronamraju, K. R., Arese, P. & Haldane, J. B. S. (2006). ***Malaria: genetic and evolutionary aspects***, Springer.

Duffy, M. F., Brown, G. V., Basuki, W., Krejany, E. O., Noviyanti, R., Cowman, A. F. & Reeder, J. C. (2002). ***Transcription of multiple var genes by individual, trophozoite-stage Plasmodium falciparum cells expressing a chondroitin sulphate A binding phenotype.*** Molecular Microbiology, 43**,** 1285-1293.

Ejigiri, I. & Sinnis, P. (2009). ***Plasmodium Sporozoite-Host Interactions From the Dermis to the Hepatocyte.*** Current opinion in microbiology, 12**,** 401-407.

Elsworth, B., Matthews, K., Nie, C. Q., Kalanon, M., Charnaud, S. C., Sanders, P. R., Chisholm, S. A., Counihan, N. A., Shaw, P. J., Pino, P., Chan, J. A., Azevedo, M. F., Rogerson, S. J., Beeson, J. G., Crabb, B. S., Gilson, P. R. & de Koning-Ward, T. F. (2014). ***PTEX is an essential nexus for protein export in malaria parasites.*** Nature, 511**,** 587-91.

Endesfelder, U., van de Linde, S., Wolter, S., Sauer, M. & Heilemann, M. (2010). ***Subdiffraction-resolution fluorescence microscopy of myosin-actin motility.*** Chemphyschem, 11**,** 836-40.

English, M., Waruiru, C., Amukoye, E., Murphy, S., Crawley, J., Mwangi, I., Peshu, N. & Marsh, K. (1996). ***Deep breathing in children with severe malaria: indicator of metabolic acidosis and poor outcome.*** Am J Trop Med Hyg, 55**,** 521-4.

Engwerda, C. R., Beattie, L. & Amante, F. H. (2005). ***The importance of the spleen in malaria.*** Trends Parasitol, 21**,** 75-80.

Fairhurst, R. M., Baruch, D. I., Brittain, N. J., Ostera, G. R., Wallach, J. S., Hoang, H. L., Hayton, K., Guindo, A., Makobongo, M. O., Schwartz, O. M., Tounkara, A., Doumbo, O. K., Diallo, D. A., Fujioka, H., Ho, M. & Wellems, T. E. (2005). ***Abnormal display of PfEMP-1 on erythrocytes carrying haemoglobin C may protect against malaria.*** Nature, 435**,** 1117-21.

Fairhurst, R. M., Bess, C. D. & Krause, M. A. (2012). ***Abnormal PfEMP1/knob display on Plasmodium falciparum-infected erythrocytes containing hemoglobin variants: fresh insights into malaria pathogenesis and protection.*** Microbes and Infection, 14**,** 851-862.

Falade, C. O., Tongo, O. O., Ogunkunle, O. O. & Orimadegun, A. E. (2010). ***Effects of malaria in pregnancy on newborn anthropometry.*** J Infect Dev Ctries, 4**,** 448-53.

Faulstich, H., Zobeley, S., Heintz, D. & Drewes, G. (1993). ***Probing the phalloidin binding site of actin.*** FEBS Lett, 318**,** 218-22.

Feeling-Taylor, A. R., Yau, S. T., Petsev, D. N., Nagel, R. L., Hirsch, R. E. & Vekilov, P. G. (2004). ***Crystallization Mechanisms of Hemoglobin C in the R State.*** Biophysical Journal, 87**,** 2621-2629.

Fenton, H. J. H. (1894). ***LXXIII.-Oxidation of tartaric acid in presence of iron.*** Journal of the Chemical Society, Transactions, 65**,** 899-910.

Ferreira, A., Marguti, I., Bechmann, I., Jeney, V., Chora, Â., Palha, Nuno R., Rebelo, S., Henri, A., Beuzard, Y. & Soares, Miguel P. (2011). ***Sickle Hemoglobin Confers Tolerance to Plasmodium Infection.*** Cell, 145**,** 398-409.

Flick, K., Scholander, C., Chen, Q., Fernandez, V., Pouvelle, B., Gysin, J. & Wahlgren, M. (2001). ***Role of Nonimmune IgG Bound to PfEMP1 in Placental Malaria.*** Science, 293**,** 2098-2100.

Flint, J., Harding, R. M., Boyce, A. J. & Clegg, J. B. (1998). ***The population genetics of the haemoglobinopathies.*** Baillieres Clin Haematol, 11**,** 1-51.

Flottmann, B. 2014. *Implementation of Multi-Color Super-Resolution Microscopy into a High-Throughput Platform for Quantitative Imaging of Cellular Structures.* Ruprecht-Karls-Universität Heidelberg.

Fowler, V. M. (2013). ***The human erythrocyte plasma membrane: a Rosetta Stone for decoding membrane-cytoskeleton structure.*** Curr Top Membr, 72**,** 39-88.

Fried, M. & Duffy, P. E. (1996). ***Adherence of Plasmodium falciparum to Chondroitin Sulfate A in the Human Placenta.*** Science, 272**,** 1502-1504.

Frischknecht, F., Baldacci, P., Martin, B., Zimmer, C., Thiberge, S., Olivo-Marin, J.-C., Shorte, S. L. & Ménard, R. (2004). ***Imaging movement of malaria parasites during transmission by Anopheles mosquitoes.*** Cellular Microbiology, 6**,** 687-694.

Gallup, J. & Sachs, J. (2001). ***The economic burden of malaria.*** The American Journal of Tropical Medicine and Hygiene, 64**,** 85-96.

Ganguly, A. K., Ranjan, P., Kumar, A. & Bhavesh, N. S. (2015). ***Dynamic association of PfEMP1 and KAHRP in knobs mediates cytoadherence during Plasmodium invasion.*** Sci Rep, 5**,** 8617.

Gardner, J. P., Pinches, R. A., Roberts, D. J. & Newbold, C. I. (1996). ***Variant antigens and endothelial receptor adhesion in Plasmodium falciparum.*** Proceedings of the National Academy of Sciences, 93**,** 3503-3508.

Gething, P. W., Van Boeckel, T. P., Smith, D. L., Guerra, C. A., Patil, A. P., Snow, R. W. & Hay, S. I. (2011). ***Modelling the global constraints of temperature on transmission of Plasmodium falciparum and P. vivax.*** Parasites & Vectors, 4**,** 92-92.

Ginsburg, H., Krugliak, M., Eidelman, O. & Cabantchik, Z. I. (1983). ***New permeability pathways induced in membranes of Plasmodium falciparum infected erythrocytes.*** Mol Biochem Parasitol, 8**,** 177-90.

Ginsburg, H. & Stein, W. D. (2004). ***The new permeability pathways induced by the malaria parasite in the membrane of the infected erythrocyte: comparison of results using different experimental techniques.*** J Membr Biol, 197**,** 113-34.

Gladwin, M. T., Sachdev, V., Jison, M. L., Shizukuda, Y., Plehn, J. F., Minter, K., Brown, B., Coles, W. A., Nichols, J. S., Ernst, I., Hunter, L. A., Blackwelder, W. C., Schechter, A. N., Rodgers, G. P., Castro, O. & Ognibene, F. P. (2004). ***Pulmonary Hypertension as a Risk Factor for Death in Patients with Sickle Cell Disease.*** New England Journal of Medicine, 350**,** 886-895.

Gokhin, D. S. & Fowler, V. M. (2016). ***Feisty filaments: actin dynamics in the red blood cell membrane skeleton.*** Curr Opin Hematol, 23**,** 206-14.

Gokhin, D. S., Nowak, R. B., Khoory, J. A., Piedra Ade, L., Ghiran, I. C. & Fowler, V. M. (2015). ***Dynamic actin filaments control the mechanical behavior of the human red blood cell membrane.*** Mol Biol Cell, 26**,** 1699-710.

Goodyer, I. D., Johnson, J., Eisenthal, R. & Hayes, D. J. (1994). ***Purification of mature-stage Plasmodium falciparum by gelatine flotation.*** Ann Trop Med Parasitol, 88**,** 209-11.

Gopalakrishnan, A. M. & Kumar, N. (2015). ***Antimalarial Action of Artesunate Involves DNA Damage Mediated by Reactive Oxygen Species.*** Antimicrobial Agents and Chemotherapy, 59**,** 317-325.

Graewe, S., Stanway, R. R., Rennenberg, A. & Heussler, V. T. (2012). ***Chronicle of a death foretold: Plasmodium liver stage parasites decide on the fate of the host cell.*** FEMS Microbiology Reviews, 36**,** 111-130.

Griffiths, G., Burke, B. & Lucocq, J. (1993). ***Fine structure immunocytochemistry***, Springer-Verlag Heidelberg.

Griffiths, G., McDowall, A., Back, R. & Dubochet, J. (1984). ***On the preparation of cryosections for immunocytochemistry.*** J Ultrastruct Res, 89**,** 65-78.

Gruenberg, J., Allred, D. R. & Sherman, I. W. (1983). ***Scanning electron microscope-analysis of the protrusions (knobs) present on the surface of Plasmodium falciparum-infected erythrocytes.*** J Cell Biol, 97**,** 795-802.

Gruring, C., Heiber, A., Kruse, F., Ungefehr, J., Gilberger, T. W. & Spielmann, T. (2011). ***Development and host cell modifications of Plasmodium falciparum blood stages in four dimensions.*** Nat Commun, 2**,** 165.

Haase, R. N., Megnekou, R., Lundquist, M., Ofori, M. F., Hviid, L. & Staalsoe, T. (2006). ***Plasmodium falciparum Parasites Expressing Pregnancy-Specific Variant Surface Antigens Adhere Strongly to the Choriocarcinoma Cell Line BeWo.*** Infection and Immunity, 74**,** 3035-3038.

Haldar, K. & Mohandas, N. (2007). ***Erythrocyte remodeling by malaria parasites.*** Curr Opin Hematol, 14**,** 203-9.

Haldar, K. & Mohandas, N. (2009). ***Malaria, erythrocytic infection, and anemia.*** Hematology Am Soc Hematol Educ Program**,** 87-93.

Hannemann, A., Weiss, E., Rees, D. C., Dalibalta, S., Ellory, J. C. & Gibson, J. S. (2011). ***The Properties of Red Blood Cells from Patients Heterozygous for HbS and HbC (HbSC Genotype).*** Anemia, 2011**,** 248527.

Hardison, R. C. (1996). ***A brief history of hemoglobins: plant, animal, protist, and bacteria.*** Proceedings of the National Academy of Sciences of the United States of America, 93**,** 5675-5679.

Heart, E., Palo, M., Womack, T., Smith, P. J. S. & Gray, J. P. (2012). ***The level of menadione redox-cycling in pancreatic β-cells is proportional to the glucose concentration: Role of NADH and consequences for insulin secretion.*** Toxicology and Applied Pharmacology, 258**,** 216-225.

Hebbel, R. P., Eaton, J. W., Balasingam, M. & Steinberg, M. H. (1982). ***Spontaneous oxygen radical generation by sickle erythrocytes.*** J Clin Invest, 70**,** 1253-9.

Hebbel, R. P., Morgan, W. T., Eaton, J. W. & Hedlund, B. E. (1988). ***Accelerated autoxidation and heme loss due to instability of sickle hemoglobin.*** Proceedings of the National Academy of Sciences, 85**,** 237-241.

Helms, G., Dasanna, A. K., Schwarz, U. S. & Lanzer, M. (2016). ***Modeling cytoadhesion of Plasmodium falciparum‐infected erythrocytes and leukocytes—common principles and distinctive features.*** Febs Letters, 590**,** 1955-1971.

Henriques, R., Griffiths, C., Hesper Rego, E. & Mhlanga, M. M. (2011). ***PALM and STORM: unlocking live-cell super-resolution.*** Biopolymers, 95**,** 322-31.

Hillmer, S., Viotti, C. & Robinson, D. G. (2012). ***An improved procedure for low-temperature embedding of high-pressure frozen and freeze-substituted plant tissues resulting in excellent structural preservation and contrast.*** Journal of Microscopy, 247**,** 43-47.

Hleb, E. Y. L. & Lapotko, D. O. (2014). ***Malaria Theranostics using Hemozoin-Generated Vapor Nanobubbles.*** Theranostics, 4**,** 761-769.

Howes, R. E., Battle, K. E., Mendis, K. N., Smith, D. L., Cibulskis, R. E., Baird, J. K. & Hay, S. I. (2016). ***Global Epidemiology of Plasmodium vivax.*** The American Journal of Tropical Medicine and Hygiene, 95**,** 15-34.

Idro, R., Carter, J. A., Fegan, G., Neville, B. G. & Newton, C. R. (2006). ***Risk factors for persisting neurological and cognitive impairments following cerebral malaria.*** Arch Dis Child, 91**,** 142-8.

Imwong, M., Suwannasin, K., Kunasol, C., Sutawong, K., Mayxay, M., Rekol, H., Smithuis, F. M., Hlaing, T. M., Tun, K. M., van der Pluijm, R. W., Tripura, R., Miotto, O., Menard, D., Dhorda, M., Day, N. P. J., White, N. J. & Dondorp, A. M. (2017). ***The spread of artemisinin-resistant Plasmodium falciparum in the Greater Mekong subregion: a molecular epidemiology observational study.*** The Lancet Infectious Diseases, 17**,** 491-497.

Janse, C. J., van der Klooster, P. F., van der Kaay, H. J., van der Ploeg, M. & Overdulve, J. P. (1986). ***DNA synthesis in Plasmodium berghei during asexual and sexual development.*** Mol Biochem Parasitol, 20**,** 173-82.

Jarolim, P., Lahav, M., Liu, S. & Palek, J. (1990). ***Effect of hemoglobin oxidation products on the stability of red cell membrane skeletons and the associations of skeletal proteins: correlation with a release of hemin.*** Blood, 76**,** 2125-2131.

Jin, Y., Kebaier, C. & Vanderberg, J. (2007). ***Direct Microscopic Quantification of Dynamics of Plasmodium berghei Sporozoite Transmission from Mosquitoes to Mice.*** Infection and Immunity, 75**,** 5532-5539.

Johnson, C. P., Tang, H.-Y., Carag, C., Speicher, D. W. & Discher, D. E. (2007). ***Forced Unfolding of Proteins Within Cells.*** Science, 317**,** 663-666.

Joice, R., Nilsson, S. K., Montgomery, J., Dankwa, S., Egan, E., Morahan, B., Seydel, K. B., Bertuccini, L., Alano, P., Williamson, K. C., Duraisingh, M. T., Taylor, T. E., Milner, D. A. & Marti, M. (2014). ***Plasmodium falciparum transmission stages accumulate in the human bone marrow.*** Science translational medicine, 6**,** 244re5-244re5.

Jones, S. A., Shim, S. H., He, J. & Zhuang, X. (2011). ***Fast, three-dimensional super-resolution imaging of live cells.*** Nat Methods, 8**,** 499-508.

Josling, G. A. & Llinás, M. (2015). ***Sexual development in Plasmodium parasites: knowing when it's time to commit.*** Nature Reviews Microbiology, 13**,** 573.

Kanias, T. & Acker, J. P. (2010). ***Biopreservation of red blood cells--the struggle with hemoglobin oxidation.*** Febs j, 277**,** 343-56.

Keohane, E. M., Smith, L. J. & Walenga, J. M. (2015). ***Rodak's hematology: clinical principles and applications***, Elsevier Health Sciences.

Kilian, N., Dittmer, M., Cyrklaff, M., Ouermi, D., Bisseye, C., Simpore, J., Frischknecht, F., Sanchez, C. P. & Lanzer, M. (2013). ***Haemoglobin S and C affect the motion of Maurer's clefts inPlasmodium falciparum-infected erythrocytes.*** Cellular Microbiology, 15**,** 1111-1126.

Kilian, N., Srismith, S., Dittmer, M., Ouermi, D., Bisseye, C., Simpore, J., Cyrklaff, M., Sanchez, C. P. & Lanzer, M. (2015). ***Hemoglobin S and C affect protein export in Plasmodium falciparum-infected erythrocytes.*** Biol Open, 4**,** 400-10.

Kirk, K., Horner, H. A., Elford, B. C., Ellory, J. C. & Newbold, C. I. (1994). ***Transport of diverse substrates into malaria-infected erythrocytes via a pathway showing functional characteristics of a chloride channel.*** J Biol Chem, 269**,** 3339-47.

Kirk, K. & Lehane, A. M. (2014). ***Membrane transport in the malaria parasite and its host erythrocyte.*** Biochemical Journal, 457**,** 1.

Klein, E. Y. (2013). ***Antimalarial drug resistance: a review of the biology and strategies to delay emergence and spread.*** International Journal of Antimicrobial Agents, 41**,** 311-317.

Kraemer, S. M. & Smith, J. D. (2006). ***A family affair: var genes, PfEMP1 binding, and malaria disease.*** Current Opinion in Microbiology, 9**,** 374-380.

Krause, M. A., Diakite, S. A. S., Lopera-Mesa, T. M., Amaratunga, C., Arie, T., Traore, K., Doumbia, S., Konate, D., Keefer, J. R., Diakite, M. & Fairhurst, R. M. (2012). ***α-Thalassemia Impairs the Cytoadherence of <italic>Plasmodium falciparum</italic>-Infected Erythrocytes.*** PLoS ONE, 7**,** e37214.

Kriek, N., Tilley, L., Horrocks, P., Pinches, R., Elford, B. C., Ferguson, D. J. P., Lingelbach, K. & Newbold, C. I. (2003). ***Characterization of the pathway for transport of the***

cytoadherence-mediating protein, PfEMP1, to the host cell surface in malaria parasite-infected erythrocytes. Molecular Microbiology, 50**,** 1215-1227.

Kudryashev, M., Lepper, S., Baumeister, W., Cyrklaff, M. & Frischknecht, F. (2010). ***Geometric constrains for detecting short actin filaments by cryogenic electron tomography***.

Kyes, S., Pinches, R. & Newbold, C. (2000). ***A simple RNA analysis method shows var and rif multigene family expression patterns in Plasmodium falciparum.*** Molecular and Biochemical Parasitology, 105**,** 311-315.

LaMonte, G., Philip, N., Reardon, J., Lacsina, J. R., Majoros, W., Chapman, L., Thornburg, C. D., Telen, M. J., Ohler, U., Nicchitta, C. V., Haystead, T. & Chi, J.-T. (2012). ***Translocation of sickle cell erythrocyte microRNAs into Plasmodium falciparum inhibits parasite translation and contributes to malaria resistance.*** Cell host & microbe, 12**,** 187-199.

Lang, P. A., Kasinathan, R. S., Brand, V. B., Duranton, C., Lang, C., Koka, S., Shumilina, E., Kempe, D. S., Tanneur, V., Akel, A., Lang, K. S., Foller, M., Kun, J. F., Kremsner, P. G., Wesselborg, S., Laufer, S., Clemen, C. S., Herr, C., Noegel, A. A., Wieder, T., Gulbins, E., Lang, F. & Huber, S. M. (2009). ***Accelerated clearance of Plasmodium-infected erythrocytes in sickle cell trait and annexin-A7 deficiency.*** Cell Physiol Biochem, 24**,** 415-28.

Lee, J. Y., Clarke, M. L., Tokumasu, F., Lesoine, J. F., Allen, D. W., Chang, R., Litorja, M. & Hwang, J. (2012). ***Absorption-Based Hyperspectral Imaging and Analysis of Single Erythrocytes.*** IEEE Journal of Selected Topics in Quantum Electronics, 18**,** 1130-1139.

Leyton-Puig, D., Kedziora, K. M., Isogai, T., van den Broek, B., Jalink, K. & Innocenti, M. (2016). ***PFA fixation enables artifact-free super-resolution imaging of the actin cytoskeleton and associated proteins.*** Biology Open, 5**,** 1001-1009.

Loor, G., Kondapalli, J., Schriewer, J. M., Chandel, N. S., Vanden Hoek, T. L. & Schumacker, P. T. (2010). ***Menadione triggers cell death through ROS-dependent mechanisms involving PARP activation without requiring apoptosis.*** Free Radical Biology and Medicine, 49**,** 1925-1936.

Lucchi, N. W., Koopman, R., Peterson, D. S. & Moore, J. M. (2006). ***Plasmodium falciparum-infected red blood cells selected for binding to cultured syncytiotrophoblast bind to chondroitin sulfate A and induce tyrosine phosphorylation in the syncytiotrophoblast.*** Placenta, 27**,** 384-94.

Lukianova-Hleb, E. Y., Campbell, K. M., Constantinou, P. E., Braam, J., Olson, J. S., Ware, R. E., Sullivan, D. J., Jr. & Lapotko, D. O. (2014). ***Hemozoin-generated vapor nanobubbles for transdermal reagent- and needle-free detection of malaria.*** Proc Natl Acad Sci U S A, 111**,** 900-5.

Lukinavičius, G., Reymond, L., D'Este, E., Masharina, A., Göttfert, F., Ta, H., Güther, A., Fournier, M., Rizzo, S., Waldmann, H., Blaukopf, C., Sommer, C., Gerlich, D. W., Arndt, H.-D., Hell, S. W. & Johnsson, K. (2014). ***Fluorogenic probes for live-cell imaging of the cytoskeleton.*** Nature Methods, 11**,** 731-733.

Lux, S. E. t. (2016). ***Anatomy of the red cell membrane skeleton: unanswered questions.*** Blood, 127**,** 187-99.

Macdonald, V. W. & Charache, S. (1982). ***Drug-induced oxidation and precipitation of hemoglobins A,S and C.*** Biochimica et Biophysica Acta (BBA) - Protein Structure and Molecular Enzymology, 701**,** 39-44.

Mackintosh, C. L., Beeson, J. G. & Marsh, K. (2004). ***Clinical features and pathogenesis of severe malaria.*** Trends in Parasitology, 20**,** 597-603.

Madhunapantula, S. V., Achur, R. N. & Gowda, D. C. (2007). ***Developmental stage- and cell cycle number-dependent changes in characteristics of Plasmodium falciparum-infected erythrocyte adherence to placental chondroitin-4-sulfate proteoglycan.*** Infect Immun, 75**,** 4409-15.

Maier, A. G., Cooke, B. M., Cowman, A. F. & Tilley, L. (2009). ***Malaria parasite proteins that remodel the host erythrocyte.*** Nat Rev Microbiol, 7**,** 341-54.

Martens, P., Kovats, R. S., Nijhof, S., de Vries, P., Livermore, M. T. J., Bradley, D. J., Cox, J. & McMichael, A. J. (1999). ***Climate change and future populations at risk of malaria.*** Global Environmental Change, 9, Supplement 1**,** S89-S107.

Marti, M., Good, R. T., Rug, M., Knuepfer, E. & Cowman, A. F. (2004). ***Targeting malaria virulence and remodeling proteins to the host erythrocyte.*** Science, 306**,** 1930-3.

Mauritz, J. M. A., Esposito, A., Ginsburg, H., Kaminski, C. F., Tiffert, T. & Lew, V. L. (2009). ***The Homeostasis of Plasmodium falciparum-Infected Red Blood Cells.*** PLoS Computational Biology, 5**,** e1000339.

Mbanefo, E. C., Ahmed, A. M., Titouna, A., Elmaraezy, A., Trang, N. T. H., Phuoc Long, N., Hoang Anh, N., Diem Nghi, T., The Hung, B., Van Hieu, M., Ky Anh, N., Huy, N. T. & Hirayama, K. (2017). ***Association of glucose-6-phosphate dehydrogenase deficiency and malaria: a systematic review and meta-analysis.*** Scientific Reports, 7**,** 45963.

Mbengue, A., Vialla, E., Berry, L., Fall, G., Audiger, N., Demettre-Verceil, E., Boteller, D. & Braun-Breton, C. (2015). ***New Export Pathway in Plasmodium falciparum-Infected Erythrocytes: Role of the Parasite Group II Chaperonin, PfTRiC.*** Traffic, 16**,** 461-75.

McDonald, K. (2007). ***Cryopreparation methods for electron microscopy of selected model systems.*** Methods Cell Biol, 79**,** 23-56.

McMillan, P. J., Millet, C., Batinovic, S., Maiorca, M., Hanssen, E., Kenny, S., Muhle, R. A., Melcher, M., Fidock, D. A., Smith, J. D., Dixon, M. W. & Tilley, L. (2013). ***Spatial and temporal mapping of the PfEMP1 export pathway in Plasmodium falciparum.*** Cell Microbiol, 15**,** 1401-18.

MDG-Monitor. (2016). *MDG 6: Combat HIV/AIDS, Malaria and other major diseases* [Online]. Available: http://www.mdgmonitor.org/mdg-6-combat-hiv-aids-malaria-and-other-diseases/ [Accessed].

Meeusen, E. N., Bischof, R. J. & Lee, C. S. (2001). ***Comparative T-cell responses during pregnancy in large animals and humans.*** Am J Reprod Immunol, 46**,** 169-79.

Miller, L. H., Ackerman, H. C., Su, X. Z. & Wellems, T. E. (2013). ***Malaria biology and disease pathogenesis: insights for new treatments.*** Nat Med, 19**,** 156-67.

Miller, L. H., Baruch, D. I., Marsh, K. & Doumbo, O. K. (2002). ***The pathogenic basis of malaria.*** Nature, 415**,** 673-9.

Mota, M. M. & Rodriguez, A. (2004). ***Migration through host cells: the first steps of Plasmodium sporozoites in the mammalian host.*** Cellular Microbiology, 6**,** 1113-1118.

Müller, M. & Moor, H. (1984). ***Cryofixation of thick specimens by high pressure freezing.*** The Science of Biological Specimen Preparation, SEM. AFM OÕHare, Chicago, IL**,** 131-138.

Mundwiler-Pachlatko, E. & Beck, H.-P. (2013). ***Maurer's clefts, the enigma of Plasmodium falciparum.*** Proceedings of the National Academy of Sciences, 110**,** 19987-19994.

Muthusamy, A., Achur, R. N., Valiyaveettil, M., Madhunapantula, S. V., Kakizaki, I., Bhavanandan, V. P. & Gowda, C. D. (2004). ***Structural characterization of the bovine tracheal chondroitin sulfate chains and binding of Plasmodium falciparum–infected erythrocytes.*** Glycobiology, 14**,** 635-645.

Nagel, R. L., Fabry, M. E. & Steinberg, M. H. (2003). ***The paradox of hemoglobin SC disease.*** Blood Reviews, 17**,** 167-178.

Nájera, J. A., González-Silva, M. & Alonso, P. L. (2011). ***Some Lessons for the Future from the Global Malaria Eradication Programme (1955–1969).*** PLoS Medicine, 8**,** e1000412.

Nans, A., Mohandas, N. & Stokes, D. L. (2011). ***Native ultrastructure of the red cell cytoskeleton by cryo-electron tomography.*** Biophys J, 101**,** 2341-50.

Oh, S. S., Voigt, S., Fisher, D., Yi, S. J., LeRoy, P. J., Derick, L. H., Liu, S. & Chishti, A. H. (2000). ***Plasmodium falciparum erythrocyte membrane protein 1 is anchored to the actin-spectrin junction and knob-associated histidine-rich protein in the erythrocyte skeleton.*** Mol Biochem Parasitol, 108**,** 237-47.

Pan, L., Yan, R., Li, W. & Xu, K. (2018). ***Super-Resolution Microscopy Reveals the Native Ultrastructure of the Erythrocyte Cytoskeleton.*** Cell Reports, 22**,** 1151-1158.

Pasternack, G. R., Anderson, R. A., Leto, T. L. & Marchesi, V. T. (1985). ***Interactions between protein 4.1 and band 3. An alternative binding site for an element of the membrane skeleton.*** J Biol Chem, 260**,** 3676-83.

Pasternak, N. D. & Dzikowski, R. (2009). ***PfEMP1: An antigen that plays a key role in the pathogenicity and immune evasion of the malaria parasite Plasmodium falciparum.*** The International Journal of Biochemistry & Cell Biology, 41**,** 1463-1466.

Pehrson, C., Mathiesen, L., Heno, K. K., Salanti, A., Resende, M., Dzikowski, R., Damm, P., Hansson, S. R., King, C. L., Schneider, H., Wang, C. W., Lavstsen, T., Theander, T. G., Knudsen, L. E. & Nielsen, M. A. (2016). ***Adhesion of Plasmodium falciparum infected erythrocytes in ex vivo perfused placental tissue: a novel model of placental malaria.*** Malaria Journal, 15**,** 1-12.

Pei, X., An, X., Guo, X., Tarnawski, M., Coppel, R. & Mohandas, N. (2005). ***Structural and functional studies of interaction between Plasmodium falciparum knob-associated histidine-rich protein (KAHRP) and erythrocyte spectrin.*** J Biol Chem, 280**,** 31166-71.

Perkins, D. J., Were, T., Davenport, G. C., Kempaiah, P., Hittner, J. B. & Ong'echa, J. M. (2011). ***Severe Malarial Anemia: Innate Immunity and Pathogenesis.*** International Journal of Biological Sciences, 7**,** 1427-1442.

Peters, A. L. & Van Noorden, C. J. F. (2009). ***Glucose-6-phosphate Dehydrogenase Deficiency and Malaria: Cytochemical Detection of Heterozygous G6PD Deficiency in Women.*** Journal of Histochemistry and Cytochemistry, 57**,** 1003-1011.

Phillips, M. A., Burrows, J. N., Manyando, C., van Huijsduijnen, R. H., Van Voorhis, W. C. & Wells, T. N. C. (2017). ***Malaria.*** Nature Reviews Disease Primers, 3**,** 17050.

Picart, C. & Discher, D. E. (1999). ***Actin protofilament orientation at the erythrocyte membrane.*** Biophysical Journal, 77**,** 865-878.

Pietro, A. (2007). ***Plasmodium falciparum gametocytes: still many secrets of a hidden life.*** Molecular Microbiology, 66**,** 291-302.

Pimenta, P. F., Touray, M. & Miller, L. (1994). ***The journey of malaria sporozoites in the mosquito salivary gland.*** J Eukaryot Microbiol, 41**,** 608-24.

Pivkin, I. V., Peng, Z., Karniadakis, G. E., Buffet, P. A., Dao, M. & Suresh, S. (2016). ***Biomechanics of red blood cells in human spleen and consequences for physiology and disease.*** Proceedings of the National Academy of Sciences of the United States of America, 113**,** 7804-7809.

Price, R. N., Nosten, F., Luxemburger, C., ter Kuile, F. O., Paiphun, L., Chongsuphajaisiddhi, T. & White, N. J. (1996). ***Effects of artemisinin derivatives on malaria transmissibility.*** Lancet, 347**,** 1654-8.

Przyborski, J. M., Nyboer, B. & Lanzer, M. (2016). ***Ticket to ride: export of proteins to the Plasmodium falciparum-infected erythrocyte.*** Molecular Microbiology, 101**,** 1-11.

Quadt, K. A., Barfod, L., Andersen, D., Bruun, J., Gyan, B., Hassenkam, T., Ofori, M. F. & Hviid, L. (2012). ***The Density of Knobs on <italic>Plasmodium falciparum</italic>-Infected Erythrocytes Depends on Developmental Age and Varies among Isolates.*** PLoS ONE, 7**,** e45658.

Rees, D. C., Williams, T. N. & Gladwin, M. T. (2010). ***Sickle-cell disease.*** Lancet, 376**,** 2018-31.

Riglar, D. T., Richard, D., Wilson, D. W., Boyle, M. J., Dekiwadia, C., Turnbull, L., Angrisano, F., Marapana, D. S., Rogers, K. L., Whitchurch, C. B., Beeson, J. G., Cowman, A. F., Ralph, S. A. & Baum, J. (2011). ***Super-Resolution Dissection of Coordinated Events during Malaria Parasite Invasion of the Human Erythrocyte.*** Cell Host & Microbe, 9**,** 9-20.

Rodriguez, M. H. & Hernández-Hernández, F. d. l. C. (2004). ***Insect–malaria parasites interactions: the salivary gland.*** Insect Biochemistry and Molecular Biology, 34**,** 615-624.

Rogerson, S. J., Hviid, L., Duffy, P. E., Leke, R. F. & Taylor, D. W. (2007). ***Malaria in pregnancy: pathogenesis and immunity.*** Lancet Infect Dis, 7**,** 105-17.

Rossi, R., Milzani, A., Dalle-Donne, I., Giannerini, F., Giustarini, D., Lusini, L., Colombo, R. & Di Simplicio, P. (2001). ***Different Metabolizing Ability of Thiol Reactants in Human and Rat Blood: BIOCHEMICAL AND PHARMACOLOGICAL IMPLICATIONS.*** Journal of Biological Chemistry, 276**,** 7004-7010.

Rowe, J. A., Claessens, A., Corrigan, R. A. & Arman, M. (2009). ***Adhesion of Plasmodium falciparum-infected erythrocytes to human cells: molecular mechanisms and therapeutic implications.*** Expert Reviews in Molecular Medicine, 11**,** null-null.

Rug, M., Cyrklaff, M., Mikkonen, A., Lemgruber, L., Kuelzer, S., Sanchez, C. P., Thompson, J., Hanssen, E., O'Neill, M., Langer, C., Lanzer, M., Frischknecht, F., Maier, A. G. & Cowman, A. F. (2014). ***Export of virulence proteins by malaria-infected erythrocytes involves remodelling of host actin cytoskeleton***.

Rug, M., Prescott, S. W., Fernandez, K. M., Cooke, B. M. & Cowman, A. F. (2006). ***The role of KAHRP domains in knob formation and cytoadherence of P falciparum-infected human erythrocytes.*** Blood, 108**,** 370-378.

Ruwende, C. & Hill, A. (1998). ***Glucose-6-phosphate dehydrogenase deficiency and malaria.*** Journal of Molecular Medicine, 76**,** 581-588.

Sachs, J. & Malaney, P. (2002). ***The economic and social burden of malaria.*** Nature, 415**,** 680.

Salanti, A., Dahlback, M., Turner, L., Nielsen, M. A., Barfod, L., Magistrado, P., Jensen, A. T., Lavstsen, T., Ofori, M. F., Marsh, K., Hviid, L. & Theander, T. G. (2004). ***Evidence for the involvement of VAR2CSA in pregnancy-associated malaria.*** J Exp Med, 200**,** 1197-203.

Salanti, A., Staalsoe, T., Lavstsen, T., Jensen, A. T. R., Sowa, M. P. K., Arnot, D. E., Hviid, L. & Theander, T. G. (2003). ***Selective upregulation of a single distinctly structured var gene in chondroitin sulphate A-adhering Plasmodium falciparum involved in pregnancy-associated malaria.*** Molecular Microbiology, 49**,** 179-191.

Salomao, M., An, X., Guo, X., Gratzer, W. B., Mohandas, N. & Baines, A. J. (2006). ***Mammalian αI-spectrin is a neofunctionalized polypeptide adapted to small highly deformable erythrocytes.*** Proceedings of the National Academy of Sciences of the United States of America, 103**,** 643-648.

Sasi, P., Burns, S. P., Waruiru, C., English, M., Hobson, C. L., King, C. G., Mosobo, M., Beech, J. S., Iles, R. A., Boucher, B. J. & Cohen, R. D. (2007). ***Metabolic acidosis and other determinants of hemoglobin-oxygen dissociation in severe childhood Plasmodium falciparum malaria.*** Am J Trop Med Hyg, 77**,** 256-60.

Sauer, M. & Heilemann, M. (2017). ***Single-Molecule Localization Microscopy in Eukaryotes.*** Chem Rev, 117**,** 7478-7509.

Scherf, A., Hernandez-Rivas, R., Buffet, P., Bottius, E., Benatar, C., Pouvelle, B., Gysin, J. & Lanzer, M. (1998). ***Antigenic variation in malaria: in situ switching, relaxed and mutually exclusive transcription of var genes during intra-erythrocytic development in Plasmodium falciparum.*** The EMBO Journal, 17**,** 5418-5426.

Scherf, A., Lopez-Rubio, J. J. & Riviere, L. (2008). ***Antigenic Variation in Plasmodium falciparum.*** Annual Review of Microbiology, 62**,** 445-470.

Schindelin, J., Arganda-Carreras, I., Frise, E., Kaynig, V., Longair, M., Pietzsch, T., Preibisch, S., Rueden, C., Saalfeld, S., Schmid, B., Tinevez, J.-Y., White, D. J., Hartenstein, V., Eliceiri, K., Tomancak, P. & Cardona, A. (2012). ***Fiji: an open-source platform for biological-image analysis.*** Nature Methods, 9**,** 676.

Schwarzer, E., Turrini, F., Ulliers, D., Giribaldi, G., Ginsburg, H. & Arese, P. (1992). ***Impairment of macrophage functions after ingestion of Plasmodium falciparum-infected erythrocytes or isolated malarial pigment.*** J Exp Med, 176**,** 1033-41.

Scott, J. A. G., Berkley, J. A., Mwangi, I., Ochola, L., Uyoga, S., Macharia, A., Ndila, C., Lowe, B. S., Mwarumba, S., Bauni, E., Marsh, K. & Williams, T. N. (2011). ***Relation between***

falciparum malaria and bacteraemia in Kenyan children: a population-based, case-control study and a longitudinal study. The Lancet, 378**,** 1316-1323.

Serjeant, G. R. (2013). ***The Natural History of Sickle Cell Disease.*** Cold Spring Harbor Perspectives in Medicine, 3**,** a011783.

Shapiro, L. L. M., Whitehead, S. A. & Thomas, M. B. (2017). ***Quantifying the effects of temperature on mosquito and parasite traits that determine the transmission potential of human malaria.*** PLOS Biology, 15**,** e2003489.

Shi, H., Liu, Z., Li, A., Yin, J., Chong, A. G. L., Tan, K. S. W., Zhang, Y. & Lim, C. T. (2013). ***Life Cycle-Dependent Cytoskeletal Modifications in Plasmodium falciparum Infected Erythrocytes.*** PLOS ONE, 8**,** e61170.

Shotton, D. M., Burke, B. E. & Branton, D. (1979). ***The molecular structure of human erythrocyte spectrin. Biophysical and electron microscopic studies.*** J Mol Biol, 131**,** 303-29.

Singh, B. & Daneshvar, C. (2013). ***Human Infections and Detection of Plasmodium knowlesi.*** Clinical Microbiology Reviews, 26**,** 165-184.

Skorokhod, O. A., Caione, L., Marrocco, T., Migliardi, G., Barrera, V., Arese, P., Piacibello, W. & Schwarzer, E. (2010). ***Inhibition of erythropoiesis in malaria anemia: role of hemozoin and hemozoin-generated 4-hydroxynonenal.*** Blood, 116**,** 4328-37.

Smith, J. D., Gamain, B., Baruch, D. I. & Kyes, S. (2001). ***Decoding the language of var genes and Plasmodium falciparum sequestration.*** Trends Parasitol, 17**,** 538-45.

Spycher, C., Rug, M., Klonis, N., Ferguson, D. J., Cowman, A. F., Beck, H. P. & Tilley, L. (2006). ***Genesis of and trafficking to the Maurer's clefts of Plasmodium falciparum-infected erythrocytes.*** Mol Cell Biol, 26**,** 4074-85.

Srivastava, S. K., Awasthi, Y. C. & Beutler, E. (1974). ***Useful agents for the study of glutathione metabolism in erythroyctes. Organic hydroperoxides.*** Biochem J, 139**,** 289-95.

Staines, H. M., Powell, T., Thomas, S. L. Y. & Clive Ellory, J. (2004). ***Plasmodium falciparum-induced channels.*** International Journal for Parasitology, 34**,** 665-673.

Sturm, A., Amino, R., van de Sand, C., Regen, T., Retzlaff, S., Rennenberg, A., Krueger, A., Pollok, J.-M., Menard, R. & Heussler, V. T. (2006). ***Manipulation of Host Hepatocytes by the Malaria Parasite for Delivery into Liver Sinusoids.*** Science, 313**,** 1287-1290.

Subramani, R., Quadt, K., Jeppesen, A. E., Hempel, C., Petersen, J. E. V., Hassenkam, T., Hviid, L. & Barfod, L. (2015). ***Plasmodium falciparum-Infected Erythrocyte Knob Density Is Linked to the PfEMP1 Variant Expressed.*** mBio, 6.

Swihart, A. H., Mikrut, J. M., Ketterson, J. B. & Macdonald, R. C. (2001). ***Atomic force microscopy of the erythrocyte membrane skeleton.*** J Microsc, 204**,** 212-25.

Talman, A. M., Domarle, O., McKenzie, F. E., Ariey, F. & Robert, V. (2004). ***Gametocytogenesis : the puberty of Plasmodium falciparum.*** Malaria Journal, 3**,** 24-24.

Taylor, S. M., Cerami, C. & Fairhurst, R. M. (2013). ***Hemoglobinopathies: Slicing the Gordian Knot of <italic>Plasmodium falciparum</italic> Malaria Pathogenesis.*** PLoS Pathog, 9**,** e1003327.

Taylor, S. M., Parobek, C. M. & Fairhurst, R. M. (2012). ***Haemoglobinopathies and the clinical epidemiology of malaria: a systematic review and meta-analysis.*** Lancet Infect Dis, 12**,** 457-68.

Thomas, S. L. Y. & Lew, V. L. (2004). ***Plasmodium falciparum and the permeation pathway of the host red blood cell.*** Trends in Parasitology, 20**,** 122-125.

Thor, H., Smith, M. T., Hartzell, P., Bellomo, G., Jewell, S. A. & Orrenius, S. (1982). ***The metabolism of menadione (2-methyl-1,4-naphthoquinone) by isolated hepatocytes. A study of the implications of oxidative stress in intact cells.*** Journal of Biological Chemistry, 257**,** 12419-12425.

Tilley, L., Dixon, M. W. A. & Kirk, K. (2011). ***The Plasmodium falciparum-infected red blood cell.*** The International Journal of Biochemistry & Cell Biology, 43**,** 839-842.

Tilley, L., Straimer, J., Gnadig, N. F., Ralph, S. A. & Fidock, D. A. (2016). ***Artemisinin Action and Resistance in Plasmodium falciparum.*** Trends Parasitol, 32**,** 682-696.

Trampuz, A., Jereb, M., Muzlovic, I. & Prabhu, R. M. (2003a). ***Clinical review: Severe malaria.*** Crit Care, 7**,** 315-23.

Trampuz, A., Jereb, M., Muzlovic, I. & Prabhu, R. M. (2003b). ***Clinical review: Severe malaria.*** CRITICAL CARE-LONDON-, 7**,** 315-323.

Trent, R. J. A. (2006). ***Diagnosis of the Haemoglobinopathies.*** Clinical Biochemist Reviews, 27**,** 27-38.

Triglia, T., Stahl, H. D., Crewther, P. E., Scanlon, D., Brown, G. V., Anders, R. F. & Kemp, D. J. (1987). ***The complete sequence of the gene for the knob-associated histidine-rich protein from Plasmodium falciparum.*** Embo j, 6**,** 1413-9.

Uneke, C. J. (2007). ***Impact of placental Plasmodium falciparum malaria on pregnancy and perinatal outcome in sub-Saharan Africa: I: introduction to placental malaria.*** Yale J Biol Med, 80**,** 39-50.

United Nations. (2017). *Sustainable Development Knowledge Platform* [Online]. Available: https://sustainabledevelopment.un.org/sdgs [Accessed].

Uyoga, S., Ndila, C. M., Macharia, A. W., Nyutu, G., Shah, S., Peshu, N., Clarke, G. M., Kwiatkowski, D. P., Rockett, K. A. & Williams, T. N. (2015). ***Glucose-6-phosphate dehydrogenase deficiency and the risk of malaria and other diseases in children in Kenya: a case-control and a cohort study.*** The Lancet Haematology, 2**,** e437-e444.

van de Linde, S., Loschberger, A., Klein, T., Heidbreder, M., Wolter, S., Heilemann, M. & Sauer, M. (2011). ***Direct stochastic optical reconstruction microscopy with standard fluorescent probes.*** Nat Protoc, 6**,** 991-1009.

van den Berg, J. J. M., Op den Kamp, J. A. F., Lubin, B. H., Roelofsen, B. & Kuypers, F. A. (1992). ***Kinetics and site specificity of hydroperoxide-induced oxidative damage in red blood cells.*** Free Radical Biology and Medicine, 12**,** 487-498.

Van der Zee, J., Van Steveninck, J., Koster, J. F. & Dubbelman, T. M. A. R. (1989). ***Inhibition of enzymes and oxidative damage of red blood cells induced by t-butylhydroperoxide-derived radicals.*** Biochimica et Biophysica Acta (BBA) - Biomembranes, 980**,** 175-180.

van Eijk, A. M., Ayisi, J. G., Ter Kuile, F. O., Slutsker, L., Shi, Y. P., Udhayakumar, V., Otieno, J. A., Kager, P. A., Lal, R. B., Steketee, R. W. & Nahlen, B. L. (2007). ***HIV, malaria, and infant anemia as risk factors for postneonatal infant mortality among HIV-seropositive women in Kisumu, Kenya.*** J Infect Dis, 196**,** 30-7.

Vaughan, A. M., Aly, A. S. I. & Kappe, S. H. I. (2008). ***Malaria Parasite Pre-Erythrocytic Stage Infection: Gliding and Hiding.*** Cell Host & Microbe, 4**,** 209-218.

Venkataramani, V., Herrmannsdorfer, F., Heilemann, M. & Kuner, T. (2016). ***SuReSim: simulating localization microscopy experiments from ground truth models.*** Nat Methods, 13**,** 319-21.

Viebig, N. K., Gamain, B., Scheidig, C., Lépolard, C., Przyborski, J., Lanzer, M., Gysin, J. & Scherf, A. (2005). ***A single member of the Plasmodium falciparum var multigene family determines cytoadhesion to the placental receptor chondroitin sulphate A.*** EMBO reports, 6**,** 775-781.

Viebig, N. K., Nunes, M. C., Scherf, A. & Gamain, B. (2006). ***The human placental derived BeWo cell line: A useful model for selecting Plasmodium falciparum CSA-binding parasites.*** Experimental Parasitology, 112**,** 121-125.

Vlachou, D., Schlegelmilch, T., Runn, E., Mendes, A. & Kafatos, F. C. (2006). ***The developmental migration of Plasmodium in mosquitoes.*** Current Opinion in Genetics & Development, 16**,** 384-391.

Waldecker, M., Dasanna, A. K., Lansche, C., Linke, M., Srismith, S., Cyrklaff, M., Sanchez, C. P., Schwarz, U. S. & Lanzer, M. (2017). ***Differential time-dependent volumetric and surface area changes and delayed induction of new permeation pathways in P. falciparum-infected hemoglobinopathic erythrocytes.*** Cell Microbiol, 19.

Watermeyer, J. M., Hale, V. L., Hackett, F., Clare, D. K., Cutts, E. E., Vakonakis, I., Fleck, R. A., Blackman, M. J. & Saibil, H. R. (2016). ***A spiral scaffold underlies cytoadherent knobs in Plasmodium falciparum–infected erythrocytes.*** Blood, 127**,** 343-351.

Weatherall, D. 2010. Beginnings: The Molecular Pathology of Hemoglobin. *In:* ***Molecular Hematology***. PROVAN , D. & GRIBBEN, J. G.doi:10.1002/9781444318531.ch1

Weiss, G. E., Gilson, P. R., Taechalertpaisarn, T., Tham, W. H., de Jong, N. W., Harvey, K. L., Fowkes, F. J., Barlow, P. N., Rayner, J. C., Wright, G. J., Cowman, A. F. & Crabb, B. S. (2015). ***Revealing the sequence and resulting cellular morphology of receptor-ligand interactions during Plasmodium falciparum invasion of erythrocytes.*** PLoS Pathog, 11**,** e1004670.

Weng, H., Guo, X., Papoin, J., Wang, J., Coppel, R., Mohandas, N. & An, X. (2014). ***Interaction of Plasmodium falciparum knob-associated histidine-rich protein (KAHRP) with erythrocyte ankyrin R is required for its attachment to the erythrocyte membrane.*** Biochim Biophys Acta, 1838**,** 185-92.

Whelan, D. R. & Bell, T. D. (2015). ***Image artifacts in single molecule localization microscopy: why optimization of sample preparation protocols matters.*** Sci Rep, 5**,** 7924.

White, N. J., Pukrittayakamee, S., Hien, T. T., Faiz, M. A., Mokuolu, O. A. & Dondorp, A. M. (2014). ***Malaria.*** Lancet, 383**,** 723-35.

White, N. J., Turner, G. D. H., Medana, I. M., Dondorp, A. M. & Day, N. P. J. (2010). ***The murine cerebral malaria phenomenon.*** Trends in Parasitology, 26**,** 11-15.

WHO. (2015a). ***Guidelines for the treatment of malaria - 3rd Ed***, World Health Organization.

WHO. (2015b). ***World Malaria Report 2015***, World Health Organization.

WHO. (2017a). *Climate change and human health* [Online]. Available: http://www.who.int/globalchange/summary/en/index5.html [Accessed].

WHO. (2017b). ***World Malaria Report 2017***, World Health Organization.

Williams, T. N. & Weatherall, D. J. (2012). ***World distribution, population genetics, and health burden of the hemoglobinopathies.*** Cold Spring Harb Perspect Med, 2**,** a011692.

Winterbourn, C. C., French, J. K. & Claridge, R. (1979). ***The reaction of menadione with haemoglobin. Mechanism and effect of superoxide dismutase.*** Biochem. J, 179**,** 665-673.

Wolter, S., Löschberger, A., Holm, T., Aufmkolk, S., Dabauvalle, M.-C., van de Linde, S. & Sauer, M. (2012). ***rapidSTORM: accurate, fast open-source software for localization microscopy.*** Nature Methods, 9**,** 1040.

Wongsrichanalai, C., Pickard, A. L., Wernsdorfer, W. H. & Meshnick, S. R. (2002). ***Epidemiology of drug-resistant malaria.*** The Lancet Infectious Diseases, 2**,** 209-218.

Yeo, T. W., Lampah, D. A., Gitawati, R., Tjitra, E., Kenangalem, E., McNeil, Y. R., Darcy, C. J., Granger, D. L., Weinberg, J. B., Lopansri, B. K., Price, R. N., Duffull, S. B., Celermajer, D. S. & Anstey, N. M. (2007). ***Impaired nitric oxide bioavailability and L-arginine reversible endothelial dysfunction in adults with falciparum malaria.*** J Exp Med, 204**,** 2693-704.

Zou, C. G., Agar, N. S. & Jone, G. L. (2001). ***Oxidative insult in sheep red blood cells induced by T-butyl hydroperoxide: the roles of glutathione and glutathione peroxidase.*** Free Radic Res, 34**,** 45-56.

8 Publications

The following publications resulted from this work:

Waldecker M, Dasanna AK, Lansche C, Linke M, **Srismith S**, Cyrklaff M, Sanchez CP, Schwarz US, Lanzer M. (2017) ***Differential time-dependent volumetric and surface area changes and delayed induction of new permeation pathways in P. falciparum-infected hemoglobinopathic erythrocytes.*** Cell Microbiol. 19, 2

Cyrklaff M, **Srismith S**, Nyboer B, Burda K, Hoffmann A, Lasitschka F, Adjalley S, Bisseye C, Simpore J, Mueller AK, Sanchez CP, Frischknecht F, Lanzer M. (2016) ***Oxidative insult can induce malaria-protective trait of sickle and fetal erythrocytes*.** Nat Commun. 8, 7

Srismith S*, Kilian N*, Dittmer M, Ouermi D, Bisseye C, Simpore J, Cyrklaff M, Sanchez CP, Lanzer M. (2015) ***Hemoglobin S and C affect protein export in Plasmodium falciparum-infected erythrocytes.*** Biol Open. 4, 3 *Equal contributions